The function of the Heg-CCM pathway in zebrafish heart development

Dissertation Advisor: Dr. John Mably Jonathan Rosen

The function of the Heg-CCM pathway in zebrafish heart development

Abstract

The Heart of glass-Cerebral Cavernous Malformation (Heg-CCM) pathway is essential for heart development in zebrafish and mouse. In zebrafish, mutants for the Heg-CCM genes *ccm1*, *ccm2*, and *heg* exhibit an extreme dilation of the heart chambers and inflow tract and completely lack blood circulation. The mechanisms by which this pathway regulates heart development are incompletely understood. Two major impediments to our knowledge are the paucity of genes known to participate in the Heg-CCM pathway and a lack of information about how the Heg-CCM pathway interacts with other signaling pathways in live embryos.

To address the first hurdle, we have undertaken two approaches. First, we performed a yeast 2-hybrid screen to identify proteins that interact with Heg, the transmembrane protein component of the Heg-CCM pathway. We find that zebrafish Heg interacts with Ccm1, which is consistent with others' findings about the mouse orthologs of these proteins, suggesting that the Heg-Ccm1 interaction is conserved across vertebrate species. Second, we employed a bioinformatic approach to identify novel proteins bearing high sequence identity to the known Heg-CCM pathway components. Using this strategy, we discovered the novel protein Ccm2-like (Ccm2l) and performed analyses of Ccm2l in zebrafish and cell culture. We found that loss of *ccm2l* causes the heart's atrium to dilate and that this phenotype can be partially rescued by overexpression of *ccm2*. Slight knockdown of *ccm2l* can enhance the heart phenotype in embryos sensitized by a low dose of morpholino against *ccm1*, and Ccm2l protein can bind

Ccm1 protein in an overexpression system. Taken together, we conclude that *ccm2l* is required for normal heart development as a component of the Heg-CCM pathway.

To address the second hurdle, we focus on the interactions between the Heg-CCM pathway and the extracellular signal-regulated kinase (Erk) pathway in the zebrafish heart. We find that global inhibition of Erk causes dilation of the atrium, while myocardial hyperactivation of Erk results in a shrunken heart. Moreover, global hyperactivation of Erk can partially rescue *heg* morphant phenotypes. We propose a model in which one function of the Heg-CCM pathway is to regulate Erk activity in the developing myocardium.

Table of Contents

Acknowledgments

I would like to thank my friends and family and the classmates, colleagues and professors who have helped me since I began graduate school in 2006.

Chapter 1: An introduction to zebrafish heart development and the Heg-CCM pathway

Zebrafish as a model for cardiovascular development

The zebrafish *Danio rerio* offers many advantages as a model for vertebrate development. First, zebrafish are fecund; a single mating pair can produce hundreds of fertilized eggs in a single morning. Second, fertilized eggs simply sink to the bottom of the breeding cage, making it trivially easy to obtain them. Third, zebrafish embryos develop externally and are transparent, allowing for direct visualization of morphogenesis throughout embryonic development. Fourth, zebrafish development is extremely rapid, with the progression from fertilized egg to free-living larva taking just 5 days. Fifth, zebrafish are amenable to increasingly sophisticated genetic manipulations, including forward genetics by mutagenesis screening, reverse genetics by targeted morpholino knockdown or TALEN knockout, and the generation of transgenic animals in which integrated genes are expressed with temporal or spatial specificity.

The zebrafish has been used extensively to study the development of many organs, including the heart, the first functional organ to form in the animal. The zebrafish heart has only two chambers: one atrium and one ventricle (Figure 1.1A). However, its function and development are similar to its mammalian counterparts'. The embryonic zebrafish heart contains two tissues: the endocardium and the myocardium (Figure 1.1B). The endocardium is a specialized endothelium lining the inside of the heart that is continuous with the rest of the animal's vasculature. The myocardium is the heart's muscle which contracts rhythmically to generate blood circulation.

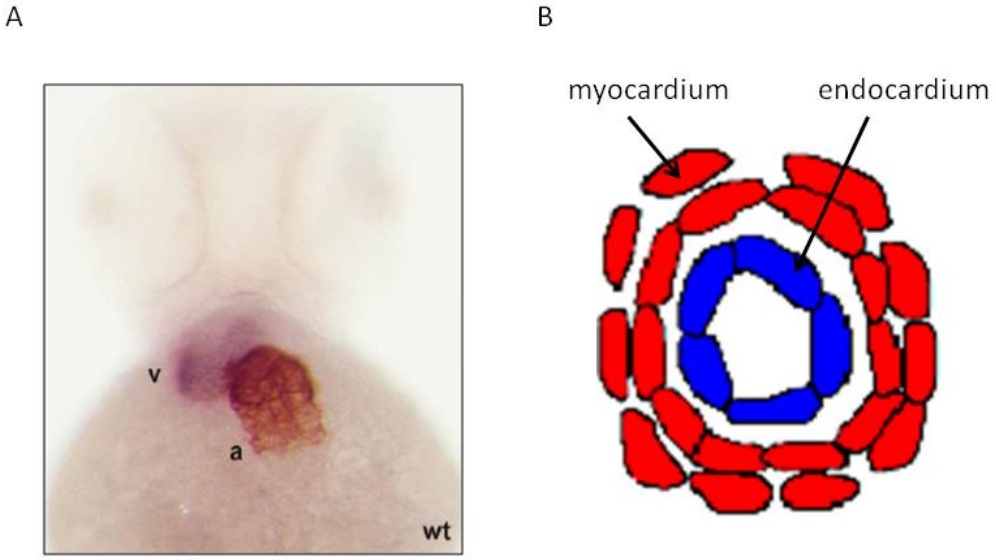

Figure 1.1. Structure of the embryonic zebrafish heart. (A) A fixed 48 hpf zebrafish embryo subjected to *in situ* hybridization and antibody staining using chamber-specific markers. The view is ventral with anterior at the top. a, atrium, v, ventricle. Figure 1.1A is taken from Mably et al., 2006. (B) Schematic depicting a cross section cut through a 48 hpf ventricle. The myocardium is red and the endocardium is blue.

It is an ongoing challenge for developmental biologists to decipher the steps that lead to the generation of a heart, and the strengths of the zebrafish system have made it immensely valuable in pursuing this goal. Owing largely to the embryo's transparency, as well as the use of transgenic zebrafish lines in which specific cell populations are labeled with fluorescent reporters, we have a detailed understanding of the morphological events required to generate a mature heart (Stainier, 2001). During somitogenesis, partially differentiated heart cells migrate from the left and right lateral plate mesoderm toward the midline. At the midline, the two converging populations form a structure called the cardiac cone, which then extends into the primitive heart tube. Around this time, a mere 22-24 hours post fertilization (hpf), the heart begins to beat. Even so, further morphological events are required to generate a mature heart. By 36 hpf, a process termed looping occurs, in which the ventricle is placed to the right of the

midline, and the atrium to the left. Endocardial cushions, the precursors to valves, form, and an extracellular matrix called cardiac jelly forms between the endocardium and the myocardium.

These morphological events are under genetic control, and zebrafish mutants isolated from mutagenesis screens have been indispensable in identifying and characterizing the relevant genes and pathways. One example of a mutant that led to unexpected discoveries about heart morphogenesis is *miles apart* (*mil*). In *mil* mutants, the bilateral populations of cardiac precursors fail to migrate to the midline. Positional cloning revealed that the *mil* gene encodes a sphingosine-1 phosphate receptor, leading to the discovery that lysosphingolipid signaling is required for heart fusion (Kupperman et al., 2000). Lysosphingolipids had been known to function in other contexts, but until the characterization of *mil* it was unknown that they play a crucial role in heart development.

ccm1, *ccm2*, and *heg* are part of a signaling pathway that is required for cardiovascular development

In the treasury of zebrafish mutants, none have heart phenotypes more striking than *santa* (*san*), *valentine* (*vtn*), and *heart of glass* (*heg*). In these mutants, early morphogenic processes such as precursor migration and fusion occur normally. The first signs that heart development is perturbed appear around 28 hpf, at which time wildtype embryos have visible blood circulation but the mutants do not. By 48 hpf, the mutant hearts and inflow tracts are massively dilated (Figure 1.2A). Mutant hearts beat, but there is no circulation of blood cells. By 72 hpf, the ventricular myocardium is 2-3 myocytes thick in wildtype embryos, but in mutants it remains a single cell layer (Mably et al., 2003). Surprisingly, the number of myocardial and endocardial

cells in these mutants is the same as in wildtype embryos; thus, the extreme increase in the size of the heart chambers is accomplished without cellular hyperproliferation (Mably et al., 2006; Mably et al., 2003). While the dilated heart is the most conspicuous phenotype in *san*, *vtn*, and *heg* mutants, other endothelial vessels are also affected, as *san* and *vtn* mutants have been shown to exhibit dilation of the subintestinal vein (SIV) and posterior cardinal vein (PCV) (Hogan et al., 2008). The animals die around 5 days post fertilization (dpf), which is typical for zebrafish embryos with any sort of severely impaired cardiovascular development.

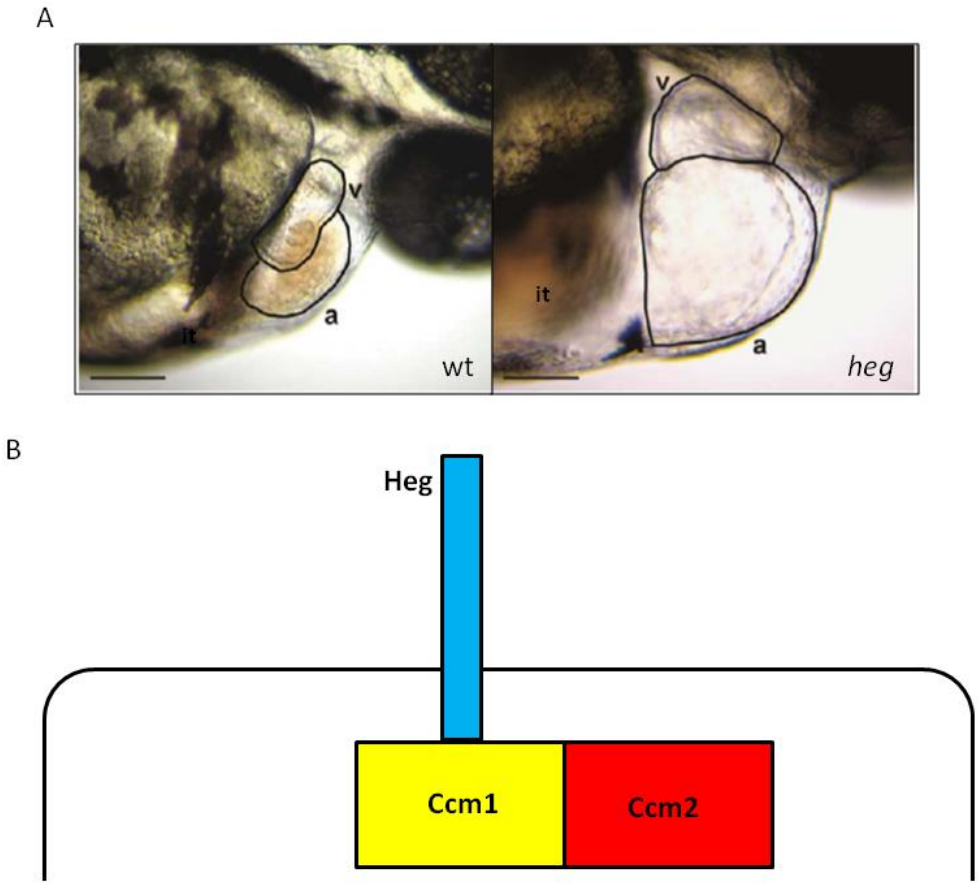

Figure 1.2. The Heg-CCM pathway is required for normal heart development. (A) In wildtype embryos at 48 hpf, the chambers of the heart are compact and the inflow tract is narrow. In *heg* mutants at 48 hpf, the heart chambers and inflow tract are massively dilated. *san* and *vtn* mutants have heart phenotypes nearly indistinguishable from *heg*. a, atrium; it, inflow tract; v, ventricle. Images taken from Mably et al., 2003. (B) Schematic showing the Heg-Ccm1-Ccm2 complex. Heg is a single-pass transmembrane protein whose intracellular domain binds Ccm1. Ccm1 binds numerous other proteins, including the cytoplasmic protein Ccm2. This schematic applies to both zebrafish and mammals.

The genes disrupted in the *san*, *vtn*, and *heg* mutants are named *cerebral cavernous malformation 1* (*ccm1*), *cerebral cavernous malformation 2* (*ccm2*), and *heg*, respectively. All three genes are conserved across vertebrate species and are also required for cardiovascular development in mouse. (See Table 1.1.) Genetic deletion of murine *Ccm1* confers numerous

cardiovascular defects in the developing embryo. The heart's atrium is enlarged and there are pericardial effusions. The aorta and intersomitic arteries are enlarged as well, and staining for the arterial marker *Efnb2* reveals a loss of arterial identity (Whitehead et al., 2004). When *Ccm2* is knocked out in the mouse instead, embryos also exhibit pericardial effusions. The branchial arch arteries fail to lumenize, and different regions of the aorta are either constricted or enlarged (Boulday et al., 2009; Whitehead et al., 2009). When *Heg1*, the mouse homolog of *heg*, is knocked out, embryos exhibit pulmonary hemorrhage, blood-filled pericardial sacs, and dilated lymphatic vessels. Additionally, in histological sections, the ventricle has a "honeycombed" appearance owing to the invagination of the heart cavity into the myocardium (Kleaveland et al., 2009). *Ccm1* and *Ccm2* knockouts die *in utero*, while half of all embryos null for *Heg1* survive until birth (Boulday et al., 2009; Kleaveland et al., 2009; Whitehead et al., 2009; Whitehead et al., 2004).

Table 1.1. Nomenclature for genes in the Heg-CCM pathway. For historical reasons, *Ccm1*, *Ccm2* and *Ccm3* each have multiple names. (*Ccm1*: *Krev interaction trapped gene 1*. *Ccm2*: *Malcavernin, Osmosensing scaffold for mekk3*. *Ccm3*: *Programmed cell death 10*.) For clarity, in this dissertation we use only the gene names presented in this table, with the established species-specific nomenclature.

Zebrafish gene	*ccm1*	*ccm2*	*heg*	*ccm3a* and *ccm3b*
Zebrafish mutant	*san*	*vtn*	*heg*	N.A.
Zebrafish protein	Ccm1	Ccm2	Heg	Ccm3a and Ccm3b
Mouse gene	*Ccm1*	*Ccm2*	*Heg1*	*Ccm3*
Mouse protein	Ccm1	Ccm2	Heg1	Ccm3
Human gene	*CCM1*	*CCM2*	*HEG1*	*CCM3*
Human protein	CCM1	CCM2	HEG1	CCM3

In contrast to mouse, where the *Heg1* knockout is quite distinct from the *Ccm1* and *Ccm2* knockouts, in zebrafish all three mutants have essentially the same phenotype: a massively dilated heart and no circulation of blood cells. Moreover, this phenotype has not been observed in any other mutants. These observations suggest that *ccm1, ccm2,* and *heg* may operate in a common pathway in zebrafish. In a test of this hypothesis, it was found that slight knockdown of any of the three genes by morpholino injection can drastically enhance heart phenotypes in embryos sensitized by a subphenotypic dose of morpholino against either of the other two (Mably et al., 2006). Similarly, in mouse, *Heg1* knockout phenotypes are enhanced in animals

haploinsufficient for *Ccm2*; approximately half of *Heg1*$^{-/-}$;*Ccm2*$^{+/+}$ embryos survive to birth, but all *Heg1*$^{-/-}$;*Ccm2*$^{+/lacZ}$ embryos die in utero (Kleaveland et al., 2009). Thus, in both zebrafish and mouse, *ccm1*, *ccm2* and *heg* interact genetically; they are core components of what is called the Heg-CCM pathway.

ccm1, *ccm2*, and *heg* and their murine counterparts are all expressed in multiple tissues, making it nontrivial to ascertain which tissue the Heg-CCM pathway is required in for normal development to occur. Fortunately, a breakthrough occurred several years ago, when two groups found that the phenotypes in the *Ccm2* null mouse are recapitulated in mice in which *Ccm2* is selectively deleted from the developing endothelium. These findings strongly suggest that the Heg-CCM pathway's activity is required in the endothelium (Boulday et al., 2009; Whitehead et al., 2009). *in situ* hybridization experiments in zebrafish embryos detect *heg* RNA in the endocardium but not the myocardium, consistent with a model in which Heg-CCM signaling in the heart's endothelium regulates heart morphology (Mably et al., 2003).

The genetic interactions among *ccm1*, *ccm2*, and *heg* are nicely complemented by biochemical evidence showing that the proteins encoded by these genes form a complex (Figure 1.2B). Ccm1 is a large cytoplasmic/nuclear protein containing three NPXY/F motifs, ankyrin repeats, and a band 4.1/ezrin/radixin/moesin (FERM) domain. In general, ankyrin repeats are thought to mediate protein-protein interactions, though the function of Ccm1's ankryrin repeats in unknown. FERM domains localize cytoplasmic proteins to the plasma membrane. Ccm2 is a smaller cytoplasmic protein. Its only domain or motif recognizable by primary amino acid sequence is a phosphotyrosine binding (PTB) domain at its N-terminal end. Co-immunoprecipitation, fluorescence resonance energy transfer (FRET), and yeast 2-hybrid experiments have demonstrated physical interactions between human CCM1 and CCM2

(Zawistowski et al., 2005; Zhang et al., 2007). Heg is a single pass transmembrane protein with epidermal growth factor (EGF)-like repeats in its extracellular domain. The intracellular domain of Heg is the most highly conserved part of the protein, and it binds the Ccm1-Ccm2 complex through Ccm1. This interaction was demonstrated by others for mammalian proteins (Kleaveland et al., 2009) and in this dissertation (Chapters 2 and 3) for the zebrafish orthologs.

Ccm1-Ccm2 binding involves an interaction between the NPXY/F motifs of Ccm1 and the PTB domain of Ccm2. A point mutation that disrupts the PTB domain of CCM2 abolishes CCM1-CCM2 binding (Zawistowski et al., 2005). There is mixed evidence in the literature on the contributions of the individual NPXY/F motifs of CCM1 to the CCM1-CCM2 interaction. One group found that the first NPXY/F motif of human CCM1 is dispensable for binding to CCM2 but that binding could be impaired by mutagenesis of the second and third NPXY/F motifs (Zhang et al., 2007). A different group found that mutagenesis of the first NPXY/F motif subtly reduced the strength of the CCM1-CCM2 interaction but did not detect any changes in CCM1-CCM2 binding upon disruption of the second or third NPXY/F motifs (Zawistowski et al., 2005). These disparate results are probably due to the groups' different strategies for disrupting the NPXY/F motifs and their different assays in measuring binding strength.

In human and mouse CCM1, there is one NPXY motif followed by two NPXF motifs. NPXY and NPXF motifs are structurally similar, but because tyrosine and not phenylalanine is a substrate for cellular kinases, typically only NPXY motifs are subject to regulation by phosphorylation. Interestingly, the second NPXF motif contains a tyrosine in the third position, and a recent mass spectrometry study found that this residue is phosphorylated while the tyrosine in the NPXY motif is not (Kim et al., 2011). The functional significance of this unusual NPXF phosphorylation event is unknown.

Cellular functions of the Heg-CCM pathway

In the last several years there have been numerous studies elucidating the cellular functions of the Heg-CCM pathway. Ccm2 was originally discovered by a yeast 2-hybrid screen using the kinase MEKK3 as bait. MEKK3 is a component of the p38 pathway, which is activated in response to hyperosmolarity and other cellular stresses. siRNA-mediated knockdown of CCM2 in cell culture inhibits the activation of p38 in response to hyperosmotic shock; thus, CCM2 is a necessary component of the p38 pathway (Uhlik et al., 2003). This role for Ccm2 was validated by another group using mouse embryonic fibroblasts (MEFs) heterozygous for Ccm2 (Zawistowski et al., 2005).

It is not easy to explain why attenuation of the p38 stress response pathway would cause the heart and vascular defects observed in Heg-CCM mutant animals. There are, however, other pathways affected by Heg-CCM gene perturbation that have the potential to at least partially explain the mutant phenotypes observed in zebrafish and mouse. Chief among them is the RhoA pathway.

RhoA is a small GTPase that promotes stress fiber formation and tissue permeability in endothelial cells. Like all GTPases, RhoA cycles between an active GTP-bound state and an inactive GDP-bound state. GTP-bound RhoA activates its effector molecule Rho-associated Protein Kinase (ROCK), which phosphorylates myosin light chain phosphatase (MLCP), preventing MLCP from deactivating (via dephosphorylation) myosin light chain (MLC).

Phosphorylated MLC promotes the formation of stress fibers and reduces cell adhesion by disrupting adherens junctions, causing tissue permeability (Spindler et al., 2010).

The link between Heg-CCM signaling and RhoA was identified on the basis of the phenotype observed in endothelial cells depleted of *CCM1* or *CCM2* by siRNA. Staining of actin in these cells shows increased stress fiber formation and monolayer permeability assays show decreased barrier function (Glading et al., 2007; Stockton et al., 2010; Whitehead et al., 2009). As these phenotypes predict, knockdown of *CCM1* or *CCM2* causes an increase in cellular levels of activated RhoA (Borikova et al., 2010; Crose et al., 2009; Stockton et al., 2010; Whitehead et al., 2009). The Heg-CCM pathway also appears to regulate RhoA in vessels in mouse, as $Ccm2^{+/-}$ adult mice exhibit a vascular leakiness phenotype that can be suppressed by administration of drugs that target the RhoA pathway (Stockton et al., 2010; Whitehead et al., 2009).

To repress the RhoA pathway, CCM proteins must reach the cell junction where RhoA is active and then somehow constrain its activity. The means by which Ccm1 arrives at the cell junction are becoming clear. Recent studies show that CCM1 normally resides on microtubules but is recruited to cell junctions by the small GTPase Rap1 (Glading et al., 2007; Liu et al., 2011). At the cell junction, it binds proteins associated with adherens junctions, including β-Catenin and p120, through its FERM domain (Glading et al., 2007). Endogenous CCM2 (Stockton et al., 2010) and overexpressed Heg1 (Kleaveland et al., 2009) both reside at cell junctions, and both are required to localize CCM1 there (Gingras et al., 2012; Stockton et al., 2010). How the Heg-CCM complex inhibits RhoA after it is assembled at the cell junction is unclear. It has been found in an overexpression system that CCM2 co-immunoprecipitates with RHOA (Whitehead et al., 2009), so the mechanism may be direct. One group has found that

CCM2 promotes the degradation of RHOA protein by recruiting the E3 ubiquitin ligase SMURF1 to the membrane (Borikova et al., 2010; Crose et al., 2009). However, in other studies, total RHOA levels were unaffected by depletion of CCM1 and CCM2 (Stockton et al., 2010; Whitehead et al., 2009). More research will have to be done to resolve the mechanism by which the Heg-CCM pathway restricts RhoA signaling.

Can the cardiovascular phenotypes in embryos homozygous mutant for Heg-CCM pathway genes be explained by RhoA hyperactivation and loss of adherens junctions? In both mouse and zebrafish, there is evidence of altered endothelial cell junctions. In the *Heg1* knockout mouse, mesenteric lymphatic vessels exhibit shortened endothelial junctions, as assayed by electron microscopy. In *ccm2* morphant zebrafish embryos, the junctions between endocardial cells are shortened as well (Kleaveland et al., 2009). It is relatively easy to explain the *Heg1* mouse knockout phenotypes by a reduction in endothelial junction length, since knockouts have defects in vascular integrity (Kleaveland et al., 2009). However, in zebrafish, where the most profound Heg-CCM mutant phenotype is the massively dilated heart (Mably et al., 2006; Mably et al., 2003), it is more challenging to attribute the Heg-CCM loss-of-function phenotype entirely to a loss of adherens junctions. While the shortened junctions between endocardial cells would result in less overlap between adjoining cells and expansion of the tissue's surface area (Figure 1.3A), it is not clear that this process would be sufficient to explain the massive increase in organ size.

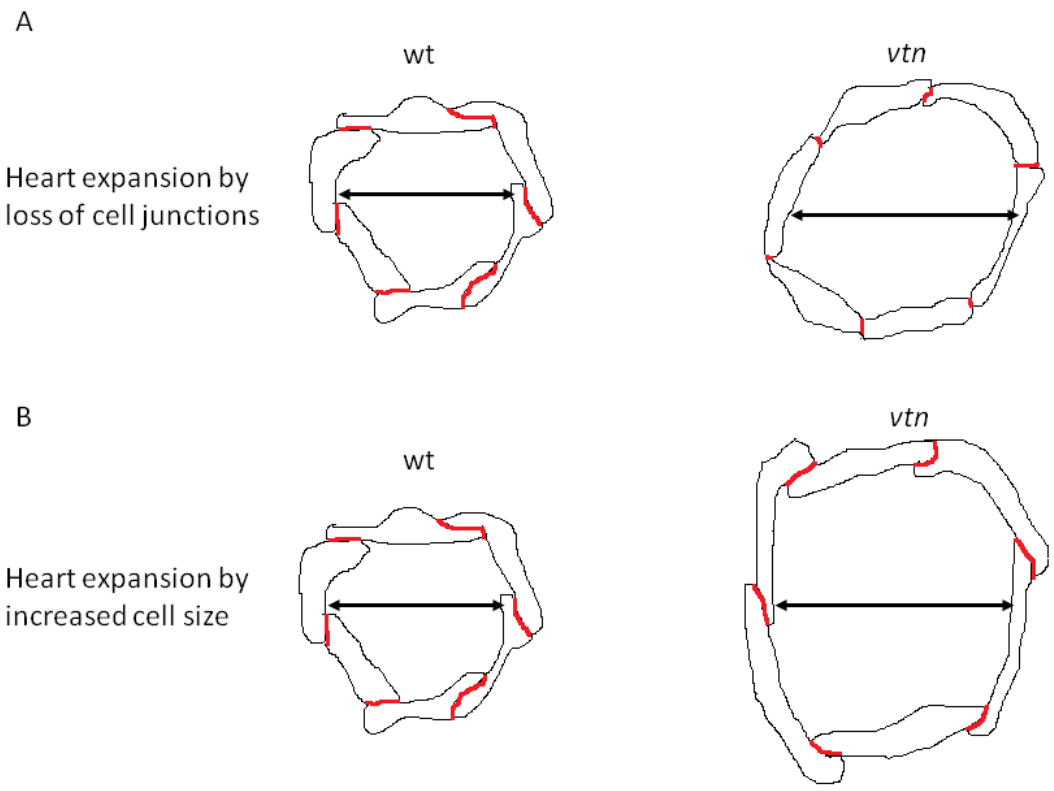

Figure 1.3. Two models for the enlargement of heart chambers in Heg-CCM pathway mutants. (A) *vtn* mutants have reduced areas of overlap between adjoining endocardial cells (Kleaveland et al., 2009). Even if endocardial cells are the same size in *vtn* mutants, this reduction in overlap would cause an expansion of the heart chamber's surface area. (B) An increase in endocardial cell size in Heg-CCM pathway mutants could also contribute to an increase in heart chamber size. Cell-cell interfaces are marked in red. Arrows show lumen diameter. For clarity, myocardium is not pictured.

In addition to altered cell junctions, changes in cell shape and size may also contribute to cardiovascular defects in *san*, *vtn*, and *heg* mutants (Figure 1.3B). Cell shape has been examined in detail in the PCV in zebrafish, and it was found that wildtype endothelial cells in this tissue have an elongated morphology, whereas *san* mutant endothelial cells are rounder and spread out with more surface area; furthermore, zebrafish transplantation experiments showed that this function of *ccm1* in controlling cell shape is cell autonomous. In this study, surprisingly, no differences in cell junctions were detected between wildtype and *san* embryos (Hogan et al.,

2008). Clearly, more research will be required to ascertain how cell junctions, cell shape, and possibly other factors contribute to the morphological defects observed in mutants of the Heg-CCM pathway.

In addition to the p38 stress response pathway and RhoA signaling, several other pathways have been shown to be affected by loss or gain of Heg-CCM gene activity. For example, one study shows that overexpression of *CCM1* in human umbilical vein endothelial cells (HUVECs) reduces activation of ERK and increases activation of AKT and Notch (Wustehube et al., 2010). (We explore the relationship between ERK and the Heg-CCM pathway in Chapter 4 of this dissertation.) Another study shows that loss of Ccm2 leads to hyperactivation of the c-Jun NH2-terminal protein kinase (JNK) pathway (Whitehead et al., 2009). Given the number of important pathways affected by manipulation of genes in the Heg-CCM pathway, it may be the case that the cardiovascular defects found in homozygous mutant fish and knockout mice are due not to a single misregulated pathway, but rather to the cumulative effects of many misregulated pathways.

Mutations in *CCM1* and *CCM2* cause cerebral cavernous malformations in humans

The genes *ccm1* and *ccm2* owe their names to the finding that mutations in their human orthologs cause vascular pathologies known as cerebral cavernous malformations (CCMs). CCMs are dilations of the vascular endothelium of the brain. Histologically, CCM lesions have a thin-walled endothelial lining and lack smooth muscle and elastic tissue. While some CCM lesions are asymptomatic, others cause devastating symptoms including severe headaches, seizures, focal neurological deficits, and even death. Typically, CCM patients first present as

adults. CCMs can be either familial or sporadic and affect approximately 0.5% of the population (Cavalcanti et al., 2012). Mutations in three genes have been shown to cause CCM disease: *CCM1* (Laberge-le Couteulx et al., 1999; Sahoo et al., 1999), *CCM2* (Denier et al., 2004; Liquori et al., 2003), and *CCM3* (Bergametti et al., 2005). The majority of CCM patients have mutations in *CCM1*; one study found that in a cohort of patients, 53% had mutations in *CCM1*, 15% had mutations in *CCM2*, and 10% had mutations in *CCM3* (Denier et al., 2006). For all three genes, inheritance of the disease follows an autosomal dominant pattern.

It is thought that familial CCM disease is caused by loss-of-function of the genes *CCM1-3*. Evidence for this hypothesis includes the finding that the majority of mutant alleles for all three genes contain premature stop codons, which can lead to either nonsense mediated decay of the mRNA or a truncated protein (Cave-Riant et al., 2002). Additionally, immunohistochemistry shows that each CCM protein is undetectable in the lesions of patients bearing mutations in that gene; for example, in a patient heterozygous for a mutant *CCM1* allele, CCM1 protein is detectable in normal tissue but not in the CCM lesion (Pagenstecher et al., 2009). Presumably, the extreme reduction or complete absence of the protein causes a loss-of-function phenotype.

Why do patients with germline mutations in *CCM1-3* develop CCM disease relatively late in life? And why, if all the cells in the body harbor the germline mutation, is CCM disease focal in nature? To answer these questions, many in the field have proposed that CCM disease is caused by a 2-hit mechanism, much like cancer. In this model, an individual who has a germline mutation in, for example, *CCM1*, will develop a CCM lesion if she acquires a somatic mutation in the other *CCM1* allele in a brain endothelial cell. As evidence for this model, sequencing of surgically resected CCM lesions from patients heterozygous for any of the three CCM-causing genes reveals biallelic mutations in that gene. Although biallelic mutations could not be detected

in every lesion, perhaps for technical reasons, the existence of biallelic mutations in even some lesions argues strongly for a two-hit model (Akers et al., 2009; Gault et al., 2009; Gault et al., 2005). In a variation of the classical two-hit model, it has also been proposed that the second hit could be environmental rather than genetic; for example, a vessel sensitized by one loss-of-function allele of a CCM gene could become leaky in response to repeated assault by cytokines (Whitehead et al., 2009).

Mouse models have provided some support for the two-hit model of CCM disease. *Ccm1*$^{+/-}$ and *Ccm2*$^{+/-}$ mice do not develop CCMs. However, this does not discount the two-hit model because the mice may simply not be long-lived enough to acquire the second mutation. (In humans, CCMs may take decades to develop.) To accelerate the rate of mutation, one disease model uses mice heterozygous for *Ccm1* and homozygous mutant for the mismatch repair component *MutS homolog 2* (*Msh2*). Interesting, approximately half of the *Ccm1*$^{+/-}$;*Msh2*$^{-/-}$ mice developed lesions in the central nervous system with histological similarity to human CCM lesions. For technical reasons, these lesions could not be sequenced to confirm a second mutation; however, Ccm1 protein is absent in a mosaic fashion, consistent with the conclusion that a somatic mutation inactivates the second allele of *Ccm1*. Mysteriously, in the same study, it was found that *Ccm2*$^{+/-}$;*Msh2*$^{-/-}$ mice do not develop CCMs (McDonald et al., 2011). Regardless, administration of the ROCK inhibitor Fasudil decreases the CCM lesion burden in *Ccm1*$^{+/-}$;*Msh2*$^{-/-}$ mice, demonstrating that the lesions that develop in this model fit with the data gathered from other studies of *Ccm1* and *Ccm2* heterozygotes and endothelial cell culture experiments. Excitingly, this study suggests that RhoA pathway inhibitors may be useful in treating human CCM patients (McDonald et al., 2012).

The function of Ccm3 is mysterious

Unlike other signaling pathways that have been studied extensively, the Heg-CCM pathway was discovered only recently and as a result remains mysterious in many ways. Questions abound as to the structure and function of this pathway. One particularly challenging problem in the field is the role of *CCM3*. There is evidence to suggest that *CCM3* functions in the same pathway as *CCM1* and *CCM2*. First, mutations in *CCM3* cause CCMs in humans (Bergametti et al., 2005). Second, in overexpression studies, CCM2 binds CCM3 (Hilder et al., 2007; Li et al., 2010; Voss et al., 2007; Zheng et al., 2010). Third, knockdown of *CCM3* in endothelial cell culture has been reported to cause an increase in RHOA activation (Borikova et al., 2010; Zheng et al., 2010). Fourth, inactivation of the two zebrafish *CCM3* paralogs, *ccm3a* and *ccm3b*, has been reported by two groups to confer a dilated heart phenotype (Voss et al., 2009; Zheng et al., 2010).

Recent studies, however, suggest that the relationship between *CCM3* and *CCM1/2* is more complicated. In one report, *Ccm2* and *Ccm3* were each knocked out of the adult mouse endothelium, and both knockouts exhibited similar CCM pathology. However, the same report found that the embryonic phenotypes caused by endothelial-specific deletion of *Ccm2* or *Ccm3* are quite distinct. These researchers also found that RhoA activation in endothelial cell culture is *not* increased by *Ccm3* knockdown, leading them to conclude that loss of *Ccm2* and *Ccm3* cause CCM disease by different mechanisms (Chan et al., 2011). In the same vein, a recent study by a different group reexamined the embryonic heart phenotype conferred by knockdown of *ccm3a/b* in zebrafish. They found that, contrary to previous reports, *ccm3a/b* morphants have pericardial edema but no enlargement of the heart chambers, unlike *san* and *vtn* mutants, which have

enormous hearts (Yoruk et al., 2012). These findings are consistent with observations previously made in our laboratory (personal communication, JDM). Moreover, *ccm3a/b* morphants exhibit an extreme dilation of cranial vessels, while *san* and *vtn* mutants do not, suggesting that *ccm3a/b* functions in a different pathway from *ccm1* and *ccm2* in zebrafish brain vasculature as well as in the heart (Yoruk et al., 2012). Clearly defining the function of Ccm3 in development and disease will be an interesting and important challenge for the community of CCM researchers in the coming years.

Zebrafish as a model to validate novel Heg-CCM pathway genes

Since loss of components of the Heg-CCM pathway causes CCM disease in humans and embryonic heart defects in zebrafish, we have considered the strengths and weaknesses of the embryonic heart as a model for understanding CCM disease. The main disadvantage of the zebrafish heart model as a means of understanding human disease is that a key aspect of cell biology is different in the two systems: *san* and *vtn* mutants have normal numbers of endothelial cells in the heart (Mably et al., 2006), while human CCMs exhibit endothelial hyperproliferation. An illustration of this disadvantage is provided by a study finding that CCM1-depleted HUVECs xenografted into mice develop CCM-like pathology, and that administration of the multiple kinase inhibitor Sorafenib could suppress the overproliferation of these cells (Wustehube et al., 2010). The zebrafish heart would not be a useful system for testing this sort of therapeutic. However, other aspects of cell biology are conserved between *san* and *vtn* hearts and human CCMs, such as the reduction in endothelial cell junctions (Kleaveland et al., 2009; Wong et al., 2000). The similarities and differences between the Heg-CCM mutant zebrafish hearts and

human CCMs are summarized in Table 1.2. Given the commonalities between the systems, we believe the mutant zebrafish heart has promise as a CCM model.

Table 1.2. A comparison of the genetics and phenotypes of the dilated zebrafish heart and human CCMs.

	Zebrafish dilated heart	**Human CCM**
Genes	*heg, ccm1, ccm2, ccm3a/b*(?)	*CCM1, CCM2, CCM3*
Inheritance	Recessive	Dominant
Tissue affected	Heart endothelium (endocardium)	Predominantly brain endothelium
Histological phenotype	Severe dilation	Severe dilation
Cell biological phenotypes	Reduced tight junctions	Reduced tight junctions, over proliferation

Why do *san* and *vtn* mutant embryos develop fatal heart defects, while patients with mutations in *CCM1* and *CCM2* develop lesions in their brain vasculature but maintain healthy hearts? This is almost certainly due not to differences between species, but to the disparate effects of homozygous and heterozygous genotypes. The *san* and *vtn* zebrafish mutants with massively dilated hearts are homozygous mutant, whereas human CCM patients are heterozygotes. Since complete loss of *Ccm1* or *Ccm2* causes embryonic lethality in mouse due to defective cardiovascular development (Boulday et al., 2009; Whitehead et al., 2009; Whitehead et al., 2004), it stands to reason that any humans homozygous for mutations in either

gene would probably die *in utero* from cardiovascular defects as well. No CCM-like lesions have been detected in the brains of heterozygous zebrafish adults (personal communication, JDM); however, since it takes most humans decades to develop CCM disease, it might be that the zebrafish is simply not long-lived enough to acquire the disease, even though the Heg-CCM pathway functions similarly in the two species.

Our comprehension of the Heg-CCM pathway in development and disease is limited not only by our lack of understanding about the interactions among the Heg-CCM genes, but also by the small number of genes known to participate in the pathway. The latter point is highlighted by a human genetics study in which DNA sequencing was performed on patients with either familial or sporadic CCM disease. The researchers found that 94% of familial cases and 57% of sporadic cases of CCMs could be explained by mutations in *CCM1-3* (Denier et al., 2006). Thus, while most familial CCM cases are attributable to mutations in known CCM-causing genes, nearly half of all sporadic CCM cases are of unknown etiology. It is very likely that the disease in these patients also has a genetic basis, and it is of great interest to identify candidate genes whose mutation could cause CCMs or enhance the pathology of CCMs caused by other factors.

The zebrafish embryo is ideal for testing candidate CCM genes. Any candidate genes can be rapidly knocked down by morpholino microinjection in large numbers of embryos, and the other embryological and genetic tools available in zebrafish can be used to analyze the relationship between the candidate gene and the known genes in the pathway. The typical Heg-CCM mutant phenotype—enlarged heart chambers, enlarged inflow tract, and lack of blood circulation—can be easily detected by low power light microscopy just two days after

fertilization. Any genes shown to interact with the Heg-CCM pathway in the zebrafish heart model would be intriguing candidates to investigate for roles in human CCM disease.

ccm2-like

One method we used to identify genes with potential roles in the Heg-CCM pathway was to query the Ensembl database using BLASTp and BLASTx algorithms for proteins bearing identity to the known Heg-CCM components. Our reasoning was that Ccm1, Ccm2, and Heg paralogs encoded by the zebrafish genome might also participate in the Heg-CCM pathway owing to their structural similarity to known Heg-CCM proteins. We identified a novel protein, which we named Ccm2-like (Ccm2l), that has high identity to Ccm2. In Chapter 2 of this dissertation, we present data that argue for a function for Ccm2l in the Heg-CCM pathway. While the relevant experiments were being performed, the function of *ccm2l* had not been analyzed in any species. While this dissertation was in preparation, however, a study of the function of *Ccm2l* in mouse was published (Zheng et al., 2012). Here I provide a summary of their findings without reference to our work. In the Discussion section of Chapter 2, I analyze the similarities and differences between the findings of Zheng *et al.* in mouse and ours in zebrafish.

Mouse *Ccm2-like* (*Ccm2l*) was identified by querying the EST and Ensemble databases with the *Ccm2* sequence. Although *Ccm2l* is expressed in a subset of endothelial cells, including those in the heart, *Ccm2l* knockout mice lack overt cardiovascular defects; they survive to adulthood and are apparently normal. Interestingly, $Ccm2l^{-/-};Heg1^{-/-}$ mice suffer embryonic lethality due to severe heart defects; these double mutants exhibit an unusually thin myocardium,

reduced ventricular trabeculation, and dilated atria. *Heg1*$^{-/-}$ null embryos often survive through embryonic development but die postnatally from similar cardiac defects. Thus, complete loss of *Ccm2l* produces no phenotype by itself, but can enhance the heart defects in *Heg1*$^{-/-}$ mice. The authors conclude that *Heg1* and *Ccm2l* function together in a pathway (Zheng et al., 2012).

Interestingly, *Ccm2l*$^{-/-}$*;Heg1*$^{-/-}$ heart defects can be rescued by loss of one *Ccm2* allele; 50% of *Ccm2l*$^{-/-}$*;Heg1*$^{-/-}$*;Ccm2*$^{+/-}$ mice survive through embryonic development, whereas *Ccm2l*$^{-/-}$*;Heg1*$^{-/-}$*;Ccm2*$^{+/+}$ mice never do. Moreover, branchial arch defects in *Ccm2*$^{+/-}$; *Heg1*$^{-/-}$ can be suppressed by loss of both alleles of *Ccm2l*. The authors propose that *Ccm2* and *Ccm2l* oppose each other in cardiovascular development (Zheng et al., 2012).

The notion of competition between Ccm2 and Ccm2l is also supported by cell culture data. Like Ccm2, Ccm2l has a PTB domain through which it binds Ccm1. In overexpression assays, Ccm2 and Ccm2l compete for binding to Ccm1. Forced expression of *Ccm2l* in endothelial cells causes an increase in activated RhoA and a decrease in monolayer permeability, consistent with disruption of Ccm1-Ccm2 binding. Unlike Ccm2, Ccm2l cannot bind Ccm3, and the authors believe this difference explains the disparate effects of Ccm2 and Ccm2l on RhoA activation and the concomitant mouse endothelial phenotypes (Zheng et al., 2012).

In the model proposed by Zheng *et al*., competition in the endothelium between Ccm2 and Ccm2l for binding to the Heg-Ccm1 complex regulates cardiovascular development. When Ccm2 binds the Heg-Ccm1 complex, RhoA signaling is suppressed and vascular stability is achieved through the maintenance of cell junctions. However, when Ccm2l binds the Heg-Ccm1 complex, a program for vascular growth is induced, and in the endocardium, growth factors that promote myocardial proliferation are released. Their model explains why loss of *Heg1* enhances both the branchial arch defects in *Ccm2*$^{+/-}$ embryos (failure to lumenize due to defective cell

junctions) and the heart defects in *Ccm2l*$^{-/-}$ embryos (insufficient myocardial growth), and why both of those phenotypes can be partially rescued by a reduction in gene dosage of the other paralog (Zheng et al., 2012).

This work

The experiments presented herein are a study of the structure and function of the Heg-CCM pathway. First, we study the Heg protein, and investigate its post-translational processing in cell culture and perform a yeast 2-hybrid screen to identify proteins that interact with its intracellular domain. We find that zebrafish Heg and Ccm1 proteins interact. Second, we use the zebrafish model to analyze the function of *ccm2l*. We conclude that *ccm2l* is required for normal heart development to occur and that *ccm2l* and *ccm2* have partially overlapping functions. Finally, we investigate the relationship between the Heg-CCM pathway and the ERK signaling system in cell culture and the zebrafish heart. We present evidence that the Erk pathway functions downstream of or parallel to the Heg-CCM pathway in regulating the size of the heart. These studies elucidate the function of the Heg-CCM pathway in regulating heart development, and it is our hope that they may provide insights into human CCM disease.

Works cited

Akers, A.L., Johnson, E., Steinberg, G.K., Zabramski, J.M., Marchuk, D.A., 2009. Biallelic somatic and germline mutations in cerebral cavernous malformations (CCMs): evidence for a two-hit mechanism of CCM pathogenesis. Hum Mol Genet 18, 919-930.

Bergametti, F., Denier, C., Labauge, P., Arnoult, M., Boetto, S., Clanet, M., Coubes, P., Echenne, B., Ibrahim, R., Irthum, B., Jacquet, G., Lonjon, M., Moreau, J.J., Neau, J.P., Parker, F., Tremoulet, M., Tournier-Lasserve, E., 2005. Mutations within the programmed cell death 10 gene cause cerebral cavernous malformations. American journal of human genetics 76, 42-51.

Borikova, A.L., Dibble, C.F., Sciaky, N., Welch, C.M., Abell, A.N., Bencharit, S., Johnson, G.L., 2010. Rho kinase inhibition rescues the endothelial cell cerebral cavernous malformation phenotype. The Journal of biological chemistry 285, 11760-11764.

Boulday, G., Blecon, A., Petit, N., Chareyre, F., Garcia, L.A., Niwa-Kawakita, M., Giovannini, M., Tournier-Lasserve, E., 2009. Tissue-specific conditional CCM2 knockout mice establish the essential role of endothelial CCM2 in angiogenesis: implications for human cerebral cavernous malformations. Dis Model Mech 2, 168-177.

Cavalcanti, D.D., Kalani, M.Y., Martirosyan, N.L., Eales, J., Spetzler, R.F., Preul, M.C., 2012. Cerebral cavernous malformations: from genes to proteins to disease. J Neurosurg 116, 122-132.

Cave-Riant, F., Denier, C., Labauge, P., Cecillon, M., Maciazek, J., Joutel, A., Laberge-Le Couteulx, S., Tournier-Lasserve, E., 2002. Spectrum and expression analysis of KRIT1 mutations in 121 consecutive and unrelated patients with Cerebral Cavernous Malformations. Eur J Hum Genet 10, 733-740.

Chan, A.C., Drakos, S.G., Ruiz, O.E., Smith, A.C., Gibson, C.C., Ling, J., Passi, S.F., Stratman, A.N., Sacharidou, A., Revelo, M.P., Grossmann, A.H., Diakos, N.A., Davis, G.E., Metzstein, M.M., Whitehead, K.J., Li, D.Y., 2011. Mutations in 2 distinct genetic pathways result in cerebral cavernous malformations in mice. The Journal of clinical investigation 121, 1871-1881.

Crose, L.E., Hilder, T.L., Sciaky, N., Johnson, G.L., 2009. Cerebral cavernous malformation 2 protein promotes smad ubiquitin regulatory factor 1-mediated RhoA degradation in endothelial cells. The Journal of biological chemistry 284, 13301-13305.

Denier, C., Goutagny, S., Labauge, P., Krivosic, V., Arnoult, M., Cousin, A., Benabid, A.L., Comoy, J., Frerebeau, P., Gilbert, B., Houtteville, J.P., Jan, M., Lapierre, F., Loiseau, H., Menei, P., Mercier, P., Moreau, J.J., Nivelon-Chevallier, A., Parker, F., Redondo, A.M., Scarabin, J.M., Tremoulet, M., Zerah, M., Maciazek, J., Tournier-Lasserve, E., 2004. Mutations within the MGC4607 gene cause cerebral cavernous malformations. American journal of human genetics 74, 326-337.

Denier, C., Labauge, P., Bergametti, F., Marchelli, F., Riant, F., Arnoult, M., Maciazek, J., Vicaut, E., Brunereau, L., Tournier-Lasserve, E., 2006. Genotype-phenotype correlations in cerebral cavernous malformations patients. Ann Neurol 60, 550-556.

Gault, J., Awad, I.A., Recksiek, P., Shenkar, R., Breeze, R., Handler, M., Kleinschmidt-DeMasters, B.K., 2009. Cerebral cavernous malformations: somatic mutations in vascular endothelial cells. Neurosurgery 65, 138-144; discussion 144-135.

Gault, J., Shenkar, R., Recksiek, P., Awad, I.A., 2005. Biallelic somatic and germ line CCM1 truncating mutations in a cerebral cavernous malformation lesion. Stroke 36, 872-874.

Gingras, A.R., Liu, J.J., Ginsberg, M.H., 2012. Structural basis of the junctional anchorage of the cerebral cavernous malformations complex. The Journal of cell biology 199, 39-48.

Glading, A., Han, J., Stockton, R.A., Ginsberg, M.H., 2007. KRIT-1/CCM1 is a Rap1 effector that regulates endothelial cell cell junctions. The Journal of cell biology 179, 247-254.

Hilder, T.L., Malone, M.H., Bencharit, S., Colicelli, J., Haystead, T.A., Johnson, G.L., Wu, C.C., 2007. Proteomic identification of the cerebral cavernous malformation signaling complex. J Proteome Res 6, 4343-4355.

Hogan, B.M., Bussmann, J., Wolburg, H., Schulte-Merker, S., 2008. ccm1 cell autonomously regulates endothelial cellular morphogenesis and vascular tubulogenesis in zebrafish. Hum Mol Genet 17, 2424-2432.

Kim, J., Sherman, N.E., Fox, J.W., Ginsberg, M.H., 2011. Phosphorylation sites in the cerebral cavernous malformations complex. J Cell Sci 124, 3929-3932.

Kleaveland, B., Zheng, X., Liu, J.J., Blum, Y., Tung, J.J., Zou, Z., Sweeney, S.M., Chen, M., Guo, L., Lu, M.M., Zhou, D., Kitajewski, J., Affolter, M., Ginsberg, M.H., Kahn, M.L., 2009. Regulation of cardiovascular development and integrity by the heart of glass-cerebral cavernous malformation protein pathway. Nature medicine 15, 169-176.

Kupperman, E., An, S., Osborne, N., Waldron, S., Stainier, D.Y., 2000. A sphingosine-1-phosphate receptor regulates cell migration during vertebrate heart development. Nature 406, 192-195.

Laberge-le Couteulx, S., Jung, H.H., Labauge, P., Houtteville, J.P., Lescoat, C., Cecillon, M., Marechal, E., Joutel, A., Bach, J.F., Tournier-Lasserve, E., 1999. Truncating mutations in CCM1, encoding KRIT1, cause hereditary cavernous angiomas. Nat Genet 23, 189-193.

Li, X., Zhang, R., Zhang, H., He, Y., Ji, W., Min, W., Boggon, T.J., 2010. Crystal structure of CCM3, a cerebral cavernous malformation protein critical for vascular integrity. The Journal of biological chemistry 285, 24099-24107.

Liquori, C.L., Berg, M.J., Siegel, A.M., Huang, E., Zawistowski, J.S., Stoffer, T., Verlaan, D., Balogun, F., Hughes, L., Leedom, T.P., Plummer, N.W., Cannella, M., Maglione, V., Squitieri, F., Johnson, E.W., Rouleau, G.A., Ptacek, L., Marchuk, D.A., 2003. Mutations in a gene

encoding a novel protein containing a phosphotyrosine-binding domain cause type 2 cerebral cavernous malformations. American journal of human genetics 73, 1459-1464.

Liu, J.J., Stockton, R.A., Gingras, A.R., Ablooglu, A.J., Han, J., Bobkov, A.A., Ginsberg, M.H., 2011. A mechanism of Rap1-induced stabilization of endothelial cell--cell junctions. Mol Biol Cell 22, 2509-2519.

Mably, J.D., Chuang, L.P., Serluca, F.C., Mohideen, M.A., Chen, J.N., Fishman, M.C., 2006. santa and valentine pattern concentric growth of cardiac myocardium in the zebrafish. Development (Cambridge, England) 133, 3139-3146.

Mably, J.D., Mohideen, M.A., Burns, C.G., Chen, J.N., Fishman, M.C., 2003. heart of glass regulates the concentric growth of the heart in zebrafish. Curr Biol 13, 2138-2147.

McDonald, D.A., Shenkar, R., Shi, C., Stockton, R.A., Akers, A.L., Kucherlapati, M.H., Kucherlapati, R., Brainer, J., Ginsberg, M.H., Awad, I.A., Marchuk, D.A., 2011. A novel mouse model of cerebral cavernous malformations based on the two-hit mutation hypothesis recapitulates the human disease. Hum Mol Genet 20, 211-222.

McDonald, D.A., Shi, C., Shenkar, R., Stockton, R.A., Liu, F., Ginsberg, M.H., Marchuk, D.A., Awad, I.A., 2012. Fasudil decreases lesion burden in a murine model of cerebral cavernous malformation disease. Stroke 43, 571-574.

Pagenstecher, A., Stahl, S., Sure, U., Felbor, U., 2009. A two-hit mechanism causes cerebral cavernous malformations: complete inactivation of CCM1, CCM2 or CCM3 in affected endothelial cells. Hum Mol Genet 18, 911-918.

Sahoo, T., Johnson, E.W., Thomas, J.W., Kuehl, P.M., Jones, T.L., Dokken, C.G., Touchman, J.W., Gallione, C.J., Lee-Lin, S.Q., Kosofsky, B., Kurth, J.H., Louis, D.N., Mettler, G., Morrison, L., Gil-Nagel, A., Rich, S.S., Zabramski, J.M., Boguski, M.S., Green, E.D., Marchuk, D.A., 1999. Mutations in the gene encoding KRIT1, a Krev-1/rap1a binding protein, cause cerebral cavernous malformations (CCM1). Hum Mol Genet 8, 2325-2333.

Spindler, V., Schlegel, N., Waschke, J., 2010. Role of GTPases in control of microvascular permeability. Cardiovasc Res 87, 243-253.

Stainier, D.Y., 2001. Zebrafish genetics and vertebrate heart formation. Nat Rev Genet 2, 39-48.

Stockton, R.A., Shenkar, R., Awad, I.A., Ginsberg, M.H., 2010. Cerebral cavernous malformations proteins inhibit Rho kinase to stabilize vascular integrity. J Exp Med 207, 881-896.

Uhlik, M.T., Abell, A.N., Johnson, N.L., Sun, W., Cuevas, B.D., Lobel-Rice, K.E., Horne, E.A., Dell'Acqua, M.L., Johnson, G.L., 2003. Rac-MEKK3-MKK3 scaffolding for p38 MAPK activation during hyperosmotic shock. Nature cell biology 5, 1104-1110.

Voss, K., Stahl, S., Hogan, B.M., Reinders, J., Schleider, E., Schulte-Merker, S., Felbor, U., 2009. Functional analyses of human and zebrafish 18-amino acid in-frame deletion pave the way

for domain mapping of the cerebral cavernous malformation 3 protein. Hum Mutat 30, 1003-1011.

Voss, K., Stahl, S., Schleider, E., Ullrich, S., Nickel, J., Mueller, T.D., Felbor, U., 2007. CCM3 interacts with CCM2 indicating common pathogenesis for cerebral cavernous malformations. Neurogenetics 8, 249-256.

Whitehead, K.J., Chan, A.C., Navankasattusas, S., Koh, W., London, N.R., Ling, J., Mayo, A.H., Drakos, S.G., Jones, C.A., Zhu, W., Marchuk, D.A., Davis, G.E., Li, D.Y., 2009. The cerebral cavernous malformation signaling pathway promotes vascular integrity via Rho GTPases. Nature medicine 15, 177-184.

Whitehead, K.J., Plummer, N.W., Adams, J.A., Marchuk, D.A., Li, D.Y., 2004. Ccm1 is required for arterial morphogenesis: implications for the etiology of human cavernous malformations. Development (Cambridge, England) 131, 1437-1448.

Wong, J.H., Awad, I.A., Kim, J.H., 2000. Ultrastructural pathological features of cerebrovascular malformations: a preliminary report. Neurosurgery 46, 1454-1459.

Wustehube, J., Bartol, A., Liebler, S.S., Brutsch, R., Zhu, Y., Felbor, U., Sure, U., Augustin, H.G., Fischer, A., 2010. Cerebral cavernous malformation protein CCM1 inhibits sprouting angiogenesis by activating DELTA-NOTCH signaling. Proceedings of the National Academy of Sciences of the United States of America 107, 12640-12645.

Yoruk, B., Gillers, B.S., Chi, N.C., Scott, I.C., 2012. Ccm3 functions in a manner distinct from Ccm1 and Ccm2 in a zebrafish model of CCM vascular disease. Dev Biol 362, 121-131.

Zawistowski, J.S., Stalheim, L., Uhlik, M.T., Abell, A.N., Ancrile, B.B., Johnson, G.L., Marchuk, D.A., 2005. CCM1 and CCM2 protein interactions in cell signaling: implications for cerebral cavernous malformations pathogenesis. Hum Mol Genet 14, 2521-2531.

Zhang, J., Rigamonti, D., Dietz, H.C., Clatterbuck, R.E., 2007. Interaction between krit1 and malcavernin: implications for the pathogenesis of cerebral cavernous malformations. Neurosurgery 60, 353-359; discussion 359.

Zheng, X., Xu, C., Di Lorenzo, A., Kleaveland, B., Zou, Z., Seiler, C., Chen, M., Cheng, L., Xiao, J., He, J., Pack, M.A., Sessa, W.C., Kahn, M.L., 2010. CCM3 signaling through sterile 20-like kinases plays an essential role during zebrafish cardiovascular development and cerebral cavernous malformations. The Journal of clinical investigation 120, 2795-2804.

Zheng, X., Xu, C., Smith, A.O., Stratman, A.N., Zou, Z., Kleaveland, B., Yuan, L., Didiku, C., Sen, A., Liu, X., Skuli, N., Zaslavsky, A., Chen, M., Cheng, L., Davis, G.E., Kahn, M.L., 2012. Dynamic regulation of the cerebral cavernous malformation pathway controls vascular stability and growth. Dev Cell 23, 342-355.

Chapter 2: Molecular analysis of Heg

Attributions

The overall experimental design for the project described in this chapter was a collaboration between Jonathan Rosen and John Mably, and all experiments were performed by Jonathan Rosen, with the exception of the bioinformatics related to the yeast 2-hybrid screen, which were performed by John Mably. Grigory Krapavinsky contributed the idea of validating yeast 2-hybrid hits by performing co-immunoprecipitations with *in vitro* translated proteins, and he also shared the relevant protocol. Various reagents were kind gifts from colleagues, as noted in Materials and Methods. Some of the text in Materials and Methods is modified from our submitted (with revisions) manuscript "*ccm2-like* is required for cardiovascular development as a novel component of the Heg-CCM pathway," in review at the time of the writing of this dissertation.

Introduction

In zebrafish, the *heart of glass* (*heg*), *santa* (*san*), and *valentine* (*vtn)* mutants—which have mutations in the genes *heg*, *cerebral cavernous malformation 1* (*ccm1*), and *cerebral cavernous malformation 2* (*ccm2*), respectively— exhibit a dramatic dilation of the embryonic heart chambers and a loss of blood circulation. The near-identical nature of the heart phenotype in the three mutants immediately suggests the possibility that the three genes operate in a common pathway. This conjecture was confirmed by morpholino coinjection experiments showing that each gene genetically interacts with the other two (Mably et al., 2006; Mably et al., 2003). *heg*, *ccm1*, and *ccm2* function as core components of the Heg-CCM pathway.

The Heg-CCM pathway is also required for cardiovascular development in mouse (Boulday et al., 2009; Kleaveland et al., 2009; Whitehead et al., 2009; Whitehead et al., 2004). Selective deletion of *Ccm2* from the developing endothelium recapitulates the whole-organism knockout phenotype, implying that the Heg-CCM pathway regulates cardiovascular development through its activity in that tissue (Boulday et al., 2009; Whitehead et al., 2009). This is likely also true in zebrafish, as *heg* is detectable in the heart's endocardium (Mably et al., 2003) and *ccm1* has been shown to have cell-autonomous functions in the posterior cardinal vein (PCV), an extra-cardiac endothelial vessel (Hogan et al., 2008).

The cellular functions of *ccm1* and *ccm2* have been investigated in considerable depth. Both genes encode cytoplasmic proteins. Ccm1 contains ankyrin repeats, a 4.1/ezrin/radixin/moesin (FERM) domain and three NPXY/F motifs. Ccm2 contains a PTB domain. Ccm1 and Ccm2 bind in an interaction that requires the NPXY/F motifs of Ccm1 and the PTB domain of Ccm2 (Zawistowski et al., 2005; Zhang et al., 2007). In endothelial cell

culture, CCM1 and CCM2 localize to endothelial cell junctions (Glading et al., 2007; Stockton et al., 2010), a finding that correlates with the defects in junctional integrity observed in both cell culture systems and mice when these proteins are depleted (Glading et al., 2007; Stockton et al., 2010; Whitehead et al., 2009).

In contrast to Ccm1 and Ccm2, little is known about Heg protein. Heg is a single-pass transmembrane protein with a highly conserved intracellular domain and a large extracellular region containing epidermal growth factor (EGF)-like repeats; the extracellular region is predicted to be heavily glycosylated (Mably et al., 2003). Based on what little is known about Heg, it is easy to imagine numerous mutually non-exclusive ways it could function in the cell. Since Ccm1 and Ccm2 localize to the membrane, it could serve to recruit or anchor them there. One can also imagine it serving as a signaling receptor, transducing signals into the cell upon binding to an unidentified extracellular ligand. The reverse is equally plausible, as Heg could act as a ligand by binding signaling receptors on adjacent cells. (In zebrafish *heg* mutants, the myocardium remains a single-cell layer instead of thickening as in wildtype embryos, and it is interesting to speculate that Heg might directly signal to the myocardium to regulate myocardial growth.) Alternatively, Heg could function as a junctional protein whose extracellular domain binds the extracellular domains of other transmembrane proteins on nearby cells to promote proper tissue architecture.

To begin to distinguish among these possibilities, we performed a yeast 2-hybrid screen, the analysis of which comprises the majority of this chapter. We reasoned that the identification of proteins that bind the intracellular domain of Heg would provide vital clues to its function. While this experiment was in progress, two important reports came out pertaining to the function of Heg. First, it was shown that Heg expression in the endothelium of the embryonic zebrafish

liver regulates the polarity of adjacent hepatocytes, raising the possibility that Heg functions as an endothelial-derived ligand in some contexts (Sakaguchi et al., 2008). Second, it was reported that the mammalian homologs of Heg and Ccm1 interact, and that Heg has a role in regulating endothelial cell junctions in mouse (Kleaveland et al., 2009). Our yeast 2-hybrid screen using zebrafish genes detects an interaction between Heg and Ccm1, demonstrating that this physical interaction is conserved across species and suggesting that other mechanistic aspects of Heg-CCM signaling may be conserved as well.

Materials and methods

Cell culture, immunoprecipitation and western blotting

Human umbilical vein endothelial cells (HUVECs) were maintained in EGM-2 media as per the manufacturer's instructions (Lonza). HUVECs at 60% confluence were transfected with siRNAs at concentrations of 10 nM or 30 nM using Silentfect reagent (Bio-rad) and Opti-mem (Life Sciences). The day after transfection, media was refreshed, and three days after transfection cells were washed in phosphate buffered saline (PBS) and lysed in radioimmunoprecipitation assay (RIPA) buffer with Complete protease inhibitor (Roche) or Trizol (Life Sciences) for generation of protein lysates or isolation of total RNA, respectively. The following silencer select siRNAs (Life Sciences) targeting *HEG1* were used: s33148, s33149, and s33150. Silencer Negative Control siRNA #1 and GAPDH siRNA (Life Sciences) were also used.

293T cells were maintained in Dulbecco's Modified Eagle Medium (DMEM) containing 10% fetal bovine serum. Cells at 80%-100% confluence were transfected using Lipofectamine-2000 reagent essentially as per the manufacturer's instructions (Life Sciences). Two days after

transfection, cells were washed in PBS and lysed in immunoprecipitation buffer (30 mM Tris, 150 mM NaCl, 1% Triton X100, and Complete protease inhibitor (Roche)). Cleared lysates to be used for immunoprecipitation experiments were incubated with antibody-conjugated agarose beads for two hours to overnight; beads were then washed several times in cold immunoprecipitation buffer. Agarose beads pre-conjugated to the following antibodies were used: anti-FLAG (Sigma), anti-Myc (Clontech), anti-HA (Roche).

HUVEC and 293T cell protein samples were diluted in NuPAGE LDS sample buffer (Life Technologies) containing DTT (final concentration 50 μM), incubated at 80°C for ten minutes, and electrophoresed on a precast acrylamide gel (Life Technologies) at 200 V. Proteins were immobilized on PVDF paper by wet transfer at 33V for 1 to 1.5 hours. PVDF papers were blocked in PBS with 0.1% tween-20 (PBT) containing 5% milk and blotted with the following antibodies in blocking solution for 1 hour at room temperature or overnight at 4 °C: FLAG M2-peroxidase 1:1000 (Sigma), HA-peroxidase 1:1000 (Roche), V5-HRP 1:2500 (Life Sciences), myc-HRP 1:1500 (Roche), Heg antibody HM2148 1:500 (see next paragraph), GAPDH 1:25000 (Millipore). Blots probed with anti-Heg antibody or anti-GAPDH antibody were washed three times and then incubated for one hour with peroxidase-conjugated anti-rabbit or anti-mouse antibodies (GE Healthcare), respectively, in blocking solution at 1:2500. After antibody incubation, blots were washed three times in PBT before developing with SuperSignal West Pico Substrate or SuperSignal West Dura Chemiluminescent Substrates (Thermo Scientific) as per the manufacturer's instructions.

A polyclonal antibody to the C-terminal region of Heg was generated by immunizing rabbits with a synthetic peptide designed from conceptual translation of the open reading frame. For the Heg C-terminal epitope antibody HM2148, the peptide PSFLSDDSRRRDYF was

synthesized, then conjugated at the N-terminus to KLH (Keyhole Limpet Hemocyanin) through a Cys-6-carbon spacer (Princeton Biomolecules). Rabbits were injected with the peptide immunogen using a typical schedule (initial sub-cutaneous injection of 500 µg followed by 5 additional boosts with 250 µg at 21 day intervals; Covance Research). The terminal exsanguination was completed at 118 days after initiation of the protocol and this serum was then affinity purified.

For experiments with lactacystin, chemical was added at a concentration of 10 µM 24 hours after transfection, and lysates were made 12 hours later. For the peptide competition assay, anti-Heg antibody was incubated in PBS with 100 molar excess of either N-terminal Heg peptide or C-terminal peptide prior to western blotting.

Plasmids

The pGBKT7-HegICD yeast 2-hybrid bait vector was generated by performing PCR on a Heg clone template with primers designed to amplify the sequence corresponding to Heg's intracellular domain. The primers contained EcoRI and BamHI restriction sites, and following PCR, the product was digested and ligated into pGBKT7, which had been digested with the same enzymes. The following primers were used: 5'-TTTGAATTCAAAAAAGACAAAAACGAC-3', 5'-TTTGGATCCTCAAAAGTAGTCTCTTCG-3'. pCMV-HA-HegICD was generated by shuttling the insert from pGBKT7 into pCMV-HA using EcoRI and SalI. FLAG-tagged preys to be expressed in 293T cells were excised from the pGADT7 yeast 2-hybrid screening vector with EcoRI and XhoI and ligated into pCMVtag2b. Ccdc80a-FLAG was generated by performing PCR on a *ccdc80a* clone with primers containing HindIII and EcoRI sites and ligating the products into pRK7 modified to contain a C-terminal FLAG tag (donated by Jamie Dempsey and

John Blenis). The following primers were used: 5'-CCCCAAGCTTGCCACCATGAGGGCACGGTATATGCTTGGTTTC-3', 5'-CCCCGAATTCATATCCATAACCCTGATGATA-3'. Full-length zebrafish *heg* was cloned into pCMV-Myc (Clontech) following PCR on a *heg* template (Open Biosystems clone 903796) using forward and reverse primers containing EcoRI and XhoI cut sites, respectively. The following primers were used:
5'-GATCGAATTCAAATGATGGAAACGTGCGCTCG-3',
5'-GATCCTCGAGTCAAAAGTAGTCTCTTCGGCGTG-3'.

FLAG-mheg-V5 was a gift from Mark Kahn. TrpM7 plasmids were a gift from Grigory Krapavinsky

Yeast 2-hybrid Screen

The yeast 2-hybrid screen was performed using the Matchmaker 2-hybrid system, as per the manufacturer's instructions (Clontech). For bait, we subcloned DNA corresponding to the intracellular domain of Heg into pGBKT7 as described above. For preys, we used a library containing inserts isolated from 3 day-old zebrafish hearts cloned into a modified pGADT7-RecAB vector. The library was a generous gift from Geoff Burns. Plasmids were recovered from positive colonies using the Easy Yeast Plasmid Isolation Kit (Clontech).

in vitro *transcription/translation*

in vitro transcription/translation was accomplished using the TNT Quick Coupled Transcription/Translation System (Promega) without radioactivity. Prey plasmids from the screen could be used without further subcloning. Each reaction contained 200 ng of plasmid in a

final volume of 10 µl. Following translation 5 µl of each prey was incubated with 5 µl of Myc-Heg-ICD for 30 minutes, at which point 290 µl immunoprecipitation buffer was added along with myc antibody-conjugated beads. Pulldowns and western blots were performed as described above.

RT-PCR

Quantitative reverse transcription polymerase chain reaction (qRT-PCR) was done with the QuantiFast SYBR Green RT-PCR Kit (Qiagen) as per the manufacturer's instructions on RNA samples extracted with Trizol (Life Sciences). The following primers were used. *GAPDH*: 5'-ATTCCATGGCACCGTCAAGG -3', 5'-GAGGGATCTCGCTCCTGGAA -3', *HEG1*: 5'-ACCACTCCTGCCGAGCATGT-3', 5'-GCGGCTGCGATCACCACAGT-3'.

Zebrafish experiments

Freshly fertilized zebrafish embryos were injected with morpholino as previously described (Rosen et al., 2009). The following morpholinos (Gene Tools) were used.
ccdc80a e3i3: 5'- GTTTTATTGCTAGTGTTACCTTCGC-3',
ccdc80a: e5i5 5'-GTGAACCATCTCTTACCCAGGTTGC-3',
Standard control morpholino: 5'-CCTCTTACCTCAGTTACAATTTATA-3'.

In experiments to characterize the *ccdc80a* knockdown phenotype, we injected 0.5 pMol *ccdc80a* e3i3 or *ccdc80a* e5i5 morpholino. For enhancer experiments, pairwise combinations of morpholino were injected as single solutions. Each 1 nL injection volume contained 0.01 pMol ccm1 MO + 0.2 pMol *ccdc80a* e3i3 MO, 0.01 pMol ccm1 MO + 0.2 pMol standard control MO,

or 0.01 pMol standard control MO + 0.2 pMol *ccdc80a* e3i3 MO. Solutions were blinded to the experimenter prior to injection and revealed after embryos were assayed at 2 dpf.

Microscopy

Live zebrafish embryos were mounted in 4% methyl cellulose on a microscope slide without a coverslip. Images were taken with a Nikon Eclipse 90i microscope equipped with a CoolSNAP HQ2 camera (Photometrics) using NIS-Elements software. Images were then processed in Adobe Photoshop.

Results

The C-terminal end of Heg is cleaved

Endothelial cell culture has been invaluable in dissecting the cellular functions of *ccm1* and *ccm2* in studies such as Glading et al., 2007 and Whitehead et al., 2009. For cell culture experiments studying *heg*, we used primary Human Umbilical Vein Endothelial Cells (HUVECs). First, we determined by RT-PCR that the human homolog of zebrafish *heg*, *HEG1*, is expressed in HUVECs (Figure 2.1A). Next, we tested three siRNAs against *HEG1* in HUVECs and found by quantitative RT-PCR that all three could efficiently knock down *HEG1* transcript (Figure 2.1B).

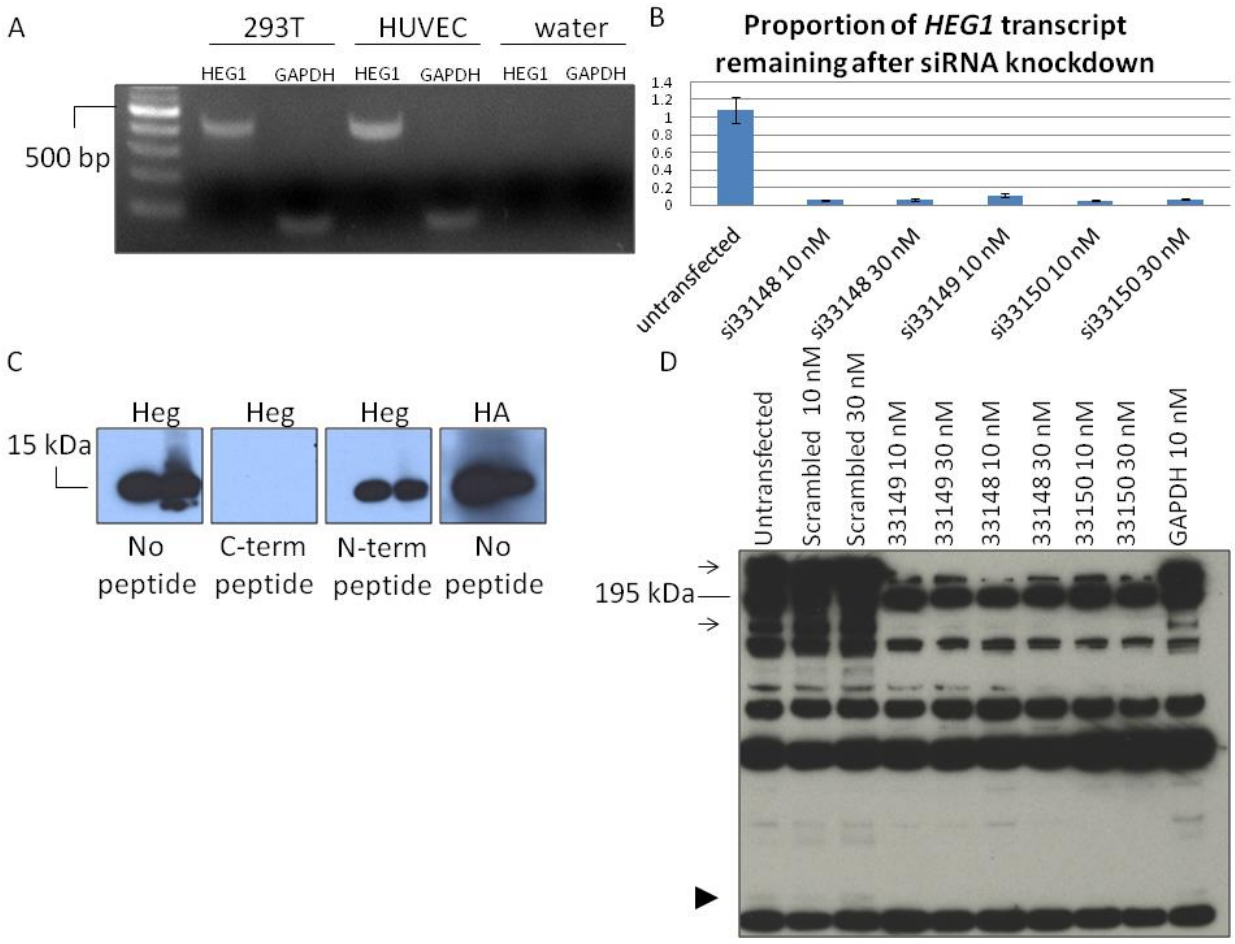

Figure 2.1. Validation of tools for studying Heg in cell culture. (A) RT-PCR detects *HEG1* transcripts in HUVECs as well as 293T cells. Ubiquitously expressed *GAPDH* is a positive control for RNA isolation and RT-PCR methodology, and water is a negative control showing that signal is not the result of contamination. (B) si33148, si33149, and si33150 all efficiently knock down *HEG1* in HUVECs at both 10 nM and 30 nM. Bars represent the ratio of *HEG1* transcript in experimental (or untransfected) samples to *HEG1* transcript in a sample transfected with negative control siRNA, all normalized to *GAPDH* expression levels. Error bars represent the standard error from three technical replicates of the same biological sample. (C) Anti-Heg and anti-HA antibodies detect overexpressed HA-HegICD protein in 293T cell lysates. In each blot, the first lane is protein immunoprecipitated with HA antibody-conjugated beads following overexpression of HA-HegICD and a FLAG-tagged Ccm1 fragment. The second lane is the input from the same sample. **(D)** Anti-Heg antibody detects endogenous HEG1 in HUVEC lysates. Two strong bands (arrows) and a faint band (arrowhead) show Heg protein specifically in samples that were untransfected or transfected with scrambled siRNA or siRNA against *GAPDH*. These bands are absent or drastically reduced in samples transfected with anti-Heg siRNAs 33148, 33149, and 33150, at either 10 nM or 30 nM. There are also several nonspecific bands detected by the antibody.

We then validated a polyclonal antibody, HM2148, generated against a peptide corresponding to the C-terminal (intracellular) region of Heg. First, we confirmed that the anti-Heg antibody could detect a tagged protein corresponding to the intracellular domain of Heg (HA-HegICD) upon overexpression in 293T cells. This interaction could be competed away by addition of C-terminal Heg peptide but not N-terminal Heg peptide (Figure 2.1C). Next, we tested the ability of the anti-Heg antibody to detect endogenous Heg in HUVECs. We found that it detected multiple protein species in lysates made from HUVECs that were untransfected, transfected with a negative control siRNA, or transfected with siRNA against GAPDH. These bands were absent or drastically reduced in lysates made from HUVECs that had been transfected with any of three different anti-Heg siRNAs (Figure 2.1D). The largest Heg-specific band runs at a molecular weight greater than 195 kDa. This is larger than 107 kDa, the expected size of full-length Heg, which suggests that Heg is subject to post-translational modifications. Indeed, based on its amino acid sequence, Heg is predicted to be heavily glycosylated.

Surprisingly, we found that in addition to the large bands presumably corresponding to full-length Heg protein, we were able to faintly detect a specific band between 15 and 20 kDa (barely visible in Figure 2.1D, arrowhead). Two explanations for the presence of this small band are that it represents a cleavage product derived from the mature protein or an isoform translated from an alternatively spliced transcript. To distinguish between these possibilities, we overexpressed a doubly tagged mouse Heg construct, FLAG-mHeg-V5, in 293T cells. Since this construct contains only exonic DNA and hence cannot be spliced, we reasoned that the presence of the small band (detected by anti-V5 antibody) in this lysate would strongly suggest that the small protein species is the result of a cleavage event. We observed the small molecular weight band when blotting with an antibody against the C-terminal V5 tag, but not with an antibody

against the N-terminal FLAG tag (Figure 2.2A). To compare the sizes of the endogenous small Heg product and the overexpressed small Heg product, we ran HUVEC and transfected 293T cell lysates on the same acrylamide gel and observed that the products are nearly the same size (Figure 2.2B). Taken altogether, we conclude that the C-terminal end of Heg is cleaved in endogenous protein in HUVECs and in overexpressed protein in 293T cells. The functional significance of this cleavage event remains mysterious and should be an interesting subject of inquiry in future research.

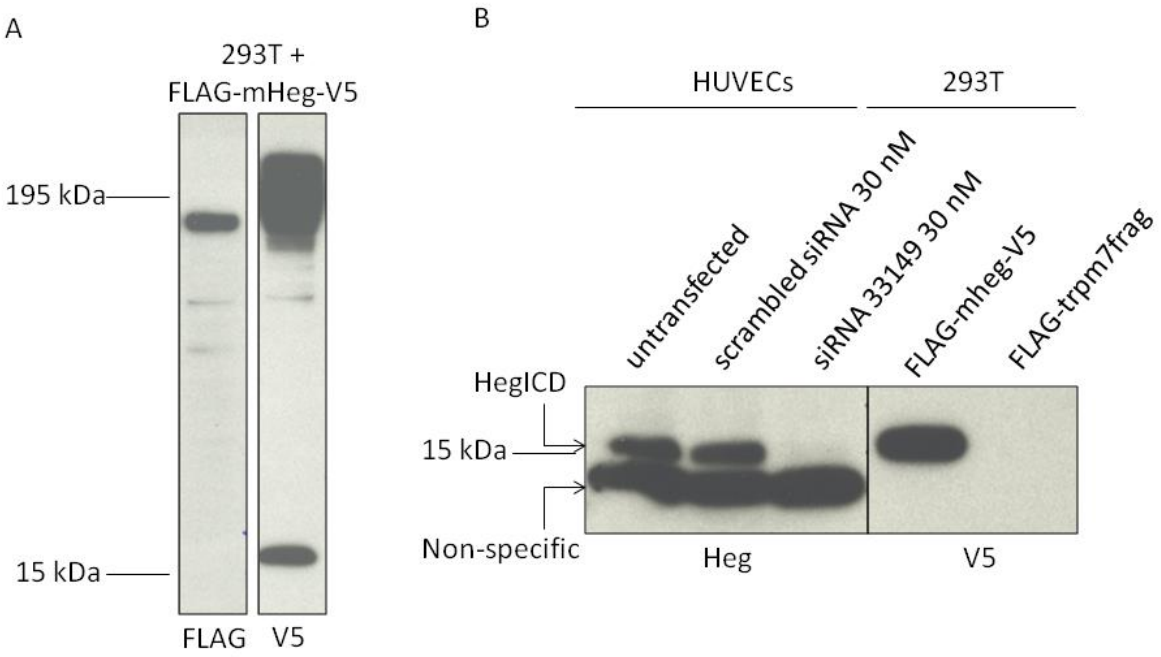

Figure 2.2. The C-terminal end of Heg is cleaved. (A) The C-terminal end of Heg is cleaved when FLAG-mHeg-V5 is overexpressed in 293T cells. Blotting with antibody against FLAG, the N-terminal epitope tag, generates a large band. Blotting with antibody against V5, the C-terminal epitope tag, produces a smear likely corresponding to differentially glycosylated species of full-length Heg, and a much smaller band slightly larger than 15 kDa. (B) The small Heg band present in HUVEC lysates (faintly visible in figure 1D) runs at approximately the same size as the small Heg band in FLAG-mHeg-V5 overexpressing 293T cells. To allow for an accurate comparison of sizes, these samples were all run on the same acrylamide gel. FLAG-TrpM7 frag (fragment) is an irrelevant protein included to show that the V5 signal for FLAG-mHeg-V5 is specific. The anti-Heg antibody also detects a smaller nonspecific band.

Yeast 2-hybird screen identifies an interaction between Heg and Ccm1

To explore the cellular function of Heg protein, we performed a yeast 2-hybrid screen to identify proteins that interact with Heg. As bait, we used a protein in which the binding domain of GAL4 is fused to HegICD. HegICD was used rather than full-length Heg because the yeast 2-hybrid assay requires translocation of proteins to the yeast nucleus, a process that would likely be impeded by the transmembrane domain of full-length Heg. Moreover, HegICD is the most highly conserved part of the protein, suggesting that it may be a particularly important domain within Heg. The prey in the yeast 2-hybrid screen were gene fragments isolated from 3 day-old embryonic zebrafish hearts, fused to the activating domain of GAL4. In response to an interaction between bait and prey, *HIS* and *lacZ* are transcribed (Figure 2.3A). The former allows for selective growth on yeast media lacking histidine, and the latter is used in a follow-up assay in which yeast colonies expressing the *lacZ* reporter turn blue after treatment with 5-bromo-4-chloro-3-indolyl-β-D-galactopyranoside (X-gal).

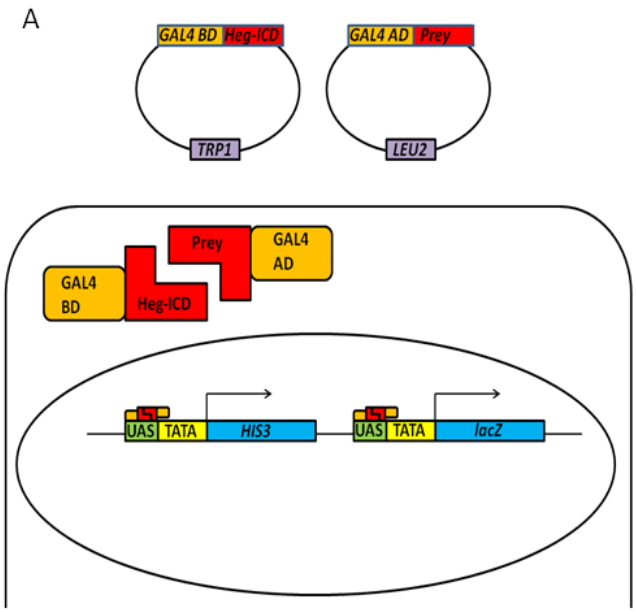

B

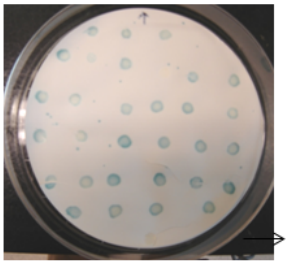

C

Gene	Representative clone	Number of hits	IP with HegICD?
ttna	138	24	N.D.
rnf2	231	12	-
flna-c	132	11	-
col1a	134	10	-
ccm1	256	10	+
cilp	230	8	-
ccdc80a-c	129	6	-
smarcb1a	40	6	-

Figure 2.3. Overview of yeast 2-hybrid screen. (A) Schematic showing yeast 2-hybrid screen. When prey proteins bind HegICD, GAL4-AD and GAL4-BD are brought into contact and transcribe the *HIS* and *LacZ* reporter genes. As a result, only clones expressing preys that interact with HegICD grow on selective media lacking histidine. (B) As a secondary assay for reporter gene activity, clones were grown on filter paper, permeabilized by liquid nitrogen, and subjected to X-gal staining. Formation of a blue product indicates *lacZ* expression. The horizontal arrow indicates a rare negative result in this assay. (C) A table of the most highly represented genes among the recovered yeast 2-hybrid clones.

We screened approximately 740,000 clones and selected 289 colonies that grew on selective media for further analysis. In the first step to validate these clones, they were restreaked on the same selective media and subjected to X-gal staining. 281 of the 289 colonies both regrew and tested positive in the X-gal assay (Figure 2.3B). We attempted to amplify the insert in all 281 colonies by PCR. We sent 254 amplified inserts for sequencing; the remainder either showed no PCR product or multiple PCR products. The insert sequences were arranged into contigs and queried against a reference RNA database using the TBLASTX algorithm to

determine what genes they represented. A complete list of the preliminary yeast 2-hybrid hits is in this dissertation's appendix.

We ranked the yeast 2-hybrid genes by how highly represented they were among the clones recovered from the screen (for top hits, see Figure 2.3C). We followed up several top hits by testing whether they co-immunoprecipitate with HA-HegICD in the 293T cell overexpression system (Figure 2.4A). Our top hit, *titin A* (*ttna*), was excluded from this analysis because of its well understood function in the heart myocardium; *collagen 1a* (*col1a*) was excluded because it was previously found by a colleague in a different yeast 2-hybrid screen to activate reporter gene expression in the absence of bait protein (personal communication, Geoff Burns). We found that only #256 immunoprecipitated with HegICD. #256 represents a fragment of *ccm1*, a known genetic interactor of *heg* (Mably et al., 2006). These results demonstrate that the proteins encoded by these two zebrafish genes can physically interact, and while our research was in progress, this was demonstrated by others for the mammalian orthologs (Kleaveland et al., 2009).

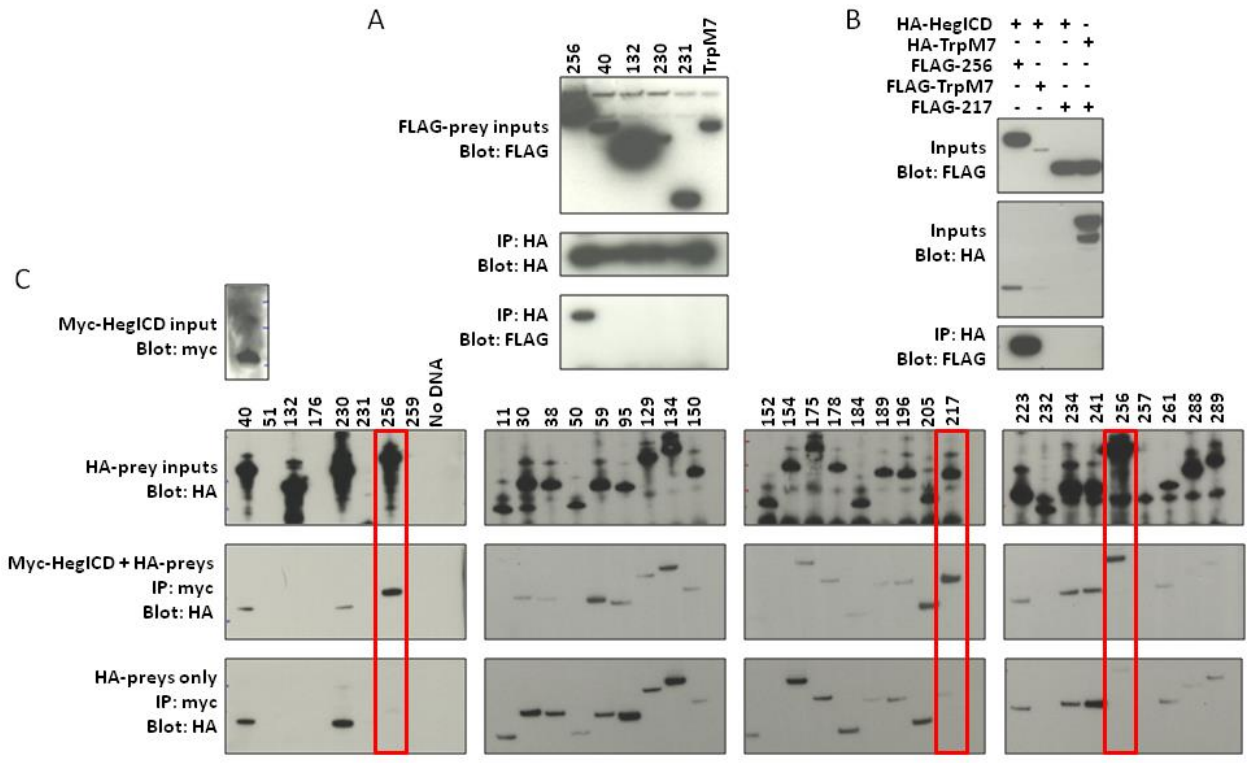

Figure 2.4. Biochemical validation of yeast 2-hybrid hits. (A) Several top yeast 2-hybrid hits, tagged with the FLAG epitope, were cotransfected into 293T cells with HA-HegICD. Only FLAG-256, corresponding to *ccm1*, was co-immunoprecipitated with HA-HegICD by anti-HA conjugated agarose beads. A TrpM7 fragment was included as an irrelevant protein control. (B) In the same assay, FLAG-217, corresponding to *cstf1*, does not bind HA-HegICD. FLAG-256 is a positive control for HegICD interactions, and HA-TrpM7 and FLAG-TrpM7 are irrelevant protein controls for specificity. (C) Thirty-four HA-tagged clones ("preys") recovered from the yeast 2-hybrid screen were transcribed and translated *in vitro* and incubated with Myc-HegICD protein generated in the same fashion. We then immunoprecipitated Myc-HegICD with anti-myc antibody-conjugated beads and blotted pulldowns with anti-HA antibody to determine which preys interact with HegICD. As a control, we simultaneously tested prey proteins (from the same *in vitro* translation reactions) for their ability to bind beads in the absence of Myc-HegICD. Interactors in this assay are defined as proteins that are immunoprecipitated more efficiently in the presence of Myc-HegICD. This assay argues for clones #256 (*ccm1*) and #217 (*cstf1*) being interactors, as shown in red boxes. The left-most column of experiments (myc input blot and pulldowns 40 through NO DNA) were performed on one date and the three rightmost columns (pulldowns 11 through 289) were performed on a later date. Clones tested represent the following genes: 40: *smarcb1a*, 51: *hmcn1*, 132: *flna*, 176: *integral membrane protein*, 230: *cilp*, 231: *rnf2*, 256: *ccm1*, 259: *cyclic nucleotide binding protein*, 11: *smox*, 30: *mapre1b*, 38: *cpt1a*, 50: *sart3*, 59: *aldob*, 95: *ptp4a3*, 129: *ccdc80*, 134: *col1a2*, 150: *aip*, 152: *fbln2*, 154: *pih1d1*, 175: *hbs1l*, 178: *ndufs2*, 184: *smad6*, 189: *cpt1a*, 196: *lox*, 205: *tbxa2r*, 217: *cstf1*, 223: *cdc20*, 232: *postn*, 234: *dhrs4*, 241: *il23r*, 256: *ccm1*, 257: *adam12*, 261: *htra2*, 288: *flnb*, 289: *nid2*.

We then decided to cast a wider net and screen a larger number of initial yeast 2-hybrid hits for physical interactions with HegICD. We generated protein from Myc-HegICD and HA-tagged prey clones by a coupled *in vitro* transcription/translation reaction and then incubated them together and tested which preys were co-immunoprecipitated with Myc-HegICD by anti-myc antibody-conjugated agarose beads (Figure 2.4C). As a negative control, we also tested whether prey proteins could bind directly to the beads in the absence of Myc-HegICD protein. We tested 34 preys in this fashion, including the five hits we had previously tested for interactions with HegICD in 293T cells. We found that 29 preys expressed protein in this assay, and only two preys were more efficiently immunoprecipitated in the presence of Myc-HegICD than by beads alone. These two hits were #256, the fragment of *ccm1*, and #217, a fragment of *cleavage stimulation factor, 3' pre-RNA, subunit 1* (*cstf1*).

While we had previously shown an interaction between clone #256 and HA-HegICD in 293T cell culture (Figure 2.4A), we were unable to identify an interaction between #217 and HA-HegICD in that system (Figure 2.4B). This analysis was complicated by an unusual feature of HA-HegICD protein: we found that following transfection, it is expressed at extremely low levels unless it is co-expressed with Ccm1 protein (Figure 2.5A). Treatment of transfected cells with the proteosome inhibitor lactacystin dramatically increased the level of HegICD protein (Figure 2.5B). These observations together suggest that HegICD is degraded by the proteosome and its interaction with Ccm1 can prevent this degradation. We did not observe this phenomenon with the cleaved Heg product following transfection with full-length Heg (Figure 2.5C), so we believe it is an artifact related to the HegICD construct rather than a biologically meaningful finding. In the context of validating yeast 2-hybrid hits, the proteosomal degradation

of HegICD makes it challenging to interpret immunoprecipitation data, as HegICD is often undetectable in inputs unless Ccm1 is present. Because HegICD is present at such a low level in samples cotransfected with clone #217, we cannot state with confidence that the lack of HegICD immunoprecipitated by #217 means that the two proteins do not bind. However, we think it is likely that if the two proteins did bind, the stability of HegICD would be enhanced, as with HegICD and Ccm1. Regardless, in the absence of convincing data that HegICD binds #217, we chose to discontinue our studies of that clone.

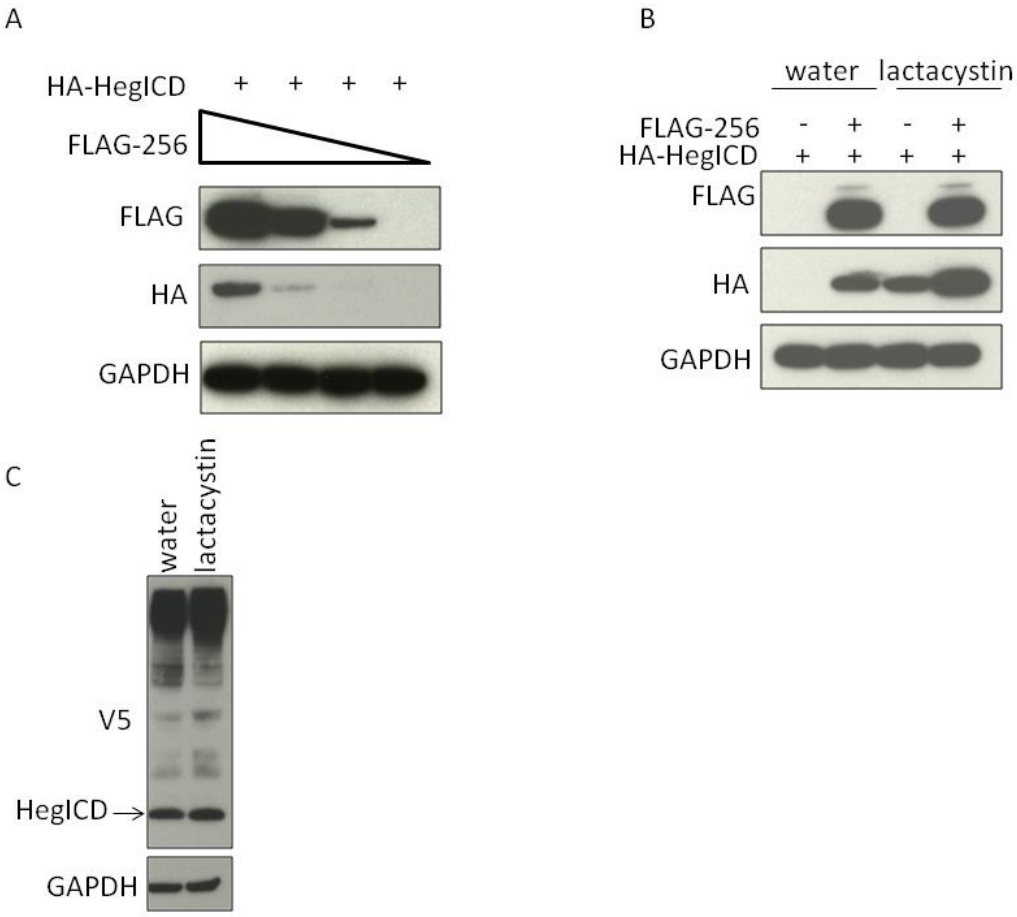

Figure 2.5. Protein derived from a HegICD construct is labile and stabilized by Ccm1. (A) Decreasing amounts of the Ccm1 construct FLAG-256 were transfected with constant amounts of HA-HegICD in 293T cells. The amount of HA-HegICD protein present 24 hours after transfection correlates with the amount of FLAG-256 protein expression. (B) Addition of the proteosome inhibitor lactacystin to cell media increases the level of HA-HegICD protein. (C) Lactacystin treatment does not affect the level of the C-terminal Heg cleavage product following transfection with the full-length Heg construct FLAG-mHeg-V5.

Zebrafish Ccm1, which is 741 amino acids long, contains a large C-terminal FERM domain comprising amino acids 414-638. The smallest *ccm1* clone recovered from the yeast 2-hybrid screen codes for Ccm1 amino acids 416-741, suggesting that the FERM domain of Ccm1

is sufficient to bind HegICD. Based on our co-immunoprecipitation experiments in Chapter 3 of this dissertation, this is indeed the case.

We followed up one other hit from the yeast 2-hybrid screen in considerable detail even though it failed to interact with HegICD in the *in vitro* transcription/translation co-immunoprecipitation experiment. Clone #129 represents *coiled-coil domain containing 80a* (*ccdc80a*), one of three zebrafish *ccdc80* paralogs. Human *CCDC80* has been shown to negatively regulate the Wnt/β-catenin signaling pathway in adiopose cell culture (Tremblay et al., 2009). Similarly, *ccm1* has been shown to suppress β-catenin signaling in endothelial cells (Glading and Ginsberg, 2010). Due to this common function of *CCDC80* and the Heg-CCM pathway member *ccm1*, we performed additional experiments to determine whether Ccdc80a and Heg interact genetically and physically.

We designed two non-overlapping morpholinos against exon-intron junctions in *ccdc80a* to determine the phenotype caused by loss of *ccdc80a* function. Both morpholinos caused enlarged atria and inflow tracts in 48 hpf embryos (Figure 2.6A). The morpholinos were validated by RT-PCR followed by sequencing; MO e3i3 causes a partial excision of exon 3 leading to a frameshift event and an in-frame stop codon in exon 4, and MO e5i5 causes the inclusion of intron 5, which also has an in-frame stop codon (Figure 2.6B).

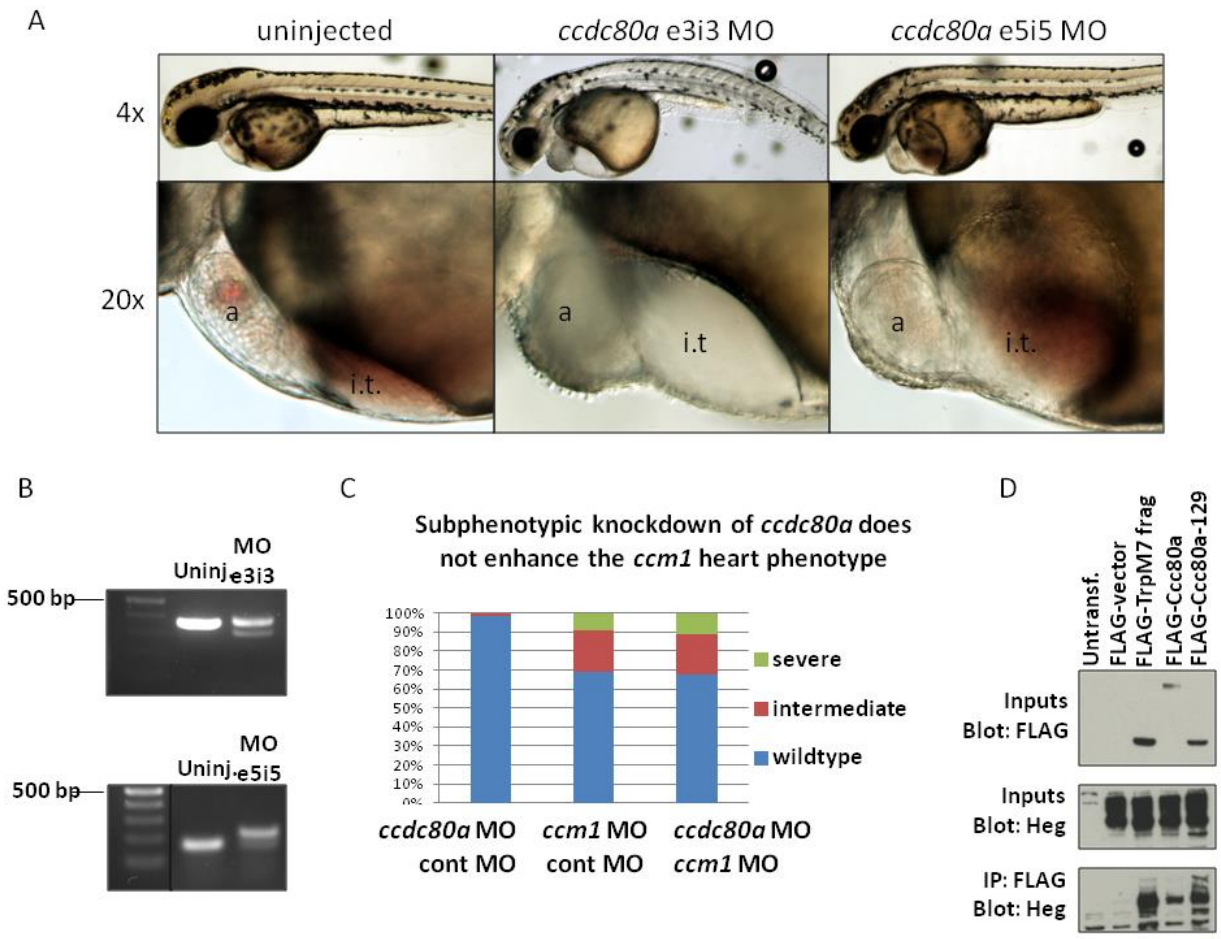

Figure 2.6. *ccdc80a* is required for heart development but does not interact with the Heg-CCM pathway. (A) Two different morpholinos targeting exon-intron junction in *ccdc80a* confer a dilated atrium and inflow tract phenotype. (B) RT-PCR showing activity of *ccdc80a* morpholinos. Irrelevant lanes have been cropped from the lower image. (C) *ccdc80a* morpholino e3i3 is no more effective than control morpholino in enhancing the dilated heart phenotype in embryos sensitized by slight *ccm1* knockdown. (D) FLAG-tagged versions of TrpM7 (an irrelevant protein control), full-length Ccdc80a, and a yeast 2-hybrid fragment isolated from the yeast 2-hybrid screen all co-immunoprecipitate overexpressed Heg in 293T cells. a, atrium; i.t., inflow tract.

The phenotypes observed are consistent with a role for *ccdc80a* in the Heg-CCM pathway. However, using a morpholino coinjection enhancer assay (see Materials and Methods), we found that *ccdc80a* knockdown does not enhance the dilated heart phenotype in embryos sensitized by a subphenotypic dose of morpholino against *ccm1* (Figure 2.6C). We also failed to detect a specific interaction between Heg and Ccdc80a proteins in the 293T cell overexpression

system (Figure 2.6D). Both full-length FLAG-Ccdc80a and the FLAG-tagged Ccdc80a fragment isolated from the yeast 2-hybrid screen co-immunoprecipitated Heg; however, a FLAG-tagged fragment of TrpM7, chosen as an irrelevant negative control protein, co-immunoprecipitated Heg as well. We conclude that overexpressed Heg protein in 293T cells binds too promiscuously for this assay to reliably identify specific interactions. (This limitation does not apply to our analysis of Heg-Ccm1 interactions in Chapter 3. In that set of experiments, the Ccm1 protein lacking a FERM domain does not bind Heg, providing an internal control for specificity.)

Discussion

Possible functions of the Heg cleavage event

The experiments in this chapter investigated Heg protein, a critical component of the Heg-CCM pathway. We studied the processing of Heg protein by performing western blots for overexpressed Heg in 293T cells and endogenous Heg in HUVECs. In both cases, we observed that antibodies against the C-terminal end of Heg detect multiple bands. As expected, there are large molecular weight bands centered around 195 kDa that likely correspond to full-length Heg proteins bearing various degrees of glycosylation. Surprisingly and interestingly, there is also a small molecular weight band that runs slightly above 15 kDa. Because this band is detectable in lysates from 293T cells overexpressing Heg cDNA that lacks introns, it probably does not represent an isoform generated by alternative splicing. We believe the most likely explanation for the existence of this small molecular weight product is that the C-terminal (intracellular) end of Heg is cleaved from the full-length protein.

We currently have no data speaking to the function of this cleavage event, but it is interesting to speculate that it is regulates the activity of the Heg-CCM pathway. One can imagine several ways this could happen. It is thought that one function of Heg is to anchor Ccm1 at the plasma membrane, where it suppresses RhoA signaling. If the intracellular portion of Heg is cleaved and released from the membrane, it could downregulate Ccm1 activity by sequestering it in the cytoplasm. Another possibility is that HegICD functions in the cell's nucleus. Ccm1 has functional nuclear localization signals (Zawistowski et al., 2005), but its nuclear activity is unknown. It is possible that Ccm1 shuttles HegICD into the nucleus where it regulates gene expression, analogous to the nuclear function of the cleaved intracellular domain of Notch protein.

The zebrafish orthologs of Heg and Ccm1 interact

We performed a yeast 2-hybrid screen using the highly conserved intracellular domain of Heg, HegICD, as bait against a library of clones isolated from embryonic zebrafish heart. We performed biochemical binding assays on 34 hits obtained in the screen and discovered that HegICD binds a Ccm1 fragment when the two are coexpressed in 293T cells and when they are expressed completely *in vitro*. The latter experiment suggests that the interaction is direct, since the coupled *in vitro* transcription/translation reaction occurs in an environment lacking most cellular proteins. The smallest *ccm1* clone recovered from the screen contains just the C-terminal, FERM-domain containing part of the Ccm1 protein, suggesting that it is this domain that interacts with Heg. This finding was confirmed in experiments presented in Chapter 3 of this dissertation.

The finding that Ccm1 binds HegICD provides a window into the molecular mechanism behind the previously observed genetic interaction between the corresponding genes (Mably et al., 2006). While this project was in progress, the biochemical interaction between Ccm1 and Heg was shown for their mammalian orthologs (Kleaveland et al., 2009). Thus, the interaction between Ccm1 and Heg is conserved between zebrafish and mouse. A recent study suggests that the function of the Heg-Ccm1 interaction is to recruit and anchor Ccm1 to the plasma membrane (Gingras et al., 2012). Additional research will be required to fully understand how binding to Heg regulates the activity of Ccm1 and the downstream components of the Heg-CCM pathway.

Works cited

Boulday, G., Blecon, A., Petit, N., Chareyre, F., Garcia, L.A., Niwa-Kawakita, M., Giovannini, M., Tournier-Lasserve, E., 2009. Tissue-specific conditional CCM2 knockout mice establish the essential role of endothelial CCM2 in angiogenesis: implications for human cerebral cavernous malformations. Dis Model Mech 2, 168-177.

Gingras, A.R., Liu, J.J., Ginsberg, M.H., 2012. Structural basis of the junctional anchorage of the cerebral cavernous malformations complex. The Journal of cell biology 199, 39-48.

Glading, A., Han, J., Stockton, R.A., Ginsberg, M.H., 2007. KRIT-1/CCM1 is a Rap1 effector that regulates endothelial cell cell junctions. The Journal of cell biology 179, 247-254.

Glading, A.J., Ginsberg, M.H., 2010. Rap1 and its effector KRIT1/CCM1 regulate beta-catenin signaling. Dis Model Mech 3, 73-83.

Hogan, B.M., Bussmann, J., Wolburg, H., Schulte-Merker, S., 2008. ccm1 cell autonomously regulates endothelial cellular morphogenesis and vascular tubulogenesis in zebrafish. Hum Mol Genet 17, 2424-2432.

Kleaveland, B., Zheng, X., Liu, J.J., Blum, Y., Tung, J.J., Zou, Z., Sweeney, S.M., Chen, M., Guo, L., Lu, M.M., Zhou, D., Kitajewski, J., Affolter, M., Ginsberg, M.H., Kahn, M.L., 2009. Regulation of cardiovascular development and integrity by the heart of glass-cerebral cavernous malformation protein pathway. Nature medicine 15, 169-176.

Mably, J.D., Chuang, L.P., Serluca, F.C., Mohideen, M.A., Chen, J.N., Fishman, M.C., 2006. santa and valentine pattern concentric growth of cardiac myocardium in the zebrafish. Development (Cambridge, England) 133, 3139-3146.

Mably, J.D., Mohideen, M.A., Burns, C.G., Chen, J.N., Fishman, M.C., 2003. heart of glass regulates the concentric growth of the heart in zebrafish. Curr Biol 13, 2138-2147.

Rosen, J.N., Sweeney, M.F., Mably, J.D., 2009. Microinjection of zebrafish embryos to analyze gene function. J Vis Exp.

Sakaguchi, T.F., Sadler, K.C., Crosnier, C., Stainier, D.Y., 2008. Endothelial signals modulate hepatocyte apicobasal polarization in zebrafish. Curr Biol 18, 1565-1571.

Stockton, R.A., Shenkar, R., Awad, I.A., Ginsberg, M.H., 2010. Cerebral cavernous malformations proteins inhibit Rho kinase to stabilize vascular integrity. J Exp Med 207, 881-896.

Tremblay, F., Revett, T., Huard, C., Zhang, Y., Tobin, J.F., Martinez, R.V., Gimeno, R.E., 2009. Bidirectional modulation of adipogenesis by the secreted protein Ccdc80/DRO1/URB. The Journal of biological chemistry 284, 8136-8147.

Whitehead, K.J., Chan, A.C., Navankasattusas, S., Koh, W., London, N.R., Ling, J., Mayo, A.H., Drakos, S.G., Jones, C.A., Zhu, W., Marchuk, D.A., Davis, G.E., Li, D.Y., 2009. The cerebral cavernous malformation signaling pathway promotes vascular integrity via Rho GTPases. Nature medicine 15, 177-184.

Whitehead, K.J., Plummer, N.W., Adams, J.A., Marchuk, D.A., Li, D.Y., 2004. Ccm1 is required for arterial morphogenesis: implications for the etiology of human cavernous malformations. Development (Cambridge, England) 131, 1437-1448.

Zawistowski, J.S., Stalheim, L., Uhlik, M.T., Abell, A.N., Ancrile, B.B., Johnson, G.L., Marchuk, D.A., 2005. CCM1 and CCM2 protein interactions in cell signaling: implications for cerebral cavernous malformations pathogenesis. Hum Mol Genet 14, 2521-2531.

Zhang, J., Rigamonti, D., Dietz, H.C., Clatterbuck, R.E., 2007. Interaction between krit1 and malcavernin: implications for the pathogenesis of cerebral cavernous malformations. Neurosurgery 60, 353-359; discussion 359.

Chapter 3: *ccm2-like* is required for cardiovascular development as a novel component of the Heg-CCM pathway

Attributions

The project described in this chapter contains intellectual contributions from Jonathan Rosen, Vanessa Sogah, and John Mably. Vanessa Sogah and John Mably initiated the project. John Mably identified zebrafish *ccm2l in silico*, and Vanessa Sogah recovered a full-length *ccm2l* clone. Vanessa Sogah also generated several plasmids, performed some of the analysis of the *ccm2l* e2i2 morpholino, and analyzed the Ccm2-Ccm2l alignment. *in situ* hybridization experiments were done by John Mably, Patrick Bailey, Brian Koh, and Lillian Ye. Lillian Ye performed some of the cell transfections and western blots, including many experimental repetitions not shown here. The rest of the experiments were performed by Jonathan Rosen. This chapter is a modified version of our submitted (with revisions) manuscript "*ccm2-like* is required for cardiovascular development as a novel component of the Heg-CCM pathway," in review at the time of the writing of this dissertation.

Introduction

The zebrafish is tremendously useful for the identification and characterization of genes that control heart development, as both heart morphology and its functional output, blood circulation, are easily visible in the transparent, externally developing embryo. The embryonic zebrafish heart contains two chambers, one atrium and one ventricle, and each consists of two tissues: endocardium, which is a specialized endothelium that lines the inside of the heart, and the muscular myocardium surrounding it that generates the organ's contractile force. Three different mutants – *santa* (*san*), *valentine* (*vtn*), and *heart of glass* (*heg*) – exhibit the same striking phenotype: the heart and inflow tract are massively dilated, and although the heart beats, there is no blood circulation (Mably et al., 2006; Mably et al., 2003). They die around 5 days post fertilization (dpf), which is a general feature of mutants that cannot form a functional cardiovascular system. The genes disrupted in *san*, *vtn*, and *heg* mutants are *ccm1*, *ccm2*, and *heg*, respectively, and they are conserved across vertebrate species; their murine homologs *Ccm1*, *Ccm2*, and *Heg1*, respectively, are essential for normal cardiovascular development in mouse (Boulday et al., 2009; Kleaveland et al., 2009; Whitehead et al., 2009; Whitehead et al., 2004).

ccm1, *ccm2*, and *heg* interact genetically as components of a signaling system known as the Heart of glass-Cerebral Cavernous Malformation (Heg-CCM) pathway. In zebrafish, slight knockdown of any of the three genes can drastically enhance heart phenotypes in embryos sensitized by a subphenotypic dose of morpholino against either of the other two (Mably et al., 2006). Similarly, the phenotype conferred by deletion of *Heg1* in mouse is enhanced in animals haploinsufficient for *Ccm2* (Kleaveland et al., 2009). CCM1, CCM2 and HEG1 proteins also

interact biochemically. Co-immunoprecipitation, FRET, and yeast 2-hybrid experiments have demonstrated physical interactions between human CCM1 and CCM2 (Zawistowski et al., 2005; Zhang et al., 2007). CCM1 contains three NPXY/F motifs, ankyrin repeats, and a *band 4.1*, ezrin, radixin, moesin (FERM) domain. CCM2 contains a phosphotyrosine binding (PTB) domain that is required for the CCM1-CCM2 interaction. The NPXY/F motifs in CCM1 are targets of the PTB domain in CCM2, and disrupting these motifs singly or pairwise causes decreased CCM1-CCM2 binding (Zawistowski et al., 2005; Zhang et al., 2007). HEG1 is a single pass transmembrane protein whose intracellular domain binds the CCM1-CCM2 complex (Kleaveland et al., 2009).

There is strong evidence that the Heg-CCM pathway functions in the endothelium. Conditional mouse knockouts where *Ccm2* is selectively deleted from the developing endothelium phenocopy the whole organism knockout, demonstrating that this pathway's activity is required in the endothelium (Boulday et al., 2009; Whitehead et al., 2009). *in situ* hybridization experiments in zebrafish embryos detect *heg* expression in the endocardium but not the myocardium, consistent with a model in which Heg-CCM signaling in the heart's endothelium regulates heart morphology (Mably et al., 2003). Adult mice heterozygous for *Ccm2* exhibit vascular leakiness (Stockton et al., 2010) and hypersensitivity to the hemorrhagic effects of VEGF injection (Whitehead et al., 2009), and this phenotype is recapitulated in endothelial cell culture where loss of *CCM1* or *CCM2* causes increased monolayer permeability (Crose et al., 2009; Glading et al., 2007; Stockton et al., 2010; Whitehead et al., 2009). These studies demonstrate that the Heg-CCM pathway is conserved across vertebrates and required in the endothelium for normal cardiovascular development and adult physiology.

The Heg-CCM pathway is so-named because mutations in the human *CCM1* and *CCM2* genes cause vascular anomalies called cerebral cavernous malformations (CCMs) (Denier et al., 2004; Laberge-le Couteulx et al., 1999; Liquori et al., 2003; Sahoo et al., 1999). CCMs, which affect approximately 0.5% of the population, are malformations of the brain vasculature characterized by an expanded endothelial vessel that can result in headache, seizure, hemorrhage and death (Revencu and Vikkula, 2006). CCMs can arise either spontaneously or as an autosomal dominant hereditary condition. In addition to *CCM1* and *CCM2*, a third gene, *CCM3*, also causes CCMs when mutated (Bergametti et al., 2005). In overexpression studies, CCM3 protein can bind CCM2 (Hilder et al., 2007; Li et al., 2010; Voss et al., 2007; Zheng et al., 2010), and knockdown of its two zebrafish homologs, *ccm3a* and *ccm3b*, affects heart development, though there are conflicting characterizations of this phenotype (Voss et al., 2009; Yoruk et al., 2012; Zheng et al., 2010). Since loss-of-function of *ccm1* and *ccm2* causes severe endothelial vessel dilation in both the embryonic zebrafish heart and the adult human brain, the zebrafish heart may provide insights into the genetic and cellular interactions that underlie human CCM disease.

Unlike other signaling pathways that have been studied extensively, the Heg-CCM pathway was discovered only recently and as a result remains incompletely understood. We employed a straightforward bioinformatic approach to identify a novel gene with sequence identity to *ccm2*, which we have named *ccm2-like* (*ccm2l*). Using morpholinos to knock down *ccm2l* in zebrafish embryos, we found that loss of *ccm2l* causes dilation of the atrium and inflow tract and a lack of blood circulation. Slight reduction of *ccm2l* causes a dilated heart phenotype in embryos sensitized by a sub-phenotypic dose of *ccm1* morpholino, defining *ccm2l* as an enhancer of the Heg-CCM pathway. Injection of *ccm2* mRNA can partially rescue

cardiovascular defects in *ccm2l* morphants, suggesting that *ccm2* and *ccm2l* have overlapping *in vivo* functions. We demonstrate that Ccm2l protein binds Ccm1; moreover, we interrogate this interaction further to define the Ccm1 NPXY/F motif requirements for this interaction, which are different from those for Ccm1-Ccm2 binding. Finally, we suggest that the human homolog of *ccm2l*, *C20ORF160*, may have relevance to human CCM disease.

Materials and methods

Zebrafish

All zebrafish husbandry procedures were performed in accordance with protocols approved by the Institutional Animal Care and Use Committee at Boston Children's Hospital. Zebrafish embryos were raised in egg water at 28.5°C. Tubingen and *(fli1*:*EGFP)*^{y1} (Lawson and Weinstein, 2002) zebrafish lines were used. For some experiments, embryos were incubated in 0.003% 1-phenyl 2-thiourea (PTU) after 1 day of development to inhibit pigment formation.

Expression analysis

in situ hybridization was performed as previously described (Mably et al., 2006; Mably et al., 2003). RT-PCR was performed either using the OneStep RT-PCR kit (Qiagen) on total RNA extracted from embryos by Trizol (Life Technologies) or by performing reverse transcription on total RNA using the QuantiTect Reverse Transcription Kit (Qiagen) followed by PCR. The following primers were used:

ccm2: 5'-CGTCTATACCGAGTCCACCA-3', 5'- AGGAGTCTTCACTGTAGATTGAG-3'.

ccm2l: 5'- AGGTCAAGTTCCTGGGACAC-3', 5'- CAGACAGACTGAGAATACAGTCC-3'.

ccm1: 5’- CATAATAGGGAAGCGTGTTGTG-3’, 5’- GGAGGAGAAATGAGCACTGG-3’.

gapdh: 5’- GGCAAACTGGTCATTGATGG-3 , 5’-CTTAATGTGAGCAGAAGCCT-3’.

cmlc2: 5’-GGAGAGAAGCTCAATGGCACA-3’, 5’-GTCATTAGCAGCCTCTTGAACTCA-3’.

insulin: 5’-GTG GAT CTC ATC TGG TCG ATG C-3’, 5’-AGG AGG AAG GAA ACC CAG AAG G-3’, as previously described (Burns and MacRae, 2006).

β-actin: 5’-GCTGTTTTCCCCTCCATTGTT-3’, 5’-TCCCATGCCAACCATCACT-3’.

For comparison of gene expression in heart and whole embryo, embryonic heart purification was performed as previously described (Burns and MacRae, 2006).

Embryo microinjection

Morpholinos, designed by Gene Tools, LLC, were diluted in water to make stock solutions and further diluted in water containing a final concentration of 0.1% phenol red for injections. Embryos were injected in the yolk with 1-2 nL of diluted morpholino no later than the 2-cell stage using a PLI-100 pico-injector (Harvard Instruments) and subsequently raised at 28.5 °C. The following morpholinos were used:

ccm1: 5’-GCTTTATTTCACCTCACCTCATAGG-3’

ccm2l: MO e4i4: 5’-ACATTTCACTCTTACTAACCAGTTT-3',

MO e2i2: 5’-TCAGACTAGACCTTGACCTCCTTCT-3’.

ccm2: 5’-GAAGCTGAGTAATACCTTAACTTCC-3’.

Standard control MO: 5'-CCTCTTACCTCAGTTACAATTTATA-3'.

In experiments to characterize the *ccm2l* knockdown phenotype, we injected 1.0 pMol MO e4i4 or 0.3 pMol MO e2i2. For enhancer experiments, pairwise combinations of

morpholino were injected as single solutions. For experiments with either MO e4i4 or MO e2i2, each 1 nL injection volume contained 0.01 pMol ccm1 MO + 0.05 pMol ccm2l MO, 0.01 pMol ccm1 MO + 0.05 pMol standard control MO, or 0.01 pMol standard control MO + 0.05 pMol ccm2l MO. The experimenter was blinded to these solutions prior to injection. For rescue experiments, embryos were first injected with morpholino (0.3 pMol MO e2i2 or 1.0 pMol MO e4i4), randomly sorted into three groups, and then injected a second time with 0.1 ng *ccm2*^{wt} mRNA or 0.1 ng *ccm2*^{m201} mRNA. (The third group was left singly injected.) The experimenter was blinded to these treatments prior to assaying phenotypes at 52 hpf.

Morpholinos against *ccm1* and *ccm2* were previously validated (Mably et al., 2006). To validate morpholinos against *ccm2l*, total RNA was isolated from embryos injected with morpholino and uninjected control embryos using Trizol reagent (Life Technologies) as per the manufacturer's instructions. The RNA was then subjected to reverse transcription PCR (RT-PCR) using the OneStep RT-PCR kit (Qiagen) with exonic primers flanking the exon-intron boundary targeted by the morpholino. RT-PCR products were visualized by SYBR safe (Life Technologies) on an agarose gel. The following PCR primers were used:

ccm2l: 5'-TGGACTATGATCCCAAGCGAACCA-3', 5'-GGGTTCAGGGAACAGGACACCCA-3'.

ccm2: 5'- ATGGAGGAGGATGTAAAGAA-3', 5'- TCAGGTATCCAGGAACTGAGG -3'.

The *ccm2l* MO e2i2 and uninjected PCR products were subcloned into the PCRII-TOPO vector (Life Technologies) and sequenced.

mRNA preparation

Capped RNA was transcribed *in vitro* from linearized pCS2-ccm2, pCS2-ccm2^{m201}, and pXT7-ccm2le2i2 templates using the mMessage mMachine SP6 or T7 Ultra kits (Life Technologies) and purified using the MEGAclear kit (Life Technologies). As the last step of the purification, RNA was eluted in water and subsequently diluted in water and phenol red (final concentration of 0.1%) prior to injection.

Cloning and plasmid generation

The generation of pCMV-Myc-heg was described in chapter 2 of this dissertation. *ccm2l* was cloned from cDNA reverse transcribed from total RNA isolated from 2 dpf zebrafish embryos. The following forward and reverse primers were designed with an EcoRI site and a XhoI site, respectively, to allow for subcloning of the PCR product into pCMV-HA (Clontech):
5'- GATCGAATTCAAATGGACTATGATCCCAAGCG-3',
5'- GATCCTCGAGTCACAAGTAATAATCCTCCTC-3'.

pCMV-HA-ccm2 was generated by performing PCR on a previously described pCS2-ccm2 template (Mably et al., 2006) with primers containing EcoRI and XhoI restriction sites followed by digestion and ligation into pCMV-HA. The following primers were used:
5'-GATCGAATTCAAATGGAGGAGGATGTAAAGAAAG-3',
5'-GATCCTCGAGTCAAGATGGCACGCCGTCTTG-3'.

Ccm1 deletion constructs were generated by performing PCR on full-length *ccm1* cDNA template with primers containing EcoRI or XhoI restriction sites and subcloning PCR fragments into pCMV-tag2b (Stratagene). The following PCR primers were used:
pCMVtag2b-ccm1:
5'-GATCGAATTCATGATGGGAAACCAAGAGCTAG-3',

5’-GATCCTCGAGTTACCCATACGCATATTTATC-3’.

pCMVtag2b-ccm1ΔNPXY/F:

5’-GGAATTCAAATGGCAGCACAGCATGACC-3’,

5’-ACCGCTCGAGTTACCCATACGCATAT -3’.

pCMVtag2b-ccm1ΔNPXY/F-ANK:

5’-GGAATTCTGGGAGGAAACCGTGAATCTC-3’,

5’- ACCGCTCGAGTTACCCATACGCATAT -3’.

pCMVtag2b-ccm1ΔFERM:

5’-GGAATTCATGGGAAACCAAGAGCTAGAG-3’,

5’-ACCGCTCGAGGAGATTCACGGTTTCCTC-3’.

FLAG-ccm1^{ty219c} and FLAG-ccm1^{m775} were generated using the same primers and vector as pCMVtag2b-ccm1, but with PCR templates containing the appropriate *ccm1* alleles.

Point mutations were inserted in pCMVtag2b-ccm1 using the QuikChange II Site-Directed Mutagenesis Kit (Stratagene). The following primers were used:

Y193A:

5'-GTGAGTAACCCGGCGGCCGCAGTGGAGAAGCA-3,

5'-TGCTTCTCCACTGCGGCCGCCGGGTTACTCAC-3'.

Y231A:

5'-CATCCAGAACCCGCTGGCCGGCTCAGATCTGCAG-3’,

5'-CTGCAGATCTGAGCCGGCCAGCGGGTTCTGGATG-3'.

Y249A,F250A:

5’-ACAGAGTGGACAAAGTCATCATCAACCCTGCCGCTGGCTTGGGAGCTCC-3,

5’- GGAGCTCCCAAGCCAGCGGCAGGGTTGATGATGACTTTGTCCACTCTGT-3’.

pXT7-ccm2le2i2 was generated by shuttling the MO e2i2 induced RT-PCR product (i.e. the upper band containing an intronic insertion) from PCRII-TOPO to pXT7.

Cell culture and western blotting

Transfections, co-immunoprecipitation, and western blotting were performed as described in chapter 2 of this dissertation. Antibodies against Heg, FLAG, and HA were used as described.

Microscopy

Images of live embryos were taken and processed as described in chapter 2.

Results

ccm2l *is a novel, conserved gene expressed during embryonic development*

To identify potential homologs of genes in the Heg-CCM pathway, we queried the NCBI databases for entries with sequence identity to Heg-CCM genes using both BLASTp and BLASTx algorithms. We identified a protein bearing 43% identity to Ccm2, which we have named Ccm2-like (Ccm2l) (Figure 3.1A). The coding sequence of *ccm2l* contains 1842 nucleotides and the corresponding protein has 613 amino acids. The only domain in Ccm2l readily predicted by the protein's primary sequence is a Pleckstrin-homology (PH) domain-like region comprised of amino acids 45-146 (Gough et al., 2001). The PH-like domain superfamily includes PTB domains; since the PH-like domain in Ccm2l has high identity to the PTB domain of Ccm2, we consider the PH-like domain to be a putative PTB domain. Ccm2l and Ccm2

contain regions of high identity not only in their PTB domains, but also in their C-terminal ends (Figure 3.1A,B). We amplified *ccm2l* from RNA isolated from 2-day old embryos using primers corresponding to the 5' and 3' ends of the coding region of the transcript. Sequencing of our clone revealed that it matches the full-length transcript predicted by the Ensembl Genome Browser. *ccm2l* homologs are found in other vertebrate species, including human, where it is called *C20ORF160*.

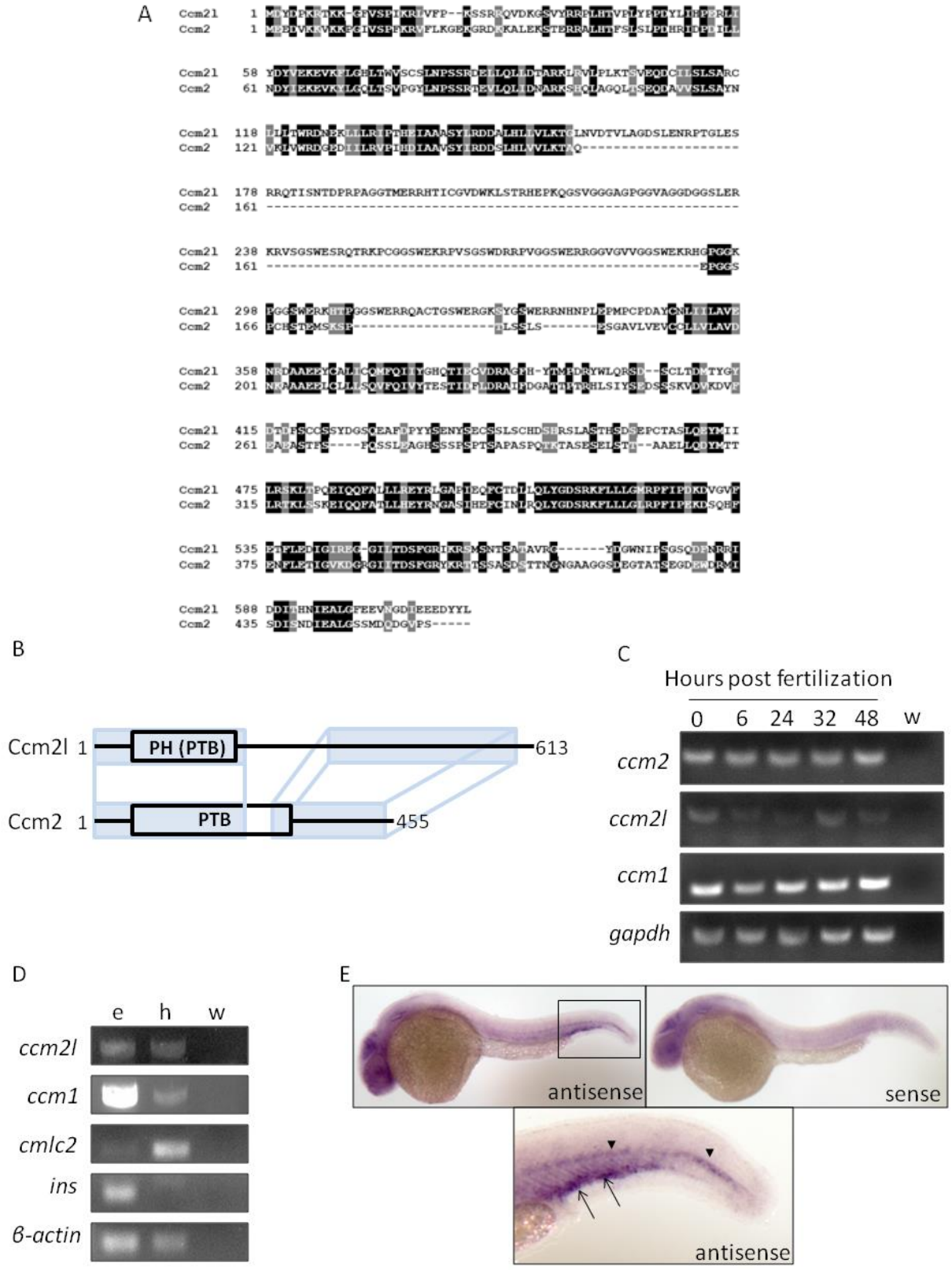
A
Ccm2l
Ccm2
B
Ccm2l 1
PH (PTB)
613
Ccm2 1
PTB
455
C
Hours post fertilization
0 6 24 32 48 w
ccm2
ccm2l
ccm1
gapdh
D
e h w
ccm2l
ccm1
cmlc2
ins
β-actin
E
antisense
sense
antisense

Figure 3.1

Figure 3.1 (Continued). Sequence and expression analysis of *ccm2l*. (A) Alignment of Ccm2l and Ccm2 protein sequences. Black residues are identical and gray residues are similar. (B) Schematic comparing the domain structures of Ccm2l and Ccm2. The N-terminal region of Ccm2l contains a putative PTB domain with high identity to the PTB domain of Ccm2. The two proteins also have regions of high identity at their C-termini. (C) RT-PCR showing expression of *ccm2*, *ccm2l*, *ccm1* and the positive control *gapdh* at five embryonic stages. All four genes are expressed at all five time points tested between 0 and 48 hpf. Water (w) is included as a negative control. (D) RT-PCR comparing expression of *ccm2l* and *ccm1* in whole embryos (e) and purified embryonic hearts (h) at 52 hpf. Both genes are expressed in the heart, with the ratio of heart expression to whole embryo expression much higher for *ccm2l*. RT-PCR for the heart-specific marker *cardiac myosin light chain* (*cmlc2*) and for a transcript absent from the heart, *insulin* (*ins*), demonstrate the quality of the heart tissue purification. (E) *in situ* hybridization analysis of *ccm2l* expression. In 30 hpf embryos, *ccm2l* expression is detected in the posterior end of the embryo in the presumptive notochord (arrowheads) and the tissue ventral to it (arrows). Embryos treated with sense probe as a negative control lack staining in these domains. PH, Pleckstrin-homology superfamily; PTB, phosphotyrosine binding domain.

We performed RT-PCR and *in situ* hybridization to analyze when and where in the embryo *ccm2l* is expressed. By RT-PCR we found that transcripts for *ccm2l*, like *ccm1* and *ccm2*, are present at all time points we tested between fertilization and 48 hours post fertilization (hpf) (Figure 3.1C). The presence of transcripts at the zygote stage implies a maternal contribution of these messages. Because the Heg-CCM pathway functions in heart development, we mechanically purified 52 hpf zebrafish embryonic hearts and performed RT-PCR for *ccm1 and ccm2l* expression, and we found that both genes are expressed in the heart (Figure 3.1D).

Next we performed *in situ* hybridization for *ccm2l*. We found that at 30 hpf, *ccm2l* is detectable in the presumptive notochord at the posterior end of the embryo and the tissue ventral to it; the corresponding negative control sense probe does not produce any signal in these domains (Figure 3.1E). This expression pattern shares features with those of *ccm1* and *ccm2*; it has previously been shown that *ccm1* is expressed in the notochord at 48 hpf and *ccm2* is expressed in the intermediate cell mass ventral to the notochord at 28 hpf (Mably et al., 2006).

The mouse homolog of *ccm2l* has previously been shown to be enriched in embryonic-stem cell derived $CD31^+$ endothelial-like cells (Mariappan et al., 2009).

ccm2l *is required for heart development*

To characterize the role of *ccm2l* in zebrafish development, we employed a morpholino loss-of-function strategy. First, we designed a morpholino, MO e4i4, to bind an exon-intron junction in the *ccm2l* pre-mRNA. Microinjection of embryos with this morpholino caused a heart phenotype with little overall toxicity, but surprisingly, we could not detect any changes to the *ccm2l* transcript when we performed RT-PCR using primers targeted to neighboring exons. Others have reported the same phenomenon and suggested that splice site morpholinos may in some cases prevent efficient translation (Schottenfeld et al., 2007). Alternatively, the morpholino-induced RNA product may be subject to rapid nonsense-mediated decay. We designed a second splice site morpholino, MO e2i2, and found that it confers a similar phenotype to MO e4i4. RT-PCR followed by sequencing demonstrated that MO e2i2 increases the amount of an endogenous alternative transcript at the expense of the expected transcript (Figure 3.2A). Sequencing revealed that the alternative transcript contains an intronic inclusion with a premature stop codon (Figure 3.2B); thus, MO e2i2 appears to cause a shift from normal Ccm2l protein to a severely

truncated isoform. Splicing of *ccm2* at the homologous exon-intron junction is not affected (Figure 3.3).

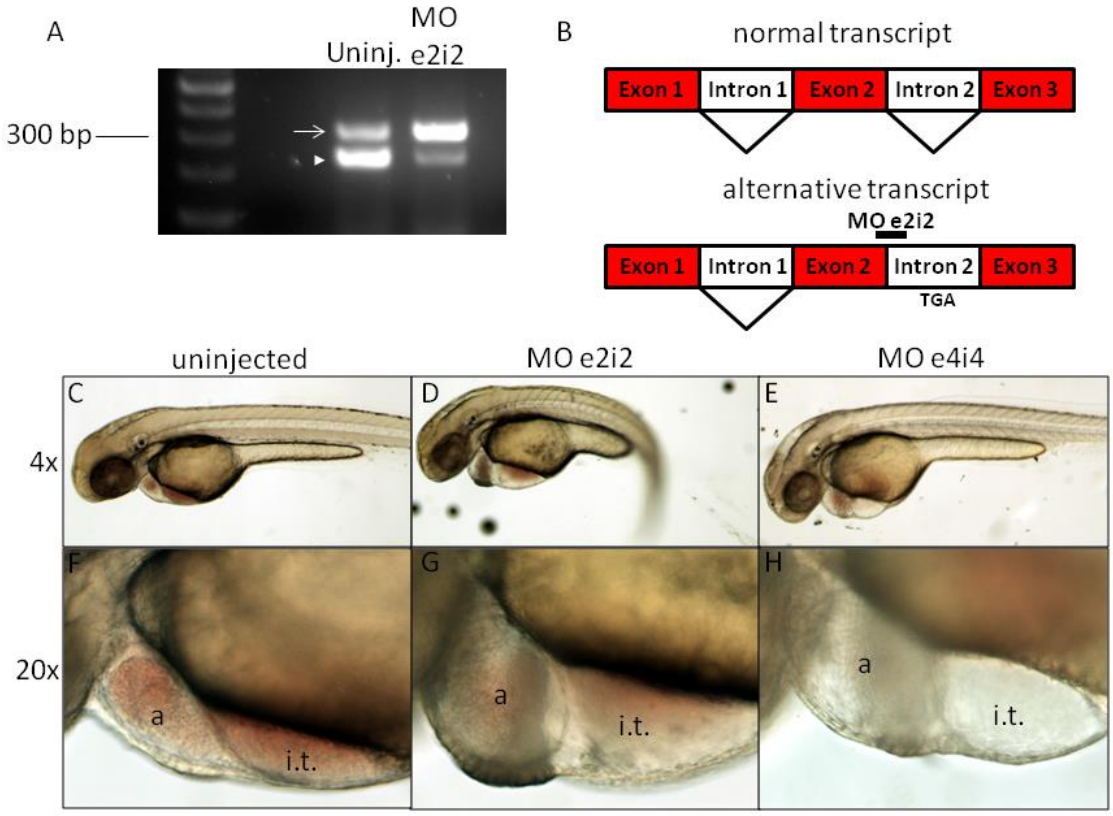

Figure 3.2. *ccm2l* morphants exhibit heart and inflow tract defects. (A) Injection of MO e2i2 increases production of an endogenous alternatively spliced product (arrow) at the expense of the presumptive functional transcript (arrowhead). (B) Sequencing reveals that the alternatively spliced *ccm2l* mRNA, which is observed at increased levels in embryos injected with MO e2i2, incorporates intron 2, leading to an in-frame stop codon. (C and F) Uninjected embryos have compact heart chambers and narrow inflow tracts. (D,E,G,H) Embryos injected at the one-cell stage with 0.3 pMol MO e2i2 (D and G) or 1.0 pMol MO e4i4 (E and H) exhibit dilation of the atrium and inflow tract. Embryos injected with MO e2i2 often have a curved body axis. All images are taken from a lateral perspective with anterior to the left. a, atrium; i.t., inflow tract.

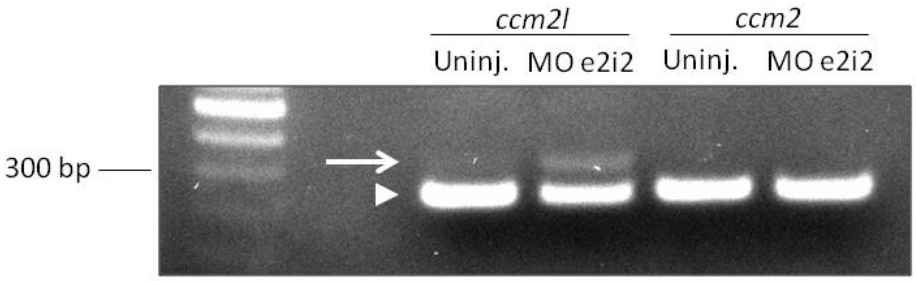

Figure 3.3. MO e2i2 affects splicing of *ccm2l* but not *ccm2*. RT-PCR using primers flanking the exon 2-intron 2 junction of *ccm2l* demonstrates a shift from the normally spliced transcript (arrowhead) to an alternative transcript (arrow) in embryos injected with MO e2i2. In contrast, primers flanking the exon 2-intron 2 junction of *ccm2* detect no difference in transcript size between uninjected embryos and embryos injected with MO e2i2.

Loss-of-function of *ccm2* in zebrafish causes a massively dilated heart phenotype (Mably et al., 2006). We began our phenotypic study of *ccm2l* by asking whether its knockdown affects heart development. At 52 hpf, uninjected embryos display compact heart chambers, a narrow inflow tract, and robust circulation (Figure 3.2C,F). In contrast, we observe dilation of the atrium in 25-50% of the embryos injected with MO e2i2 (Figure 3.2D,G). This heart phenotype is coincident with dilation of the inflow tract and in some embryos a complete cessation of blood circulation despite a rhythmic heart beat. Experiments with MO e2i2 require a relatively low dose of morpholino, as higher doses cause global developmental defects. Even at low doses, typically some embryos had to be excluded from analysis due to global defects. Embryos injected with MO e4i4 exhibit a phenotype similar to those injected with MO e2i2, consisting of dilated inflow tracts often accompanied by dilated atria at 2 dpf (Figure 3.2E,H), at a lower penetrance of 18%. Heart phenotypes caused by either *ccm2l* morpholino are less severe than those observed in *san*, *vtn*, and *heg* mutants; it is unknown whether this distinction is biologically relevant or simply due to incomplete *ccm2l* knockdown.

Because our RT-PCR data show that MO e2i2 can cause heart phenotypes even though a substantial amount of normal transcript remains in the embryo, we considered the possibility that the inclusion of intron 2 generates a dominant negative protein. To test this hypothesis, we injected mRNA containing the open reading frame of the morpholino-induced transcript and found that although a small number of embryos had heart or circulatory defects, the majority appeared to have morphologically normal hearts and blood circulation (Figure 3.4A-D). Thus, we favor the hypothesis that MO e2i2 does not generate a protein with dominant negative activity, but rather exerts a phenotype by incompletely knocking down levels of Ccm2l. Similarly, we found that morpholino against *ccm2* can confer an intermediate heart phenotype when injected at doses that allow for a substantial amount of normal transcript to endure (Figure 3.4E-K).

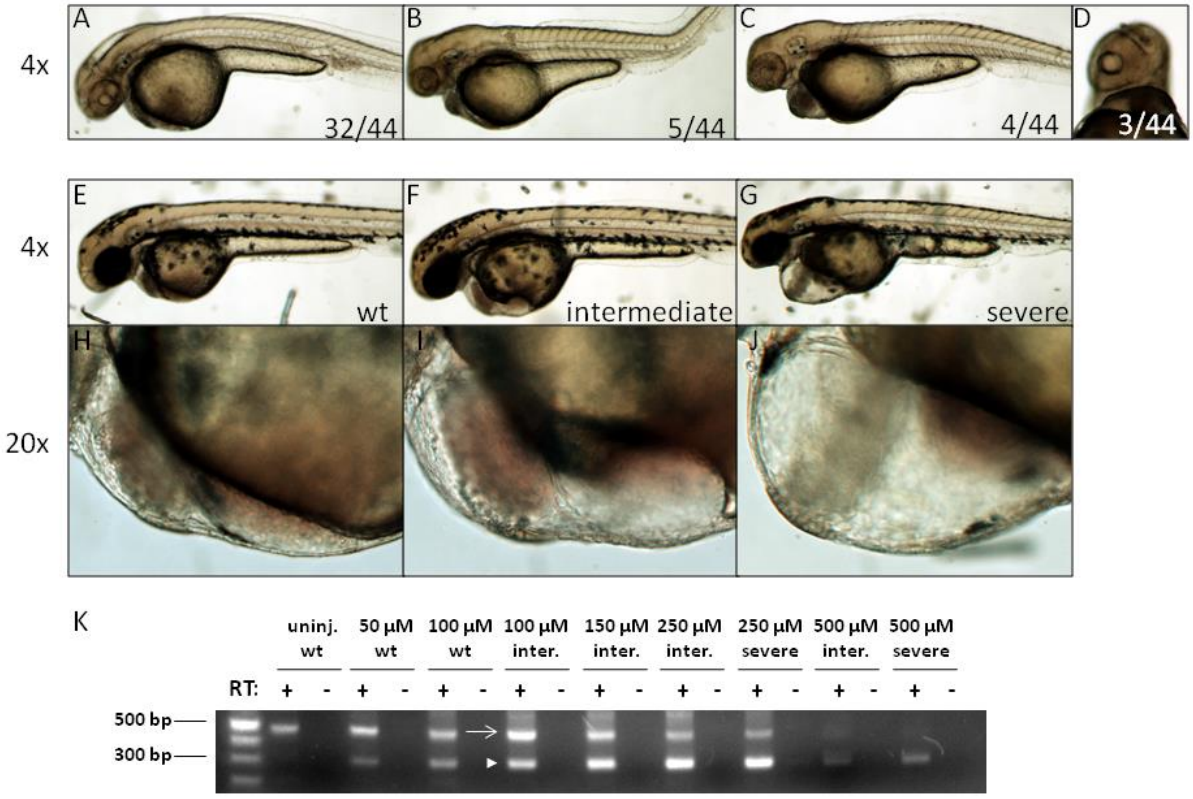

Figure 3.4. MO e2i2 does not appear to generate a dominant negative product. Embryos were injected with mRNA corresponding to the upper band in Figure 3.2a. This mRNA contained exon 1, exon 2, intron 2 (containing a stop codon), and part of exon 3 from *ccm2l*. (A) The majority of embryos (32/44) injected with this mRNA had a morphologically normal heart and circulation. (B) Five of 44 embryos had a morphologically normal heart and no circulation. (C) Four of 44 embryos had an enlarged heart and no circulation. (D) Three of 44 embryos exhibited cyclopia, an effect often seen with mRNA overexpression. (E-J) Embryos were injected with varying amounts of *ccm2* MO and grouped at 2 dpf as either wildtype, intermediate, or severe. (K) RNA was isolated and subjected to RT-PCR using primers corresponding to the exons flanking the morpholino target site. The upper band (arrow, 465 bp) represents normal *ccm2* transcript, while the lower band (arrowhead, 288 bp) represents aberrant *ccm2* transcript lacking exon 2. Embryos in which a substantial amount of *ccm2* transcript is unaffected can still exhibit a phenotype (see 100 µM, intermediate). RT, reverse transcriptase; wt, wildtype; inter., intermediate.

Next, we examined the effects of morpholino-mediated *ccm2l* knockdown on the embryonic vasculature using the *(fli1:EGFP)*^{y1} transgenic line, in which all endothelial cells are

labeled with EGFP (Lawson and Weinstein, 2002). We compared the morphology of several vessels in embryos injected with a standard control morpholino (cont MO) and those injected with MO e4i4; we chose this morpholino for analysis because its low toxicity prevents secondary vascular phenotypes caused by global developmental defects. We examined the endocardium, common cardinal vein (CCV), and mesencephalic veins (MsVs) at 52 hpf, the intersegmental veins (ISVs) at 58 hpf and the subintestinal veins (SIVs) at 72 hpf. For this analysis, we selected embryos displaying heart and inflow tract defects. As expected, the morphant endocardium appears dilated compared to embryos injected with cont MO (Figure 3.5A,B). The CCVs in affected embryos are generally normal (Figure 3.5C,D). (We have observed some CCVs exhibiting developmental delay at 2 dpf that appear normal by 3 dpf.) We observe relatively minor defects in the ISVs and SIVs; the ISVs in affected embryos are normally patterned but a small number of vessels fail to lumenize (Figure 3.5E,F), and SIVs frequently display an irregular growth pattern (Figure 3.5G,H). These defects may be explained by a reduction in blood circulation, as *silent heart* (*sih*) mutants, which completely lack blood flow owing to a defect in cardiac contractility, exhibit more severe versions of those phenotypes (Hogan et al., 2008; Mably and Childs, 2010). It was recently reported that combined knockdown of *ccm3a* and *ccm3b*, but not *ccm1* or *ccm2*, causes extreme dilation of the MsVs in zebrafish, a phenotype of particular interest because of its similarity to dilated brain vessels in patients with CCM disease (Yoruk et al., 2012). We observed that MsVs in cont MO-injected embryos are approximately the same width as those in MO e4i4-injected embryos (Figure 3.5I-K). Taken together, these data suggest that *ccm2l* function may be more crucial for development of the endocardium than for the other major vessels we investigated.

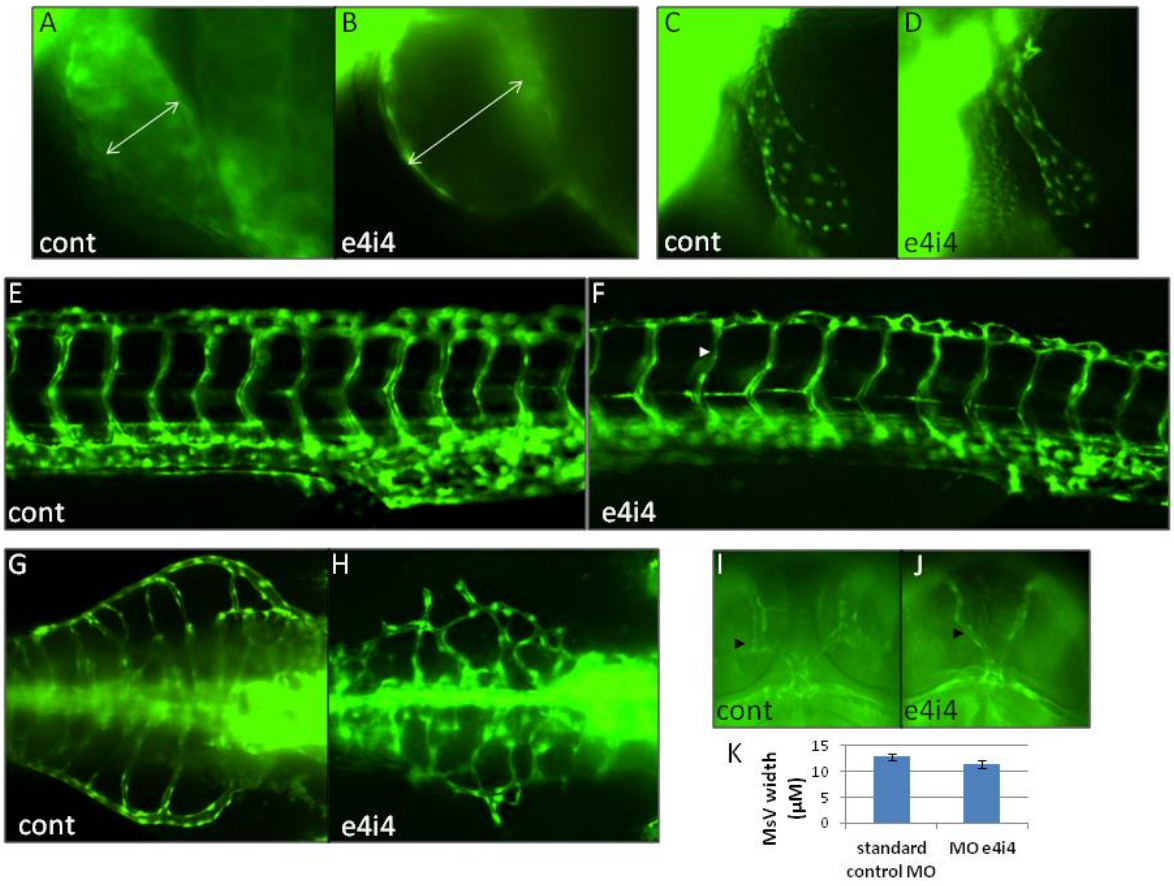

Figure 3.5. Effects of *ccm2l* disruption on embryonic vasculature. (A and B) At 52 hpf, control embryos have an appropriately constricted endocardium, while *ccm2l* morphants exhibit endocardial dilation. (Arrows show lumen diameter). (C and D) Morphology of the CCV at 52 hpf is generally normal in *ccm2l* morphants. (E and F) At 58 hpf, ISVs are mostly insensitive to *ccm2l* loss-of-function, although some affected embryos have ISVs that are not fully dilated (arrowhead). (G and H) At 72 hpf, SIVs in affected embryos are frequently mispatterned. (I -K) At 52 hpf, MsVs are approximately the same width in control embryos and affected embryos (arrowheads). A and B are 20x magnification; C-J are 10x magnification. A-F are taken from a lateral perspective with anterior to the left; G and H are dorsal images with anterior to the right. I and J are taken from a dorsal perspective with the anterior end tilted upward. In K, error bars represent standard error. Cont, standard control morpholino.

ccm2l *is an enhancer of the Heg-CCM pathway*

The heart phenotype conferred by *ccm2l* morpholino injection is consistent with a role for *ccm2l* in the Heg-CCM pathway. To directly test whether there is a genetic interaction between *ccm2l* and the Heg-CCM pathway, we undertook a morpholino co-injection approach that has

previously been used to demonstrate genetic interactions among *ccm1*, *ccm2*, and *heg* (Mably et al., 2006). We determined subphenotypic doses of *ccm2l* and *ccm1* morpholinos and injected them either together or individually with control morpholino. At 52 hpf, we assayed embryos for the dilated heart phenotype we observe in *heg*, *ccm1*, and *ccm2* mutants. Embryos were scored under light microscopy as either wildtype, intermediate, or severe. Wildtype embryos have heart morphology and blood circulation comparable to uninjected embryos; intermediate embryos have moderately dilated hearts and inflow tracks and often sluggish circulation; and severe embryos have largely dilated hearts and inflow tracts and completely lack circulation of red blood cells (Figure 3.6A). Due to the somewhat subjective nature of this rubric and the extreme sensitivity of the experiment's outcome to the precise injection volume each embryo receives, the morpholino solutions were blinded to the experimenter prior to injection and revealed after all embryos were scored.

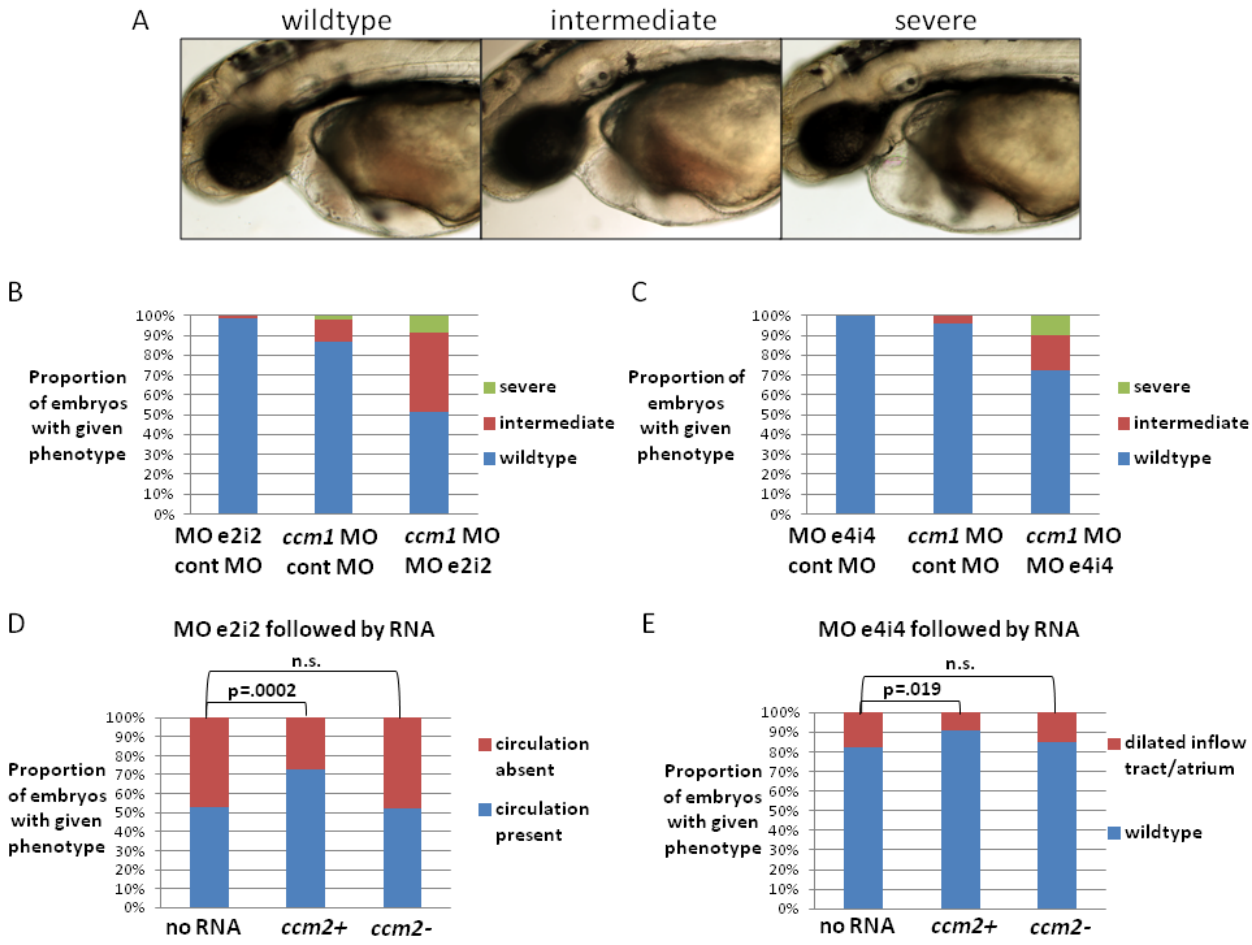

Figure 3.6. *ccm2l* interacts genetically with the Heg-CCM pathway. (A-C) For enhancer experiments, embryos were injected with low doses of control morpholino, *ccm1* morpholino and *ccm2l* morpholino in pairwise combinations and assayed at 52 hpf for heart morphology and function. (A) Embryos classified as "wildtype" have a heart and inflow tract comparable to uninjected embryos and strong blood circulation. "Intermediate" embryos exhibit moderate dilation of the atrium and inflow tract but maintain some level of blood circulation. "Severe" embryos have extreme dilation of the heart and inflow tract and lack blood circulation. (B and C) Compared to a control morpholino with no predicted cellular targets, MO e2i2 and MO e4i4 both increase the proportion of moderate and severe phenotypes in embryos sensitized with *ccm1* morpholino. Images of embryos were taken at 10x magnification from a lateral perspective with anterior to the left. Graphs represent data pooled from at least three independent experiments. For each group, n>98 embryos. (D,E) For rescue experiments, embryos were injected with *ccm2l* morpholino and subsequently injected with mRNA transcribed *in vitro* from either wildtype *ccm2* cDNA (*ccm2+*) or from cDNA corresponding to the *ccm2* mutant allele *ccm2*^{m201}(*ccm2-*). (D) *ccm2*^{wt} RNA rescued circulation in a significant proportion of embryos injected with MO e2i2, while *ccm2*^{m201} RNA did not. (E) Similarly, *ccm2*^{wt} RNA but not *ccm2*^{m201} RNA rescued heart and inflow tract morphology in a significant proportion of embryos injected with MO e4i4. Embryos exhibiting an enlarged inflow tract and/or enlarged atrium were labeled as "dilated inflow tract/atrium." Graphs represent data pooled from three

(Figure 3.6, continued) independent experiments. For each group, n>130 embryos. p-values are calculated from a 2x2 contingency table using Fisher's exact test. n.s., not significant.

We found that both *ccm2l* morpholinos enhance the dilated heart phenotype in embryos sensitized with *ccm1* morpholino. In experiments with MO e2i2, 49% of embryos receiving *ccm1* and *ccm2l* morpholinos had either intermediate or severe phenotypes, while only 15% of embryos that received *ccm1* morpholino with the equivalent amount of control morpholino had those phenotypes. Just 2% of embryos receiving MO e2i2 with control morpholino had a heart phenotype (Figure 3.6B). In experiments with MO e4i4, 28% of embryos receiving *ccm1* and *ccm2l* morpholinos had either intermediate or severe phenotypes, while only 4% of embryos that received *ccm1* morpholino with the equivalent amount of control morpholino had those phenotypes. No embryos injected with MO e4i4 and control morpholino developed abnormal heart phenotypes (Figure 3.6C). We conclude that *ccm2l* is an enhancer of the Heg-CCM heart phenotype.

ccm2 *overexpression partially rescues* ccm2l *morphant phenotypes*

Due to the high degree of homology between Ccm2 and Ccm2l, our observation that their knockdown confers similar phenotypes, and our finding that *ccm2l* knockdown can enhance the heart phenotype in *ccm1* morpholino-sensitized embryos, we hypothesized that *ccm2* and *ccm2l* have overlapping *in vivo* functions. To test this hypothesis, we attempted to rescue *ccm2l* morpholino-injected embryos with synthetic *ccm2* mRNA. Since the severity of phenotype caused by our *ccm2l* morpholinos is sensitive to the volume of morpholino received by the embryo, we used a double-injection approach to insure that all groups, on average, received the same amount of *ccm2l* morpholino. First we injected a large pool of embryos with *ccm2l*

morpholino and then randomly divided the pool into three groups. One group was re-injected with wildtype *ccm2* mRNA, the second group was re-injected with *ccm2* mRNA transcribed from a loss-of-function allele isolated from the zebrafish mutant vtn^{m201} as a negative control, and the third group did not receive a second injection. At 52 hpf, embryos were assayed in a blind fashion.

In experiments with MO e2i2, we used circulation down the trunk of the embryo as a functional readout for cardiovascular rescue. Embryos injected with only MO e2i2 or MO e2i2 and $ccm2^{m201}$ mRNA had blood circulation at rates of 53% and 52%, respectively. In contrast, embryos that received MO e2i2 and $ccm2^{wt}$ mRNA had circulation at a frequency of 73% (Figure 3.6D). We observed the same trend with MO e4i4. In rescue experiments with this morpholino, we scored embryos by heart and inflow tract morphology rather than blood circulation because MO e4i4 exhibits low penetrance and rarely causes circulatory block. We found that 82% and 85% of embryos injected with only MO e4i4 or MO e4i4 and $ccm2^{m201}$ mRNA, respectively, had normal hearts and inflow tracts. However, 91% of embryos that received MO e4i4 and $ccm2^{wt}$ mRNA had normal hearts and inflow tracts (Figure 3.6E). For both morpholinos, rescue achieved by $ccm2^{wt}$ mRNA was statistically significant, whereas any rescue achieved by $ccm2^{m201}$ mRNA was not.

Ccm2l binds Ccm1

Next, we sought a molecular explanation for our phenotypic results linking *ccm2l* to the Heg-CCM pathway. Based on its homology to Ccm2, which is known to bind Ccm1 (Zawistowski et al., 2005; Zhang et al., 2007), we hypothesized that Ccm2l binds Ccm1 as well. To test this hypothesis, we overexpressed epitope-tagged versions of Ccm1 and Ccm2l in 293T

cells, and then immunoprecipitated Ccm1 and blotted for Ccm2l. As a positive control, we performed the same experiment with Ccm1 and Ccm2. We found that both HA-ccm2 and HA-ccm2l bind FLAG-ccm1 (Figure 3.7). Since we previously showed that *ccm1* and *ccm2l* are both expressed in the heart (Figure 3.1D), this interaction in cell culture likely recapitulates an endogenous interaction.

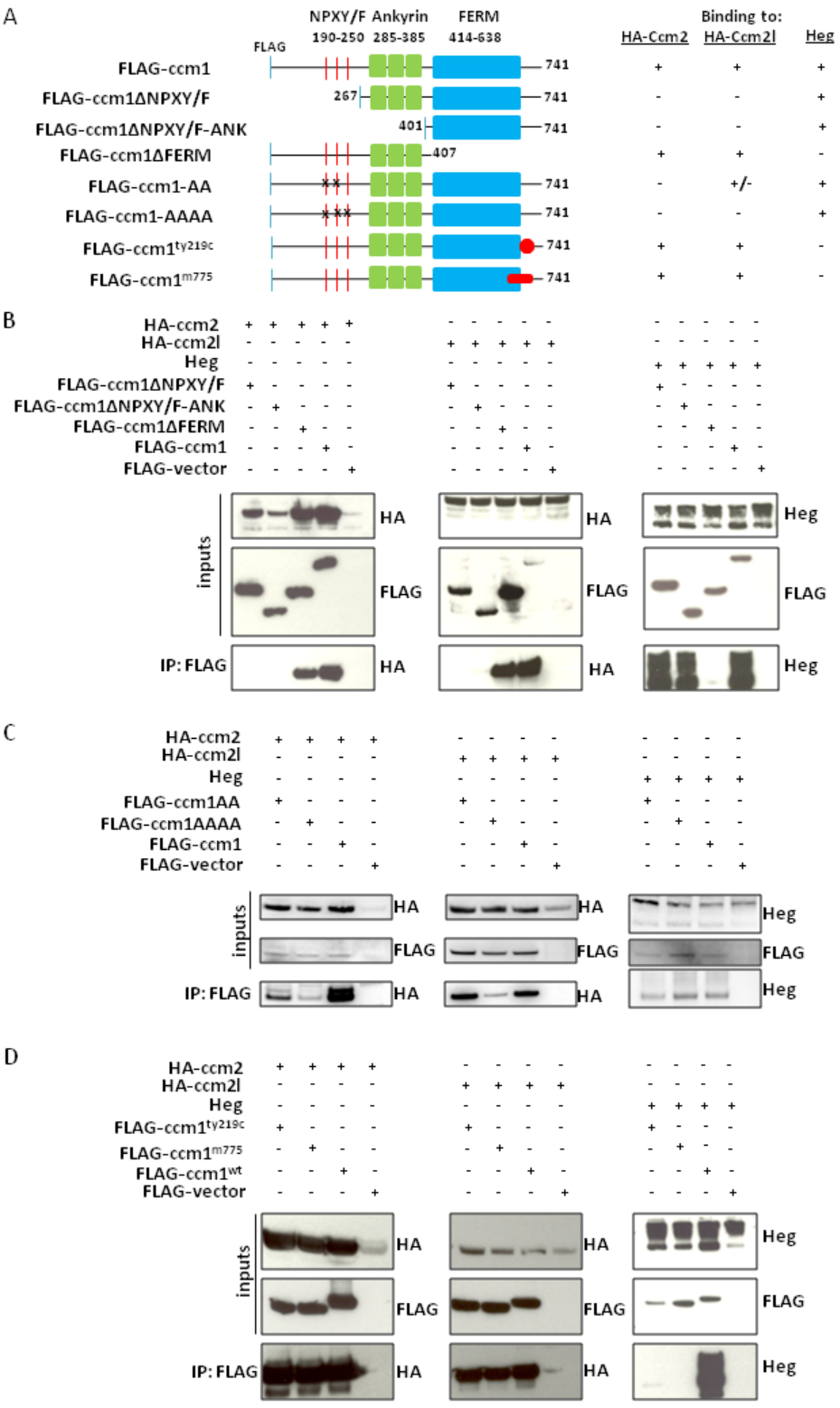
A
NPXY/F Ankyrin FERM
190-250 285-385 414-638
FLAG
Binding to:
HA-Ccm2 HA-Ccm2l Heg
FLAG-ccm1
FLAG-ccm1ΔNPXY/F
FLAG-ccm1ΔNPXY/F-ANK
FLAG-ccm1ΔFERM
FLAG-ccm1-AA
FLAG-ccm1-AAAA
FLAG-ccm1ty219c
FLAG-ccm1m775
741
267
401
407
B
HA-ccm2
HA-ccm2l
Heg
FLAG-ccm1ΔNPXY/F
FLAG-ccm1ΔNPXY/F-ANK
FLAG-ccm1ΔFERM
FLAG-ccm1
FLAG-vector
inputs
IP: FLAG
HA
FLAG
Heg
C
HA-ccm2
HA-ccm2l
Heg
FLAG-ccm1AA
FLAG-ccm1AAAA
FLAG-ccm1
FLAG-vector
D
HA-ccm2
HA-ccm2l
Heg
FLAG-ccm1ty219c
FLAG-ccm1m775
FLAG-ccm1wt
FLAG-vector

Figure 3.7

Figure 3.7 (Continued). Biochemical interactions among proteins of the Heg-CCM pathway. (A) Schematic of all Ccm1 constructs used for co-immunoprecipitation experiments and a summary of binding results. (B) FLAG-ccm1 and FLAG-ccm1ΔFERM co-immunoprecipitate HA-ccm2 and HA-ccm2l, while the N-terminal Ccm1 deletion proteins do not bind HA-ccm2 and HA-ccm2l. In contrast, FLAG-ccm1ΔFERM does not co-immunoprecipitate Heg, while the N-terminal Ccm1 deletion proteins do. (C) HA-ccm2 binding to FLAG-ccm1 is severely weakened by mutation of Ccm1's two NPXY motifs and further disrupted by mutations in the NPXF motif. The strength of the interaction between HA-ccm2l and FLAG-ccm1 is unaffected by mutation of Ccm1's NPXY motifs but is severely diminished when all three NPXY/F motifs are mutated. Heg-Ccm1 interactions appear unaffected by mutation of either two or all three NPXY/F motifs in Ccm1. (D) The mutant Ccm1 proteins FLAG-ccm1^{ty219c} and FLAG-ccm1^{m775} bind HA-ccm2 and HA-ccm2l as well as wildtype FLAG-ccm1 does, but they do not bind Heg.

To further define the interaction between Ccm2l and Ccm1, we performed a deletion analysis to determine which domains of Ccm1 bind Ccm2l. We generated two N-terminal Ccm1 deletion constructs, one lacking the three NPXY/F motifs and the other lacking these motifs as well as the ankyrin repeats, and a C-terminal deletion construct lacking the FERM domain. All these constructs contain an N-terminal FLAG tag (Figure 3.7A). In the 293T cell overexpression system, we found that protein generated from the C-terminal deletion construct, FLAG-ccm1ΔFERM, efficiently bound HA-ccm2l. In contrast, FLAG-ccm1ΔNPXY/F and FLAG-ccm1ΔNPXY/F-ANK did not bind HA-ccm2l (Figure 3.7B). We observed the same result for Ccm1 binding to Ccm2 (Figure 3.7B), consistent with others' work demonstrating an interaction between the N-terminal domain of human CCM1 and CCM2 (Zhang et al., 2007).

We also performed the same deletion analysis to determine which domains of Ccm1 are necessary to bind Heg, using a polyclonal antibody against Heg. We found that Ccm1 proteins with N-terminal deletions efficiently co-immunoprecipitate Heg. In contrast, Ccm1 protein lacking the FERM domain does not (Figure 3.7B). We saw the same result when we replaced full-length Heg with Heg protein lacking its entire extracellular domain (Figure 3.8). Thus, the C-terminal FERM domain-containing region of Ccm1 is necessary and sufficient to bind the

intracellular domain of Heg. These results are in contrast to Ccm1's interactions with Ccm2 and Ccm2l, for which the C-terminal region of Ccm1 is dispensable but the N-terminal region is essential. Consistent with our studies of the zebrafish proteins, it was recently shown that human HEG1 interacts with the FERM domain of CCM1 (Gingras et al., 2012).

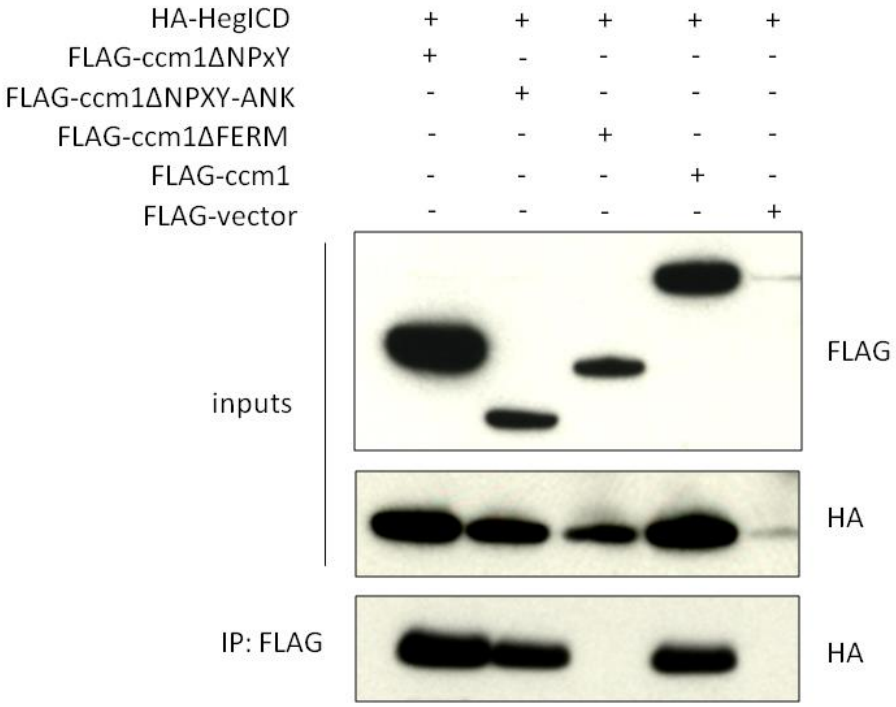

Figure 3.8. The FERM domain of Ccm1 is necessary and sufficient to bind the intracellular domain of Heg. FLAG-tagged Ccm1 deletion constructs were cotransfected with a HA-tagged construct corresponding to the intracellular domain of Heg (HA-HegICD). Protein complexes were immunoprecipitated with FLAG antibody and blotted for FLAG and HA. As with full-length Heg, the FERM domain of Ccm1 is necessary and sufficient to co-immunoprecipitate HA-HegICD.

The N-terminal region of zebrafish Ccm1 contains two NPXY motifs and one NPXF motif. Since Ccm2l contains a putative PTB domain, we hypothesized that the Ccm2l-Ccm1 interaction requires these motifs. To test this hypothesis, we generated two mutant *ccm1*

constructs (Figure 3.7A). In the first, FLAG-ccm1-AA, we altered both NPXY motifs by mutating the tyrosine residue in each to alanine. The second, FLAG-ccm1-AAAA, contains those mutations as well as two mutations in the NPXF motif. We doubly mutated the NPXF motif because the residue occupying the third position ("X") is a tyrosine. Since either the tyrosine or the phenylalanine could be mediating a protein binding interaction, we converted both to alanine. We found that FLAG-ccm1-AA binds HA-ccm2l as strongly as wildtype FLAG-ccm1, but binding of FLAG-ccm1-AAAA to HA-ccm2l is extremely diminished. In contrast, we found that the interaction between FLAG-ccm1-AA and HA-ccm2 is diminished relative to the interaction between wildtype FLAG-ccm1 and HA-ccm2, and that the interaction between FLAG-ccm1-AAAA and HA-ccm2 is weaker still (Figure 3.7C). Thus, the NPXY motifs of Ccm1 are required for strong binding of Ccm1 to Ccm2 but dispensable for binding of Ccm1 to Ccm2l. As a control, we also tested the interactions between Ccm1 NPXY/F mutant proteins and Heg. Consistent with our finding that the N-terminal region of Ccm1 is not required for binding to Heg, FLAG-ccm1-AA and FLAG-ccm1-AAAA bind Heg as strongly as wildtype FLAG-Ccm1 (Figure 3.7C).

Finally, we sought to determine whether the defective Ccm1 proteins produced by our *san* mutant fish are capable of binding Ccm2l, Ccm2, and Heg. The mutant alleles *ccm1*^{ty219c} and *ccm1*^{m775} have a point mutation and deletion, respectively, within the 3' end of the mRNA that are predicted to disrupt the FERM domain in both cases (Mably et al., 2006) (Figure 3.7A). We subcloned these mutant alleles into expression plasmids with FLAG tags and found that both produce proteins that can bind Ccm2 and Ccm2l. However, neither mutant Ccm1 protein can bind Heg (Figure 3.7D). The FERM domain of Ccm1 has been shown to bind the small GTPase RAP1 and membrane proteins such as β-Catenin (Glading et al., 2007; Liu et al., 2011). We

hypothesize that the *san*^{m775} and *san*^{ty219c} mutant embryos exhibit their heart phenotype owing to an inability of Ccm1 to bind these proteins as well as Heg, rather than an inability to bind Ccm2 and Ccm2l.

Discussion

ccm2l *is required for normal cardiovascular development*

We identified Ccm2l as a novel, conserved protein bearing considerable identity to Ccm2, and performed a loss-of-function analysis using two nonoverlapping morpholinos targeted to exon-intron junctions in the *ccm2l* pre-mRNA. *ccm2l* morphants exhibit dilation of the atrium and inflow tract and in severely affected embryos reduced or absent blood circulation. The heart and inflow tract phenotypes we observe in *ccm2l* morphants are reminiscent of but less severe than the phenotypes in *san*, *vtn*, and *heg* mutants. *ccm2l* morphants may have a more mild heart phenotype than these mutants because *ccm2l* has a more subtle role in heart development, or the difference could simply be a reflection of incomplete *ccm2l* knockdown. In the future, generation of a *ccm2l* null mutant will be crucial to resolving this ambiguity.

Morpholino disruption of *ccm2l* also confers subtle defects in other regions of the vasculature; in *ccm2l* morphants, a small number of ISVs fail to lumenize, and many SIVs have unusual growth patterns. The ISV and SIV phenotypes may be due to compromised blood flow in the embryo, since *sih* mutants, which have no blood circulation, have more severe versions of these phenotypes (Hogan et al., 2008; Mably and Childs, 2010). While we favor the interpretation that the primary function of *ccm2l* is to regulate heart morphology and the extra-cardiac vascular defects in *ccm2l* morphants are due to reduced blood circulation caused by heart

dilation, we cannot yet rule out the possibility that *ccm2l* functions directly in vessels outside the heart.

Our *in situ* hybridization data showing *ccm2l* expression in the notochord and ICM do not correlate with our findings that *ccm2l* is essential for heart development. While it is possible that *ccm2l* could regulate heart morphogenesis from a distant location, we believe the more likely explanation for the discrepancy between expression pattern and phenotype is that our *in situ* hybridization protocol is insufficiently sensitive to detect *ccm2l* in the heart. In support of this reasoning, we can detect by RT-PCR *ccm2l* transcript in hearts dissociated from 2 dpf embryos. The case with *ccm1* is similar; *ccm1* is required for heart development and is detectable in purified hearts by RT-PCR, yet we have been unable to detect *ccm1* expression in the embryonic heart by *in situ* hybridization. Based on our phenotypic and RT-PCR data, as well as the literature in the field, we think that the Heg-CCM pathway, including *ccm2l*, has a tissue-autonomous function in the heart's endocardium. Tissue-specific manipulations of the Heg-CCM pathway in zebrafish will be required to demonstrate this.

ccm2l *is a component of the Heg-CCM pathway*

We conclude that *ccm2l* is a component of the Heg-CCM pathway based on four lines of evidence. First, disruption of *ccm2l* by morpholino injection causes dilation of the atrium and inflow tract. These phenotypes are less severe than those conferred by knockdown of *ccm1*, *ccm2,* or *heg,* but qualitatively similar. Second, mild knockdown of *ccm2l* enhances the dilated heart phenotype in embryos treated with a subphenotypic dose of *ccm1* morpholino. This morpholino co-injection technique was previously used to link *heg* to the CCM pathway (Mably et al., 2006), and that finding was subsequently validated by genetic and biochemical

experiments in mouse (Kleaveland et al., 2009). Third, *ccm2l* knockdown phenotypes can be partially rescued by overexpression of *ccm2*, suggesting that the two genes have partially overlapping *in vivo* functions. Fourth, Ccm2l protein can bind Ccm1.

We propose a model in which Ccm2 and Ccm2l function similarly in the Heg-CCM complex (Figure 3.6). Both Ccm2 and Ccm2l bind the N-terminal region of Ccm1 through Ccm1's NPXY/F motifs, and we speculate that there is overlap between the downstream signaling events triggered by both interactions. In our model, when *ccm2l* is knocked down, exogenously supplied *ccm2* can recover the downstream signaling events that are common to the two complexes. Thus, overexpression of *ccm2* can rescue *ccm2l* morphant defects in a significant proportion of embryos. Our rescue data are also consistent with models in which *ccm2* functions downstream of *ccm2l*, but we favor the interpretation that they have interchangeable *in vivo* functions because of their structural similarity and our finding that Ccm2l, like Ccm2, binds Ccm1.

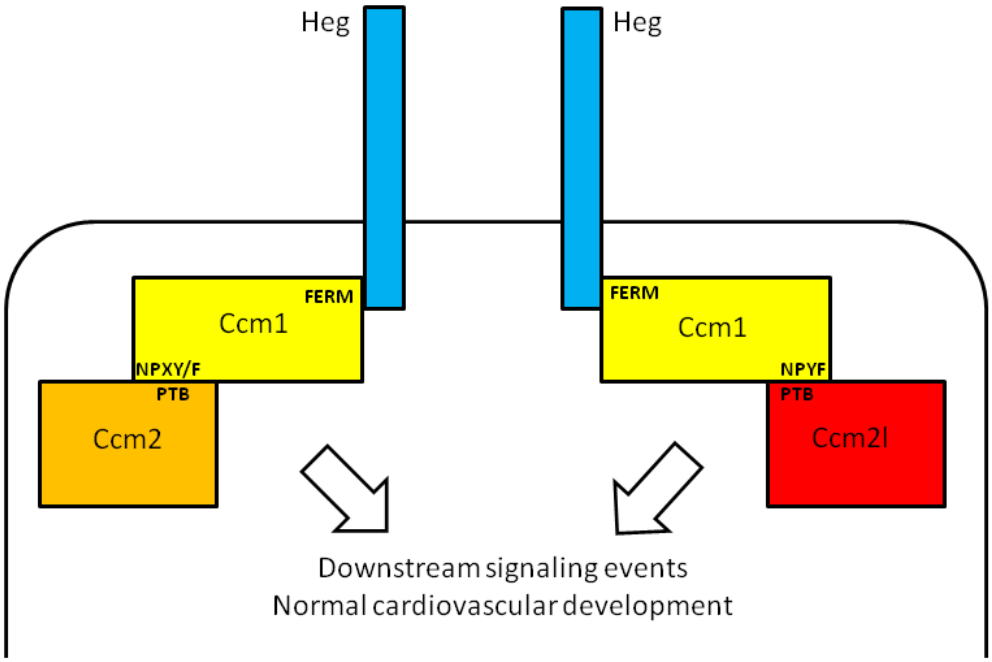

Figure 3.9. Model for the function of *ccm2l* in cardiovascular development. In our model, Ccm2l binds Ccm1 through Ccm1's N-terminal region. When the two NPXY motifs in Ccm1 are disrupted, the NPYF motif is sufficient to allow binding between Ccm1 and Ccm2l. This differs from the Ccm2-Ccm1 interaction, for which the NPXY motifs are required for full-strength binding. We hypothesize that although the NPXY/F motif requirements for the Ccm1-Ccm2l and Ccm1-Ccm2 interactions differ, the two complexes transduce partially overlapping signals. Thus, when Ccm2l levels are reduced, exogenously supplied Ccm2 can rescue heart morphology and blood circulation in a substantial proportion of embryos. The downstream signaling events common to the Ccm1-Ccm2 and Ccm1-Ccm2l interactions are essential for normal cardiovascular development, and in their absence the endocardium and inflow tract become dilated and blood circulation is compromised.

The molecular details of how Ccm2l interacts with other proteins in the Heg-CCM pathway are unknown. For example, it is unclear whether Ccm1 binds to Ccm2 and Ccm2l in a mutually exclusive manner *in vivo*, or whether Ccm2 and Ccm2l can simultaneously bind Ccm1. It is interesting to note here that the first two NPXY/F motifs in Ccm1 are jointly necessary for binding to Ccm2 but dispensable for binding to Ccm2l, which raises the possibility that Ccm2

and Ccm2l bind different NPXY/F motifs *in vivo* and might be able to bind Ccm1 simultaneously. Finer mutational analysis of the NPXY/F motifs in Ccm1 and biochemical characterization of *in vivo* Heg-CCM complexes will be required to resolve this question. Additionally, more analysis will be required to determine whether the third NPXY/F motif in Ccm1 is the site of Ccm2l binding, or whether due to redundancy, any NPXY/F motif by itself would be sufficient for binding to Ccm2l.

The third NPXY/F motif, the only one of the three motifs with a phenylalanine (F) instead of a tyrosine (Y) in the fourth position, is also interesting for another reason. In general, NPXY and NPXF motifs bind similar targets but only NPXY motifs can be regulated by tyrosine phosphorylation. However, in Ccm1, the third position in the NPXF motif is occupied by a conserved tyrosine, and a recent mass spectrometry study found that this residue was the only detectable phosphotyrosine in human CCM1 (Kim et al., 2011). In future studies it will be valuable to determine whether phosphorylation at this site regulates binding of Ccm1 to Ccm2 and/or Ccm2l.

ccm2l *in zebrafish and in mouse*

While this paper was under review, our colleagues published a study of the function of the mouse ortholog of *ccm2l* (Zheng et al., 2012). Some of the findings of Zheng et al. on the role of *Ccm2L* in mouse are consistent with our findings on the role of *ccm2l* in zebrafish, and some are different. Zheng *et al.* generate a *Ccm2L* knockout mouse and find that it is viable with no gross cardiovascular defects, unlike *ccm2l* morpholino-injected zebrafish embryos that exhibit cardiac dilation. However, in a $Ccm2L^{-/-}$ background, the $Heg1^{-/-}$ phenotype is enhanced; $Heg1^{-/-}$;$Ccm2L^{+/-}$ mice can survive to birth, while $Heg1^{-/-}$;$Ccm2L^{-/-}$ animals die in utero from cardiac

defects. This elegant genetic experiment is analogous to our morpholino co-injection experiments, in which we find that slight knockdown of *ccm2l* can enhance the cardiac defects in embryos sensitized with a low dose of *ccm1* morpholino. Thus, in both zebrafish and mouse, knockdown of *Ccm2L* enhances heart defects in embryos that already have a hit to the Heg-CCM pathway. Interestingly, in mouse, this enhancement can be suppressed by loss of one allele of *Ccm2*. That is, $Heg1^{-/-}$;$Ccm2L^{-/-}$;$Ccm2^{+/+}$ mice invariably die *in utero,* but a significant proportion of $Heg1^{-/-}$;$Ccm2L^{-/-}$;$Ccm2^{+/-}$ mice survive until birth. These genetic data arguing for antagonistic functions for *Ccm2* and *Ccm2L* contrast with our zebrafish data showing rescue of *ccm2l* knockdown phenotypes by overexpression of *ccm2.*

We hypothesize that the difference in the relationships between *ccm2* and *ccm2l* in zebrafish and mouse is due to the disparate mechanisms of heart growth that operate in the two species. Zheng et al. show that $Heg1^{-/-}$;$Ccm2L^{-/-}$ hearts have a reduction in both trabeculation and expression of growth factors known to be secreted by the endocardium to promote myocardial proliferation. As a result, embryos die from inadequate heart growth, a phenotype that can be rescued by loss of one *Ccm2* allele. In zebrafish, however, neither trabeculation nor myocardial proliferation are prominent features of development during the stages of embryogenesis we examine. Trabeculation in the zebrafish ventricle does not begin until 72 hpf (Liu et al., 2010), a time point outside of the scope of our experiments. Although the number of cardiomyocytes increases between 24 and 48 hpf, proliferating cardiomyocytes are scarce; instead, the main mechanism of heart growth is the addition of newly differentiated cardiomyocytes (de Pater et al., 2009). Given the absence of trabeculation and significant myocardial proliferation, we believe the control of heart development by competitive interactions between *Ccm2* and *Ccm2L* observed by Zheng *et al.* in mouse would likely not be conserved in

the early zebrafish embryo. It is also possible that some of the apparently species-specific differences are due to different methods of gene knockdown. In the future, it will be extremely valuable to analyze the function of *ccm2l* using a zebrafish null mutant.

The zebrafish heart as a model for CCM disease

In humans, loss-of-function mutations in *CCM1* and *CCM2* cause vascular malformations of the nervous system called CCMs. CCMs share certain features with *ccm1* and *ccm2* mutant zebrafish hearts. In both cases, vessels become severely dilated and electron microscopy reveals defects in the formation of tight junctions between endothelial cells (Kleaveland et al., 2009; Wong et al., 2000). Owing to the genetic and cell biological similarities between the dilated heart phenotype in zebrafish embryos and human CCMs, we propose that the zebrafish heart has promise as a model to understand CCM disease. In one human genetics study, 94% and 57% of patients with familial and sporadic CCM disease, respectively, had mutations in the coding regions of the three known CCM-associated genes (Denier et al., 2006). Thus, there are likely more malformation-causing genes to be found. Moreover, CCMs range from asymptomatic to fatal, so even in patients with known disease-causing mutations there may be other genetic modifiers that influence disease severity. It stands to reason that genes that modify the *ccm1* and *ccm2* loss-of-function heart phenotypes in zebrafish may also influence CCM pathogenesis in humans. In our studies, we identify *ccm2l* as an enhancer of the dilated heart phenotype in the zebrafish embryo. We propose that the human homolog of *ccm2l*, *C20ORF160*, is an intriguing candidate gene to be investigated for mutations in patients with CCM disease of unknown genetic etiology or in patients with characterized mutations but unusually severe disease progression.

Conclusions

We conclude that *ccm2l* is essential for cardiovascular development in zebrafish due to its function in the Heg-CCM pathway. When *ccm2l* is knocked down, the embryonic atrium and inflow tract become dilated and blood flow is compromised. Slight perturbation of *ccm2l* enhances the dilated heart phenotype in embryos sensitized by morpholino against *ccm1*, defining *ccm2l* as an enhancer of the Heg-CCM pathway. Overexpression of *ccm2* partially rescues *ccm2l* morphant defects, which suggests that *ccm2* and *ccm2l* have overlapping *in vivo* functions. *ccm2l* and *ccm1* are both expressed in the heart, and Ccm2l protein binds Ccm1 in an interaction that requires Ccm1's NPXY/F motifs; however, unlike Ccm2, Ccm2l can bind Ccm1 even when the first two of the three NPXY/F motifs are mutated. Based on the role of *ccm2l* in the Heg-CCM pathway in zebrafish, the human ortholog of *ccm2l*, *C20ORF160*, may be relevant to human CCM disease.

Works cited

Bergametti, F., Denier, C., Labauge, P., Arnoult, M., Boetto, S., Clanet, M., Coubes, P., Echenne, B., Ibrahim, R., Irthum, B., Jacquet, G., Lonjon, M., Moreau, J.J., Neau, J.P., Parker, F., Tremoulet, M., Tournier-Lasserve, E., 2005. Mutations within the programmed cell death 10 gene cause cerebral cavernous malformations. American journal of human genetics 76, 42-51.

Boulday, G., Blecon, A., Petit, N., Chareyre, F., Garcia, L.A., Niwa-Kawakita, M., Giovannini, M., Tournier-Lasserve, E., 2009. Tissue-specific conditional CCM2 knockout mice establish the essential role of endothelial CCM2 in angiogenesis: implications for human cerebral cavernous malformations. Dis Model Mech 2, 168-177.

Burns, C.G., MacRae, C.A., 2006. Purification of hearts from zebrafish embryos. Biotechniques 40, 274, 276, 278 passim.

Crose, L.E., Hilder, T.L., Sciaky, N., Johnson, G.L., 2009. Cerebral cavernous malformation 2 protein promotes smad ubiquitin regulatory factor 1-mediated RhoA degradation in endothelial cells. The Journal of biological chemistry 284, 13301-13305.

de Pater, E., Clijsters, L., Marques, S.R., Lin, Y.F., Garavito-Aguilar, Z.V., Yelon, D., Bakkers, J., 2009. Distinct phases of cardiomyocyte differentiation regulate growth of the zebrafish heart. Development (Cambridge, England) 136, 1633-1641.

Denier, C., Goutagny, S., Labauge, P., Krivosic, V., Arnoult, M., Cousin, A., Benabid, A.L., Comoy, J., Frerebeau, P., Gilbert, B., Houtteville, J.P., Jan, M., Lapierre, F., Loiseau, H., Menei, P., Mercier, P., Moreau, J.J., Nivelon-Chevallier, A., Parker, F., Redondo, A.M., Scarabin, J.M., Tremoulet, M., Zerah, M., Maciazek, J., Tournier-Lasserve, E., 2004. Mutations within the MGC4607 gene cause cerebral cavernous malformations. American journal of human genetics 74, 326-337.

Denier, C., Labauge, P., Bergametti, F., Marchelli, F., Riant, F., Arnoult, M., Maciazek, J., Vicaut, E., Brunereau, L., Tournier-Lasserve, E., 2006. Genotype-phenotype correlations in cerebral cavernous malformations patients. Ann Neurol 60, 550-556.

Gingras, A.R., Liu, J.J., Ginsberg, M.H., 2012. Structural basis of the junctional anchorage of the cerebral cavernous malformations complex. The Journal of cell biology 199, 39-48.

Glading, A., Han, J., Stockton, R.A., Ginsberg, M.H., 2007. KRIT-1/CCM1 is a Rap1 effector that regulates endothelial cell cell junctions. The Journal of cell biology 179, 247-254.

Gough, J., Karplus, K., Hughey, R., Chothia, C., 2001. Assignment of homology to genome sequences using a library of hidden Markov models that represent all proteins of known structure. J Mol Biol 313, 903-919.

Hilder, T.L., Malone, M.H., Bencharit, S., Colicelli, J., Haystead, T.A., Johnson, G.L., Wu, C.C., 2007. Proteomic identification of the cerebral cavernous malformation signaling complex. J Proteome Res 6, 4343-4355.

Hogan, B.M., Bussmann, J., Wolburg, H., Schulte-Merker, S., 2008. ccm1 cell autonomously regulates endothelial cellular morphogenesis and vascular tubulogenesis in zebrafish. Hum Mol Genet 17, 2424-2432.

Kim, J., Sherman, N.E., Fox, J.W., Ginsberg, M.H., 2011. Phosphorylation sites in the cerebral cavernous malformations complex. J Cell Sci 124, 3929-3932.

Kleaveland, B., Zheng, X., Liu, J.J., Blum, Y., Tung, J.J., Zou, Z., Sweeney, S.M., Chen, M., Guo, L., Lu, M.M., Zhou, D., Kitajewski, J., Affolter, M., Ginsberg, M.H., Kahn, M.L., 2009. Regulation of cardiovascular development and integrity by the heart of glass-cerebral cavernous malformation protein pathway. Nature medicine 15, 169-176.

Laberge-le Couteulx, S., Jung, H.H., Labauge, P., Houtteville, J.P., Lescoat, C., Cecillon, M., Marechal, E., Joutel, A., Bach, J.F., Tournier-Lasserve, E., 1999. Truncating mutations in CCM1, encoding KRIT1, cause hereditary cavernous angiomas. Nat Genet 23, 189-193.

Lawson, N.D., Weinstein, B.M., 2002. In vivo imaging of embryonic vascular development using transgenic zebrafish. Dev Biol 248, 307-318.

Li, X., Zhang, R., Zhang, H., He, Y., Ji, W., Min, W., Boggon, T.J., 2010. Crystal structure of CCM3, a cerebral cavernous malformation protein critical for vascular integrity. The Journal of biological chemistry 285, 24099-24107.

Liquori, C.L., Berg, M.J., Siegel, A.M., Huang, E., Zawistowski, J.S., Stoffer, T., Verlaan, D., Balogun, F., Hughes, L., Leedom, T.P., Plummer, N.W., Cannella, M., Maglione, V., Squitieri, F., Johnson, E.W., Rouleau, G.A., Ptacek, L., Marchuk, D.A., 2003. Mutations in a gene encoding a novel protein containing a phosphotyrosine-binding domain cause type 2 cerebral cavernous malformations. American journal of human genetics 73, 1459-1464.

Liu, J., Bressan, M., Hassel, D., Huisken, J., Staudt, D., Kikuchi, K., Poss, K.D., Mikawa, T., Stainier, D.Y., 2010. A dual role for ErbB2 signaling in cardiac trabeculation. Development (Cambridge, England) 137, 3867-3875.

Liu, J.J., Stockton, R.A., Gingras, A.R., Ablooglu, A.J., Han, J., Bobkov, A.A., Ginsberg, M.H., 2011. A mechanism of Rap1-induced stabilization of endothelial cell--cell junctions. Mol Biol Cell 22, 2509-2519.

Mably, J.D., Childs, S.J., 2010. Developmental Physiology of the Zebrafish Cardiovascular System, in: Perry, S.F., Ekker, M., Farrell, A.P., Brauner, C.J. (Eds.), Zebrafish: Fish Physiology, First ed. Academic Press, London, pp. 249-287.

Mably, J.D., Chuang, L.P., Serluca, F.C., Mohideen, M.A., Chen, J.N., Fishman, M.C., 2006. santa and valentine pattern concentric growth of cardiac myocardium in the zebrafish. Development (Cambridge, England) 133, 3139-3146.

Mably, J.D., Mohideen, M.A., Burns, C.G., Chen, J.N., Fishman, M.C., 2003. heart of glass regulates the concentric growth of the heart in zebrafish. Curr Biol 13, 2138-2147.

Mariappan, D., Niemann, R., Gajewski, M., Winkler, J., Chen, S., Choorapoikayil, S., Bitzer, M., Schulz, H., Hescheler, J., Sachinidis, A., 2009. Somitovasculin, a novel endothelial-specific transcript involved in the vasculature development. Arterioscler Thromb Vasc Biol 29, 1823-1829.

Revencu, N., Vikkula, M., 2006. Cerebral cavernous malformation: new molecular and clinical insights. J Med Genet 43, 716-721.

Sahoo, T., Johnson, E.W., Thomas, J.W., Kuehl, P.M., Jones, T.L., Dokken, C.G., Touchman, J.W., Gallione, C.J., Lee-Lin, S.Q., Kosofsky, B., Kurth, J.H., Louis, D.N., Mettler, G., Morrison, L., Gil-Nagel, A., Rich, S.S., Zabramski, J.M., Boguski, M.S., Green, E.D., Marchuk, D.A., 1999. Mutations in the gene encoding KRIT1, a Krev-1/rap1a binding protein, cause cerebral cavernous malformations (CCM1). Hum Mol Genet 8, 2325-2333.

Schottenfeld, J., Sullivan-Brown, J., Burdine, R.D., 2007. Zebrafish curly up encodes a Pkd2 ortholog that restricts left-side-specific expression of southpaw. Development (Cambridge, England) 134, 1605-1615.

Stockton, R.A., Shenkar, R., Awad, I.A., Ginsberg, M.H., 2010. Cerebral cavernous malformations proteins inhibit Rho kinase to stabilize vascular integrity. J Exp Med 207, 881-896.

Voss, K., Stahl, S., Hogan, B.M., Reinders, J., Schleider, E., Schulte-Merker, S., Felbor, U., 2009. Functional analyses of human and zebrafish 18-amino acid in-frame deletion pave the way for domain mapping of the cerebral cavernous malformation 3 protein. Hum Mutat 30, 1003-1011.

Voss, K., Stahl, S., Schleider, E., Ullrich, S., Nickel, J., Mueller, T.D., Felbor, U., 2007. CCM3 interacts with CCM2 indicating common pathogenesis for cerebral cavernous malformations. Neurogenetics 8, 249-256.

Whitehead, K.J., Chan, A.C., Navankasattusas, S., Koh, W., London, N.R., Ling, J., Mayo, A.H., Drakos, S.G., Jones, C.A., Zhu, W., Marchuk, D.A., Davis, G.E., Li, D.Y., 2009. The cerebral cavernous malformation signaling pathway promotes vascular integrity via Rho GTPases. Nature medicine 15, 177-184.

Whitehead, K.J., Plummer, N.W., Adams, J.A., Marchuk, D.A., Li, D.Y., 2004. Ccm1 is required for arterial morphogenesis: implications for the etiology of human cavernous malformations. Development (Cambridge, England) 131, 1437-1448.

Wong, J.H., Awad, I.A., Kim, J.H., 2000. Ultrastructural pathological features of cerebrovascular malformations: a preliminary report. Neurosurgery 46, 1454-1459.

Yoruk, B., Gillers, B.S., Chi, N.C., Scott, I.C., 2012. Ccm3 functions in a manner distinct from Ccm1 and Ccm2 in a zebrafish model of CCM vascular disease. Dev Biol 362, 121-131.

Zawistowski, J.S., Stalheim, L., Uhlik, M.T., Abell, A.N., Ancrile, B.B., Johnson, G.L., Marchuk, D.A., 2005. CCM1 and CCM2 protein interactions in cell signaling: implications for cerebral cavernous malformations pathogenesis. Hum Mol Genet 14, 2521-2531.

Zhang, J., Rigamonti, D., Dietz, H.C., Clatterbuck, R.E., 2007. Interaction between krit1 and malcavernin: implications for the pathogenesis of cerebral cavernous malformations. Neurosurgery 60, 353-359; discussion 359.

Zheng, X., Xu, C., Di Lorenzo, A., Kleaveland, B., Zou, Z., Seiler, C., Chen, M., Cheng, L., Xiao, J., He, J., Pack, M.A., Sessa, W.C., Kahn, M.L., 2010. CCM3 signaling through sterile 20-like kinases plays an essential role during zebrafish cardiovascular development and cerebral cavernous malformations. The Journal of clinical investigation 120, 2795-2804.

Zheng, X., Xu, C., Smith, A.O., Stratman, A.N., Zou, Z., Kleaveland, B., Yuan, L., Didiku, C., Sen, A., Liu, X., Skuli, N., Zaslavsky, A., Chen, M., Cheng, L., Davis, G.E., Kahn, M.L., 2012. Dynamic regulation of the cerebral cavernous malformation pathway controls vascular stability and growth. Dev Cell 23, 342-355.

Chapter 4: Heg-CCM and ERK signaling

Attributions

The experiments in this chapter were designed by Jonathan Rosen and John Mably, and performed by Jonathan Rosen. Bobby Bolcome and Joanne Chan first observed the heart phenotype in embryos treated with CI-1040, and they provided helpful tips for working with the hsp70:mek1DD zebrafish, as well as the fish themselves.

Introduction

In all animals, signaling pathways control crucial cell functions. One important family of signaling pathways is the mitogen-activated protein kinase (MAPK) pathways, which transmit information about the extracellular environment to the cell's nucleus through ordered kinase cascades. Like the other MAPK pathways, the extracellular signal-regulated kinase (ERK) pathway is an ancient, highly conserved signaling system that is crucial to normal embryonic development and adult physiology.

The structure of the ERK pathway has been studied extensively (Figure 4.1). Activation of the ERK pathway frequently begins with binding of a growth factor to its receptor on the plasma membrane. Through intermediate scaffold proteins, activation of the receptor results in the conversion of GDP-bound Ras, the inactive form of the small GTPase, into Ras-GTP. Ras-GTP activates the kinase Raf, which in turn activates the kinases MEK1 and MEK2 by phosphorylation. Finally, MEK1 and MEK 2 activate the two ERK paralogs, ERK1 and ERK2. ERK1 and ERK2, themselves kinases, phosphorylate a dizzying array of cytoplasmic and nuclear substrates, including kinases, cytoskeletal components, and transcription factors (Roskoski, 2012).

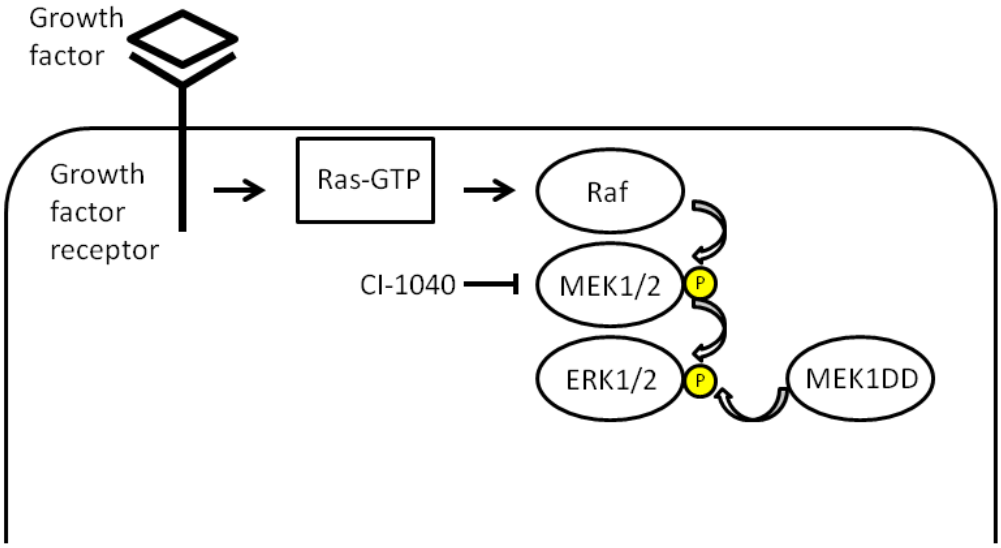

Figure 4.1. The ERK pathway. This diagram represents a simplified version of the ERK pathway and indicates where CI-1040 and the MEK1DD protein inhibit and activate the pathway, respectively. MEK1DD is constitutatively active because, unlike endogenous MEK1, it is not subject to regulation by the pathway's upstream components.

Properly regulated Erk signaling is required for normal heart development in zebrafish. Embryos injected with morpholinos targeting either *erk1* or *erk2* exhibit, amongst other severe defects, pericardial edema and possibly enlarged heart chambers (Krens et al., 2008). Similarly, sustained treatment with the MEK1/2 inhibitor PD0325901 causes pericardial edema and a blockage of circulation in many embryos (Anastasaki et al., 2012). When the upstream activator *raf1* is knocked down by morpholino injection, affected embryos exhibit enlarged atria (Razzaque et al., 2007). Conversely, when Erk is hyperactivated by global expression of a constitutatively active *mek1* construct, a proportion of embryos exhibit small, dysfunctional hearts (Bolcome and Chan, 2010).

Since *Cerebral cavernous malformation 2* (*Ccm2*) was originally discovered as a necessary component of the p38 MAPK complex (Uhlik et al., 2003), much research has been

devoted to understanding the functions of Heart of glass-Cerebral Cavernous Malformation (Heg-CCM) pathway members in regulating MAPK pathways. It has been shown that CCM1 negatively regulates ERK in human umbilical vein endothelial cells (HUVECs). Moreover, ERK is hyperactivated in resected CCM lesions, and in a model of CCM disease involving transplantation of CCM1-depleted HUVECs into mice, chemical inhibition of ERK ameliorated the HUVECs' CCM-like phenotype (Wustehube et al., 2010). Thus, there is evidence that Ccm1 negatively regulates ERK in the context of CCM disease; however, the nature of the relationship between the Heg-CCM pathway and ERK in heart development is unknown.

In this chapter, we investigate the relationship between HEG1 and ERK in HUVECs and in the developing zebrafish heart. We find that Heg and Erk interact differently in these two biological contexts. We show that Erk hyperactivation can partially rescue *heg* morphant cardiovascular defects and propose a model whereby endocardial Heg positively regulates myocardial Erk.

Materials and methods

Zebrafish experiments

Tubingen (wildtype) and hsp70:mek1DD zebrafish were used (Bolcome and Chan, 2010). Embryos from the former were maintained at 28.5 °C, while embryos from the latter were maintained at 26 °C to avoid undesired heat shock. cmlc2:mek1DD fish were generated by performing tol2 cloning with the mek1DD middle entry vector (Bolcome and Chan, 2010) and a 5' entry vector we previously generated containing the *cmlc2* promoter (Sogah et al., 2010).

Injections were performed as previously described (Rosen et al., 2009) using a previously validated morpholino against *heg* (Mably et al., 2003). Embryos were treated with 1.5 µM CI-1040 (Axon Medchem) in dimethyl sulfoxide (DMSO) or an equivalent amount of vehicle starting at 24 hpf. Heat shock was performed for 2-3 hours early on the second day of development.

Cell culture and western blotting

HUVECs were maintained and transfected and western blots were performed as described in chapter 2 of this dissertation. Phosphorylated ERK and total ERK antibodies were used on western blots as per the manufacturer's instructions (Cell Signaling Technology). GAPDH and Heg antibodies were used as described in Chapter 2 of this dissertation. Quantitative densitometry analysis of western blots was performed using ImageJ software.

Microscopy

Images of live zebrafish embryos were captured and processed as described in Chapter 2.

Results

Because depletion of CCM1 protein in HUVECs has been shown to cause an increase in ERK activation (Wustehube et al., 2010), we were interested to determine whether HEG1, which binds CCM1, also works to suppress ERK activity. We found that siRNA-mediated knockdown of HEG1 protein in HUVECs causes an increase in both phosphorylated ERK and total ERK protein when cells are starved and then stimulated with full media (Figure 4.2A). Densitometry

analysis of western blot bands revealed that although the proportion of ERK that is phosphorylated is not affected by HEG1 knockdown, the ratio of phosphorylated ERK to GAPDH is increased (Figure 4.2B). Thus, HEG1 seems to restrict the abundance of activated ERK protein not by regulating the phosphorylation of ERK, but by controlling the levels of total ERK.

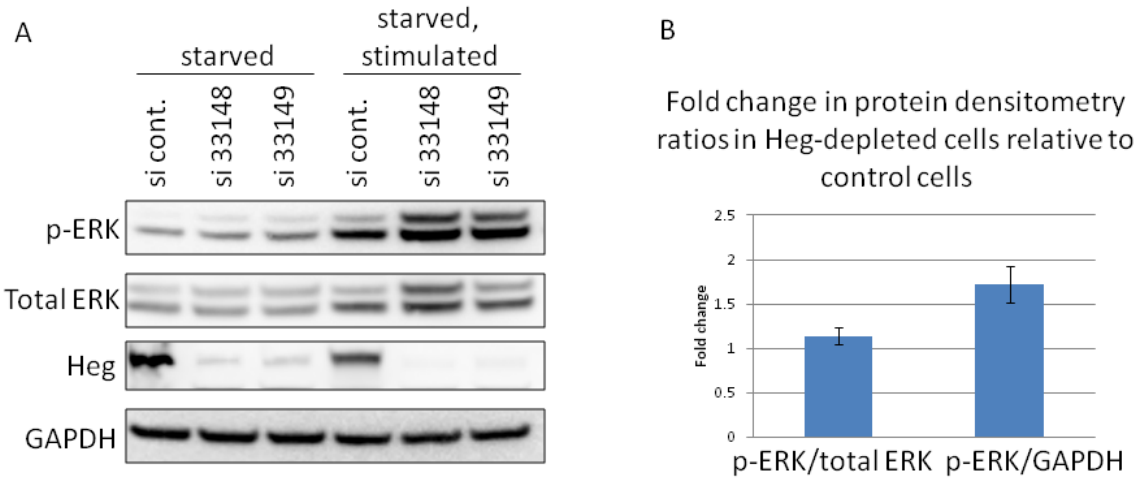

Figure 4.2. Heg knockdown increases p-ERK levels in HUVECs. (A) Knocking down HEG1 in HUVECs with two different siRNAs causes an increase in phosphorylated ERK (p-ERK) and total ERK, relative to cells transfected with negative control siRNA. (B) Densitometry analysis was performed on bands from western blot experiments comparing protein levels in HUVECs transfected with anti-HEG1 siRNA 33148 and HUVECs transfected with negative control siRNA. The p-ERK/total ERK ratio is unaffected by depletion of HEG1, but the p-ERK/GAPDH ratio is more than 1.5 fold higher in cells lacking HEG1. Error bars represent standard error from three independent experiments.

Since HEG1 negatively regulates ERK in HUVECs, we hypothesized that Heg opposes Erk in zebrafish heart development as well. According to our hypothesis, inhibition of Erk signaling ought to decrease the size of the heart, as opposed to Heg knockdown, which increases the size of the heart. Interestingly, we observed the opposite result. We incubated embryos in

CI-1040, a highly specific small molecule that inhibits Mek1 and Mek2, the two kinases that activate Erk. We frequently observed increases in the size of the atrium, reminiscent of *heg* mutant embryos (Figure 4.3A,B). Consistent with this result, it has been shown by others that global activation of Erk due to organism-wide induction of a phosphomimetic *mek1* gene, which produces a constitutatively active Mek1 protein (Mek1DD) that hyperactivates Erk, confers a severe reduction in the size of the heart (Bolcome and Chan, 2010). Thus, like Heg, Erk activity appears to restrict the size of the heart. Moreover, we generated transgenic fish in which Erk is hyperactivated just in the myocardium by tissue-specific expression of the same transgene and found that this is sufficient to cause an extreme reduction in heart size (Figure 4.3C).

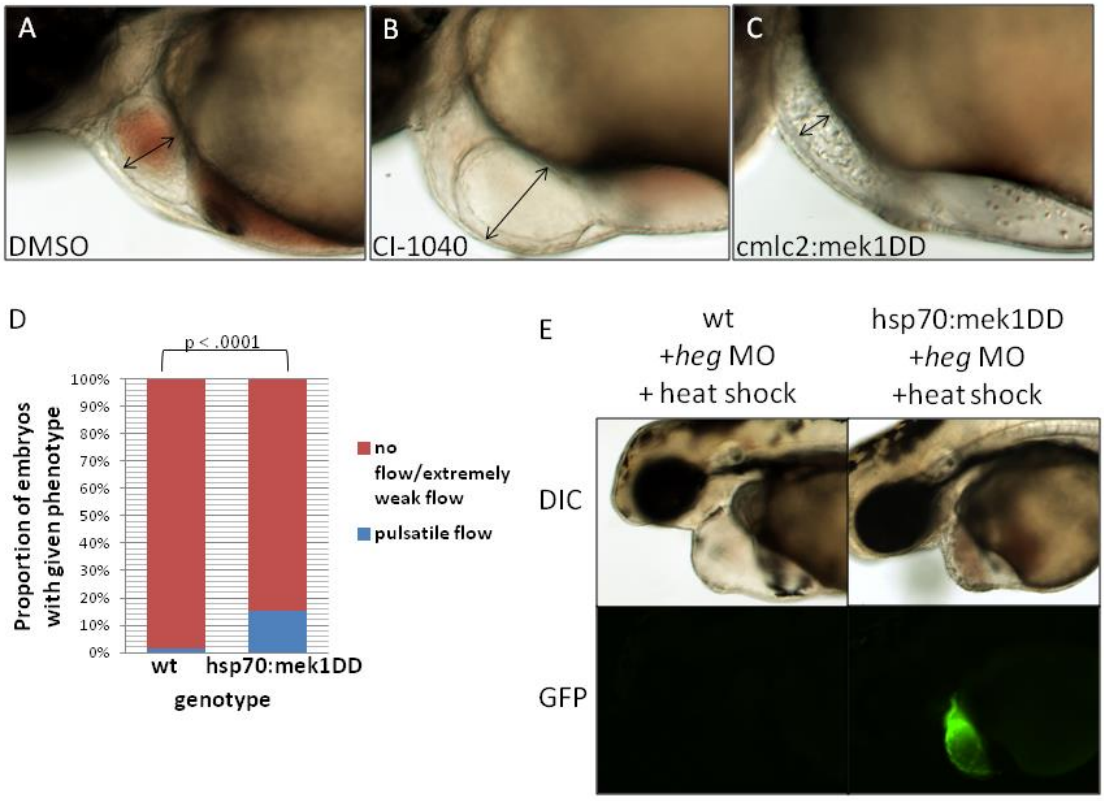

Figure 4.3. Global Erk activation rescues circulation in *heg* morphants. (A-C) Chemical inhibition of the Erk pathway causes an increase in the size of the atrium, while genetic hyperactivation of the Erk pathway causes a decrease in the size of the atrium. (D) Following *heg* knockdown, transgenic activation of Erk signaling restores circulation in a statistically significant proportion of embryos. The p-value was calculated from a 2x2 contingency table using Fisher's exact test. (E) Examples of embryos from the rescue experiments. Both embryos pictures were injected with *heg* morpholino and heat shocked; the embryo on the left was genetically wildtype and exhibited a severe heart phenotype including a lack of circulation, while the embryo on the right expressed the transgene, had heart morphology that was closer to normal, and had robust circulation of red blood cells.

Since we found that Erk and Heg regulate heart morphology in similar fashions, we sought to test the hypothesis that Erk is a downstream effector of Heg. For this experiment, we used the hsp70:mek1DD fish line, in which heat shock induction leads to global expression of Mek1DD and Erk hyperactivation (Bolcome and Chan, 2010). We crossed hsp70:mek1DD fish with wildtype fish to create clutches containing comparable numbers of transgenic and wildtype

embryos. We injected embryos with *heg* morpholino and heat shocked them early on the second day of development. At 48 hpf, we separated transgenic embryos from their wildtype siblings on the basis of whether they express the transgene's GFP reporter, and scored for circulation down the trunk of the embryo. We used circulation for our assay rather than heart morphology to distinguish whether expression of the transgene merely shrinks the big heart or actually restores cardiovascular function in *heg* morphants. We found that after heat shock, a higher proportion of transgenic embryos than wildtype embryos had circulation (Figure 4.3D). The difference between groups is modest in the sense that regardless of genotype, the majority of embryos lack circulation. However, the difference is statistically highly significant. Thus, hyperactivation of Erk partially rescues *heg* morphant cardiovascular defects.

Discussion

The relationships between Heg and Erk in HUVECs and in the zebrafish heart

In this chapter, we investigate the relationship between Heg and ERK signaling in primary endothelial cells and the zebrafish heart. We find that in HUVECs, siRNA-mediated depletion of HEG1 causes an increase in the levels of total ERK and phosphorylated ERK, suggesting an antagonistic relationship between HEG1 and ERK. Paradoxically, Heg and Erk appear to regulate zebrafish heart morphology in similar ways, such that inhibition of either causes severe dilation, raising the possibility that the two genes function cooperatively in the zebrafish heart. The notion of a cooperative interaction between the two genes is supported by our findings that Erk activation can rescue *heg* morpholino-induced circulatory block in a statistically significant proportion of embryos.

To reconcile our phenotypic results suggesting that Erk functions downstream of Heg in heart development with our data showing that HEG1 negatively regulates ERK in HUVECs, we hypothesize that when we rescue *heg* morphant embryos by globally activating Erk, the relevant Erk activity is in the myocardium. That is to say, it may be the case that in *heg* morphants there is a glut of activated Erk in the endocardium, as in HEG1-depleted HUVECs, but it is the activity of Erk in the myocardium that is controlling heart size. This hypothesis is supported by our finding that hyperactivation of Erk solely in the myocardium is sufficient to shrink the heart.

Two models to explain the rescue of heg morphant defects by Erk hyperactivation

We propose two models to explain our rescue results (Figure 4.4). In our first model, endocardial Heg positively regulates Erk activity in the myocardium, and Erk in the myocardium regulates heart morphology. When Heg is lost from the endocardium, Erk activity in the myocardium is reduced, and the heart dilates as in embryos treated with the Mek1/2 inhibitor CI-1040. It is possible that endocardial Heg, being a transmembrane protein, could directly contact the myocardium to regulate the Erk pathway at a time point before the two heart tissues are separated by extracellular matrix. Alternatively, there could be a secreted endocardial factor downstream of Heg that activates Erk in the myocardium. This model is not mutually exclusive with models for Heg-CCM function that emphasize the role of that pathway in regulating endothelial junctions and vessel structure. It may be the case that the *heg*$^{-/-}$ heart is so big because Heg constrains heart size by multiple mechanisms, all of which are lost in the mutant.

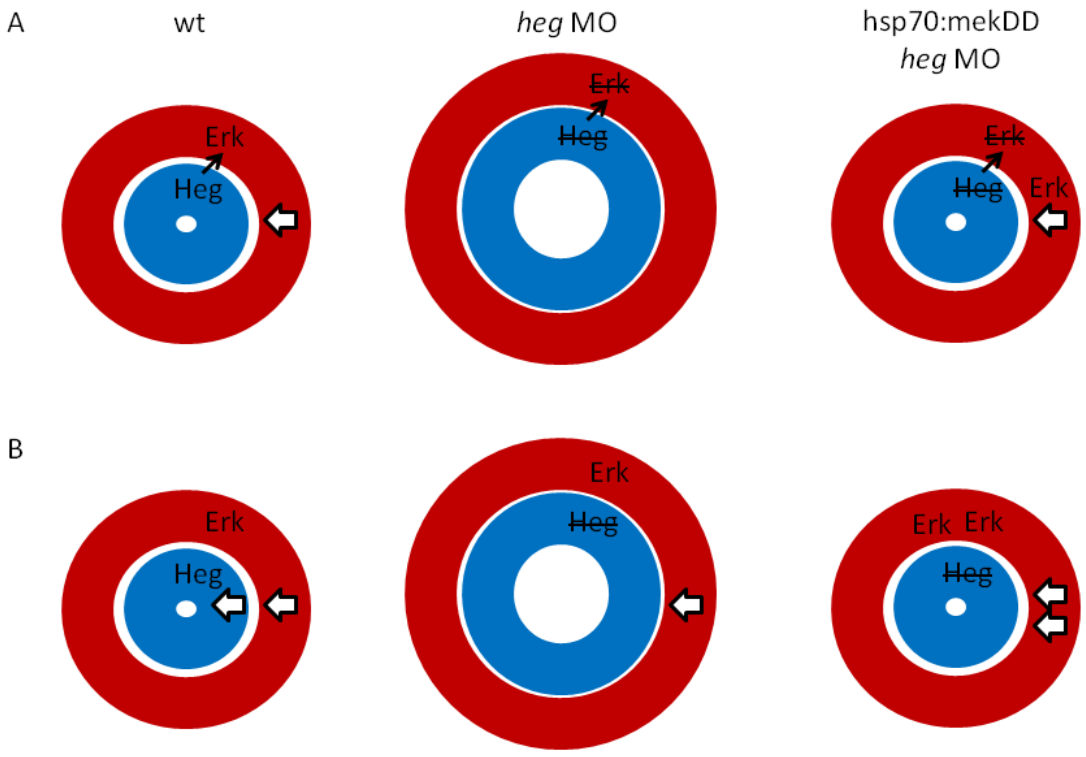

Figure 4.4. Models to explain the rescue of *heg* morphants by Erk activation. These schematics illustrate a cross-sectional view through a heart chamber, with the endocardium in blue and the myocardium in red. (A) and (B) represent two different models. (A) In a wildtype embryo, endocardial Heg activates Erk in the myocardium. Myocardial Erk constrains the size of the heart. When Heg is depleted by morpholino, Erk activity is lost from the myocardium, and the heart expands. When Erk is added back through a transgene, the myocardial Erk lost due to Heg depletion is restored, and heart size is constrained as normal. (B) In a wildtype embryo, Heg in the endocardium and Erk in the myocardium independently constrain the size of the heart. When Heg is depleted by morpholino, myocardial Erk is unaffected, but the constraining force of Erk is insufficient to prevent dilation of the heart. When Erk is added by a transgene, the extra size-constraining activity in the myocardium can make up for the same activity lost in the endocardium by Heg knockdown.

Our second model posits an indirect relationship between Heg and Erk in heart development. In this model, the Heg-CCM pathway and Erk function independently in the regulation of heart size, such that Erk activity is not reduced in the *heg* morphant. Even so, because Erk functions in the myocardium to restrict the size of the heart, experimental hyperactivation of Erk reverses the *heg* morphant phenotype.

To distinguish between these models, it will be crucial to determine whether Erk activation in the myocardium is decreased in *heg* mutants, either by comparing phosphorylated Erk or the mRNA levels of Erk transcriptional targets in wildtype and *heg* mutant embryos. If Erk activity is indeed decreased in the myocardium of *heg* mutants, that would argue for our first model. To confirm either of our models, it will also be necessary to demonstrate that myocardial-specific loss of Erk function can increase the size of the heart, as myocardial-specific Erk gain-of-function can shrink it. With the exception of a study demonstrating a non-autonomous role for Heg in regulating hepatic polarization (Sakaguchi et al., 2008), most research on the Heg-CCM pathway has focused on its tissue-autonomous functions; the project summarized in this chapter, still in its infancy, should be valuable in helping us understand Heg-CCM pathway-mediated interactions between tissues.

Works cited

Anastasaki, C., Rauen, K.A., Patton, E.E., 2012. Continual low-level MEK inhibition ameliorates cardio-facio-cutaneous phenotypes in zebrafish. Dis Model Mech 5, 546-552.

Bolcome, R.E., 3rd, Chan, J., 2010. Constitutive MEK1 activation rescues anthrax lethal toxin-induced vascular effects in vivo. Infect Immun 78, 5043-5053.

Krens, S.F., He, S., Lamers, G.E., Meijer, A.H., Bakkers, J., Schmidt, T., Spaink, H.P., Snaar-Jagalska, B.E., 2008. Distinct functions for ERK1 and ERK2 in cell migration processes during zebrafish gastrulation. Dev Biol 319, 370-383.

Mably, J.D., Mohideen, M.A., Burns, C.G., Chen, J.N., Fishman, M.C., 2003. heart of glass regulates the concentric growth of the heart in zebrafish. Curr Biol 13, 2138-2147.

Razzaque, M.A., Nishizawa, T., Komoike, Y., Yagi, H., Furutani, M., Amo, R., Kamisago, M., Momma, K., Katayama, H., Nakagawa, M., Fujiwara, Y., Matsushima, M., Mizuno, K., Tokuyama, M., Hirota, H., Muneuchi, J., Higashinakagawa, T., Matsuoka, R., 2007. Germline gain-of-function mutations in RAF1 cause Noonan syndrome. Nat Genet 39, 1013-1017.

Rosen, J.N., Sweeney, M.F., Mably, J.D., 2009. Microinjection of zebrafish embryos to analyze gene function. J Vis Exp.

Roskoski, R., Jr., 2012. ERK1/2 MAP kinases: structure, function, and regulation. Pharmacological research : the official journal of the Italian Pharmacological Society 66, 105-143.

Sakaguchi, T.F., Sadler, K.C., Crosnier, C., Stainier, D.Y., 2008. Endothelial signals modulate hepatocyte apicobasal polarization in zebrafish. Curr Biol 18, 1565-1571.

Sogah, V.M., Serluca, F.C., Fishman, M.C., Yelon, D.L., Macrae, C.A., Mably, J.D., 2010. Distinct troponin C isoform requirements in cardiac and skeletal muscle. Dev Dyn 239, 3115-3123.

Uhlik, M.T., Abell, A.N., Johnson, N.L., Sun, W., Cuevas, B.D., Lobel-Rice, K.E., Horne, E.A., Dell'Acqua, M.L., Johnson, G.L., 2003. Rac-MEKK3-MKK3 scaffolding for p38 MAPK activation during hyperosmotic shock. Nature cell biology 5, 1104-1110.

Wustehube, J., Bartol, A., Liebler, S.S., Brutsch, R., Zhu, Y., Felbor, U., Sure, U., Augustin, H.G., Fischer, A., 2010. Cerebral cavernous malformation protein CCM1 inhibits sprouting angiogenesis by activating DELTA-NOTCH signaling. Proceedings of the National Academy of Sciences of the United States of America 107, 12640-12645.

Chapter 5: Discussion

In this dissertation, I describe experiments designed to elucidate the function of the Heg-CCM pathway. Chapters 2 through 4 each contain a Discussion section that summarizes and discusses our findings. This chapter begins by highlighting findings of particular interest for further discussion, with an emphasis on future directions, and ends with a comparison between the Heart of glass-Cerebral Cavernous Malformation (Heg-CCM) pathway in zebrafish and mammals and a discussion of the utility of the zebrafish heart as a CCM disease model.

Heg undergoes a cleavage event of unknown function

We have found that the C-terminal, intracellular domain of the transmembrane protein Heg is cleaved from the full-length protein. This occurs with endogenous Heg in human umbilical vein endothelial cells (HUVECs) and when Heg is transfected in 293T cells. The former suggests that the cleavage is authentic and not an artifact of overexpression; the latter suggests that the small protein product is the result of cleavage and not alternative splicing, since alternative splicing cannot occur in RNA transcribed from a plasmid lacking introns.

The function of this cleavage event is unknown and a ripe target for future research. One hypothesis is that the cleaved fragment has activity distinct from the full-length protein, and that the cleavage of Heg is a regulated event necessary for certain outputs of the Heg-CCM pathway. One way this could occur would be if cleaved Heg were released from the plasma membrane and allowed to interact with previously inaccessible targets in the cytoplasm. The intracellular domain of Heg (HegICD) has a NPXF motif, and NPXF motifs are known to interact with PTB domains. The FERM domain of Ccm1, Heg's only known interactor, contains a PTB subdomain; surprisingly, however, the NPXF motif in HegICD is not required for the HEG1-

CCM1 interaction (Gingras et al., 2012). Perhaps HegICD's NPXF motif is involved in other, cytoplasmic interactions.

It is also possible that HegICD has activity in the nucleus. Ccm1 has been shown to have functional nuclear localization sequences (NLS) (Zawistowski et al., 2005), but its nuclear function is unknown. HegICD has no NLS, but it is interesting to speculate that Ccm1 could transport it across the nuclear membrane. Although HegICD does not have DNA binding domains, one can imagine it affecting gene expression by forming complexes with transcription factors or other DNA or chromatin regulators. The extensively studied Notch protein may serve as a useful analogy to understand Heg function. Heg and Notch are both single-pass transmembrane proteins with extracellular domains that are subject to glycosylation and contain EGF-like repeats. After Notch interacts with its transmembrane ligand, sequential cleavage events result in the release of the Notch intracellular domain (NICD) from the plasma membrane. NICD then translocates to the nucleus, where it complexes with CBF1–SU(H)–LAG1 (CSL) and the transcriptional co-activator Mastermind-like (Mml) to activate target genes (Guruharsha et al., 2012).

In the future, it will be interesting to determine whether HegICD behaves similarly to NICD. One useful approach will be to perform immunofluorescent antibody staining for endogenous HegICD to chart its localization under different conditions. If cleavage requires binding of a particular ligand to the extracellular domain of Heg, then isolation of this ligand might be a challenging but necessary task. It will also be informative to perform Edman Degradation to determine the exact site of cleavage, which might yield clues as to the regulation of that event.

Alternatively, the cleavage of Heg might be a regulatory mechanism to decrease Heg-CCM signaling. Heg is thought to anchor Ccm1 to endothelial cell junctions (Gingras et al., 2012), where it suppresses RhoA activity (Borikova et al., 2010; Stockton et al., 2010) and inhibits the expression of Wnt target genes by preventing the internalization of β-Catenin (Glading and Ginsberg, 2010). Cleavage of HegICD might lead to the release of Ccm1 from the junction, relieving to some degree the inhibition of the RhoA and Wnt pathways. Since cleavage of Heg is presumably a more rapid event than transcriptional regulation, this strategy would allow the cell to quickly respond to situations requiring the downregulation of Heg-CCM signaling.

ccm2l

We found that the novel, conserved gene *ccm2l* is required for normal heart development in the zebrafish embryo. When we knock down *ccm2l* with two different morpholinos targeted to exon-intron junctions, we observe dilation of the heart and inflow tract, and in extreme cases, a complete cessation of blood circulation. Slight knockdown of *ccm2l* can enhanced the dilated heart phenotype in embryos sensitized with a low dose of *ccm1* morpholino, overexpression of *ccm2* can partially rescue *ccm2l* morphant defects, and Ccm2l protein can bind Ccm1.

Our results led us to propose a model in which *ccm2* and *ccm2l* have partially overlapping functions in heart development. In our model, Heg-CCM protein complexes can contain either Ccm2 or Ccm2l, and these two different complexes have partially overlapping downstream signaling targets. We believe that in our rescue experiments, overexpressed *ccm2* leads to an increased number of Heg-Ccm1-Ccm2 complexes that can reach the targets normally

acted upon by the Heg-Ccm1-Ccm2l complex. This leads to rescue of cardiovascular development.

Although *ccm2* and *ccm2l* have partially overlapping functions in heart development, they do not function redundantly, as knockdown of either individually is sufficient to confer a heart phenotype. This suggests that, although exogenous *ccm2* can rescue *ccm2l* morphant defects, the embryo does not have a mechanism to increase expression of *ccm2* in response to loss of *ccm2l*. (Alternatively, the embryo may upregulate *ccm2* expression at a level insufficient to induce rescue in all embryos; measurement of transcript levels by quantitative RT-PCR would be required to determine this.) We also emphasize that our phenotypic data indicate that the functions of *ccm2* and *ccm2l* are partially overlapping but not identical, since *ccm2* mRNA injection rescues nearly 100% of *vtn* mutants (Mably et al., 2006) but only approximately 50% of affected *ccm2l* morphants.

Why is the *ccm2* loss-of-function phenotype more severe than that for *ccm2l*? One possibility is that the *ccm2l* phenotype is relatively mild because knockdown is incomplete. Another possibility is that the protein complexes containing Ccm2 generate the bulk of the downstream Heg-CCM signals, either because that complex has greater activity or because Ccm2 is present at a higher level in the cell than Ccm2l. Thus, loss of *ccm2* would have a more profound effect on the embryo than loss of *ccm2l*.

The downstream targets of Ccm2 and Ccm2l in heart development are unknown, and their identification should provide a wealth of knowledge about how the Heg-CCM pathway regulates cardiac morphology. According to our model, some of these targets would be shared by Ccm2 and Ccm2l, and others would be unique to one or the other. In the last several years, multiple pathways have been shown to be affected by loss of *ccm2*, both in cell culture and in the

adult mouse vasculature. These pathways, which include RhoA/ROCK (Crose et al., 2009; Stockton et al., 2010; Whitehead et al., 2009) , Wnt/ β-catenin signaling (Glading and Ginsberg, 2010), and the p38 stress response (Uhlik et al., 2003), represent a rich pool of candidates to be tested as downstream effectors of Ccm2 and Ccm2l in heart development.

Heg and Erk regulate heart development

It has previously been shown in HUVECs that depletion of CCM1 leads to hyperactivation of ERK and that overexpression of CCM1 leads to a reduction in ERK activation (Wustehube et al., 2010). We used siRNAs to deplete HEG1 from HUVECs and found that this causes an increase in the amount of activated ERK. Since loss of *heg* and *ccm1* in zebrafish affect heart development in the same way, it is not surprising that HEG1, like CCM1, negatively regulates ERK in HUVECs.

What is surprising, however, is that the relationship between Heg and Erk in heart development appears to be quite different from their relationship in HUVECs. Chemical inhibition of Mek1/2, the kinases that activate Erk, results in a dilated heart phenotype reminiscent of the *heg* mutant, suggesting that Heg does not negatively regulate Erk in the heart. Moreover, global activation of Erk in transgenic embryos rescues circulation in a statistically significant proportion of embryos injected with morpholino against *heg*. This finding raises the possibility that Heg positively regulates Erk *in vivo*.

Our zebrafish data suggesting that Heg positively regulates Erk and our HUVEC data showing a negative interaction can be reconciled by models emphasizing signaling between the two tissues of the zebrafish heart. We hypothesize that endocardial Heg may negatively regulate

endocardial Erk, recapitulating the interaction we observed in HUVECs. However, in our model, endocardial Heg *positively* regulates Erk in the myocardium, and it is myocardial Erk rather than endocardial Erk that regulates heart morphogenesis. A crucial function for myocardial Erk in heart development is suggested by our finding that hyperactivation of Erk specifically in the myocardium results in a shrunken heart.

In the future, several key experiments will have to be done to validate this model. First, it will need to be shown that Erk signaling is decreased in the myocardium of *heg* mutants. This can be done either with a phospho-specific Erk antibody or by measuring mRNA levels of Erk transcriptional targets. Second, this model requires that myocardial-specific loss of Erk activity be sufficient to cause severe heart dilation. This can be determined by generating zebrafish expressing a dominant negative *mek1* transgene specifically in the myocardium. Third, our rescue experiments ought to be repeated with myocardial-specific activation of Erk. This presents a challenge, as we have shown that this condition causes a dramatic shrinkage of the heart, a phenotype that would probably preclude embryos from exhibiting rescue of the *heg* phenotype. A possible solution to this problem would be to generate transgenic zebrafish employing the Tet-On system, in which temporal specificity can be achieved by administration of doxycycline. Perhaps by activating Erk in the myocardium relatively late in development, we could avoid the extreme defects we see in cmlc2:mek1DD embryos. The Tet-On system has been used successfully to temporally regulate expression of transgenes in the myocardium (Huang et al., 2005).

An alternative model to explain the rescue of *heg* morphant embryos by global Erk activation is that Heg and Erk regulate heart size similarly but independently. In other words, Heg and Erk both restrain the size of the heart, but neither affects the function of the other. If we

found that *heg* mutants exhibit normal levels of phospho-Erk and transcription of Erk-regulated genes, that would be evidence for this model. To distinguish between the two models, it will also be informative to perform cell counts on embryos treated with the MEK1/2 inhibitor CI-1040. An interesting feature of the *heg* mutant is that, although the heart is enormous, the number of cardiomyocytes is the same as in wildtype embryos. If this is the case for CI-1040 treated embryos, that would be consistent with the notion of Erk and Heg operating by a common mechanism. If CI-1040 treated embryos have more cardiomyocytes that normal, that would argue for inhibition of Erk and Heg causing an enlarged heart by independent mechanisms.

The Heg-CCM pathway in zebrafish and mammals

In this dissertation we use the zebrafish to analyze various aspects of the Heg-CCM pathway, with a mind toward applying our findings to the understanding of human CCM disease. In this final section, I compare our work in zebrafish to analogous studies in mouse and human and finish by describing the strengths and limitations of the zebrafish heart as a model for understanding CCM disease.

We performed a yeast 2-hybrid screen using the intracellular domain of zebrafish Heg as bait, and we recovered a large number of clones encoding fragments of Ccm1. We subsequently validated the Heg-Ccm1 interaction through co-immunoprecipitation of proteins generated by *in vitro* translation and in the 293T cell overexpression system. While our work was in progress, it was published by others that the mouse orthologs of Heg and Ccm1 bind as well (Kleaveland et al., 2009). Thus, the Heg-Ccm1 interaction is conserved between zebrafish and mammals. Our

finding that this interaction is mediated by the FERM domain of Ccm1 was validated in mammals as well (Gingras et al., 2012).

In zebrafish, the physical interaction between Heg and Ccm1 was predicted by the finding that the *heg* and *san* mutants have nearly identical phenotypes (Mably et al., 2006). In mouse, interestingly, the *Ccm1* and *Heg1* knockouts have quite different phenotypes; *Ccm1* knockouts die *in utero* from severe vascular defects (Whitehead et al., 2004), while *Heg1* knockouts usually die postnatally from cardiac or pulmonary rupture (Kleaveland et al., 2009). The discrepancy between the *Ccm1* and *Heg1* mouse phenotypes makes it particularly remarkable that the biochemical interaction is conserved. One possible explanation for why the mouse *Heg1* knockout phenotype is relatively weak is that mammals have additional transmembrane proteins that offer some redundancy. This would also explain why, to date, no *HEG1* mutations have been identified in CCM patients.

A comparison of our study of *ccm2l* in zebrafish to the analogous study in mouse (Zheng et al., 2012) provides another example of Heg-CCM biochemical interactions being conserved between species; however, in this case, the developmental function of the same interaction seems to be different in mouse and zebrafish. In both species, it was found that *ccm1* and *ccm2l* are expressed in the heart and their protein products can physically interact. However, in zebrafish, the *gain* of *ccm2* rescues heart defects in *ccm2l* morphants, whereas in mouse, the *loss* of *ccm2* rescues heart defects in *Ccm2l*$^{-/-}$*;Heg1*$^{-/-}$ animals. As we explain in the discussion section of Chapter 3 of this dissertation, we hypothesize that this difference in the relationship between *ccm2* and *ccm2l* relates to the different modes of heart development in zebrafish and mouse. In the mouse embryo, heart growth is accomplished primarily by myocardial proliferation, a process promoted by *ccm2l*. However, in early zebrafish embryos, heart growth is mainly

accomplished by differentiation of new cardiomyocytes, not proliferation of existing ones (de Pater et al., 2009). Thus, we hypothesize, an antagonistic relationship between *ccm2* and *ccm2l* in regulation of heart growth would not be conserved in the early zebrafish embryo, even though Ccm2l may interact with the same proteins in both systems.

A third interaction we studied—between Heg and Erk—is quite different in human CCMs and the zebrafish heart. We have found that global inhibition of Erk with the Mek1/2 inhibitor CI-1040 results in a dilated heart, myocardial-specific activation of Erk results in a shrunken heart, and, most interestingly, global activation of Erk can rescue *heg* morphant heart defects. Given the histological and cell biological similarities between *heg* mutant hearts and CCM lesions, this finding raises the possibility that pharmaceuticals that activate ERK might be useful in treating CCMs in human patients. A limited number of small molecules that activate ERK are available and have shown promise in animal models of a different disease (Maher et al., 2011).

And yet, despite the similarities between the two systems, treatment of CCM disease with ERK activators would be unwise. Unlike the endothelium in *heg* and *san* mutants, CCM lesion endothelium is hyperproliferative, a phenotype thought to contribute to the disease. ERK is known to stimulate proliferation generally, and it has been shown that resected CCM lesions have increased ERK activation. Furthermore, in a CCM model in which HUVECs depleted of CCM1are grafted into mice and form vessels with features of CCM pathology, treatment with the ERK pathway inhibitor Sorafenib (which inhibits other kinases as well) can ameliorate CCM-like phenotypes (Wustehube et al., 2010). It stands to reason that drugs that activate ERK could worsen outcomes in CCM patients.

Why are Heg-CCM loss-of-function phenotypes rescued by Erk *activation* in the zebrafish heart but by ERK *inhibition* in a mouse CCM model? Here, the discrepancy is probably not due to species-specific roles for Heg-CCM genes and ERK, but rather to organ-specific roles for Heg-CCM genes and ERK. Erk activation likely rescues circulation in *heg* morphants due to its effects in the myocardium, a tissue that is probably irrelevant to human CCM disease. And Sorafenib rescues CCM-like pathology in the mouse model by suppressing endothelial hyperproliferation, a defect absent from the mutant zebrafish heart's endocardium.

All that considered, does the embryonic zebrafish heart have value as a model for CCM disease? The answer is probably yes—but with certain limitations. Human CCM lesions are dilated, have reduced cell junctions, and are hyperproliferative. The zebrafish Heg-CCM mutants have the first two phenotypes but not the third; thus, for chemical or genetic interventions targeting vessel dilation and cell junctions, the zebrafish heart may faithfully recapitulate the human disease, while interventions that could improve patient outcomes by reducing endothelial proliferation might have no effect on the zebrafish heart. The second challenge is posed by the myocardium. It is easy to envision large scale screens designed to identify small molecules that can rescue *heg*, *san*, or *vtn* heart defects as a proxy for CCM lesions. Any hits from such a screen would have to be evaluated in a tissue-specific fashion, as there is no reason to expect that treatments that work primarily by affecting the myocardium would have a beneficial role in the brain vasculature. However, a molecule that rescued the mutant heart by primarily affecting the endocardium might be an interesting candidate as a therapeutic for CCM disease.

Works cited

Borikova, A.L., Dibble, C.F., Sciaky, N., Welch, C.M., Abell, A.N., Bencharit, S., Johnson, G.L., 2010. Rho kinase inhibition rescues the endothelial cell cerebral cavernous malformation phenotype. The Journal of biological chemistry 285, 11760-11764.

Crose, L.E., Hilder, T.L., Sciaky, N., Johnson, G.L., 2009. Cerebral cavernous malformation 2 protein promotes smad ubiquitin regulatory factor 1-mediated RhoA degradation in endothelial cells. The Journal of biological chemistry 284, 13301-13305.

de Pater, E., Clijsters, L., Marques, S.R., Lin, Y.F., Garavito-Aguilar, Z.V., Yelon, D., Bakkers, J., 2009. Distinct phases of cardiomyocyte differentiation regulate growth of the zebrafish heart. Development (Cambridge, England) 136, 1633-1641.

Gingras, A.R., Liu, J.J., Ginsberg, M.H., 2012. Structural basis of the junctional anchorage of the cerebral cavernous malformations complex. The Journal of cell biology 199, 39-48.

Glading, A.J., Ginsberg, M.H., 2010. Rap1 and its effector KRIT1/CCM1 regulate beta-catenin signaling. Dis Model Mech 3, 73-83.

Guruharsha, K.G., Kankel, M.W., Artavanis-Tsakonas, S., 2012. The Notch signalling system: recent insights into the complexity of a conserved pathway. Nat Rev Genet 13, 654-666.

Huang, C.J., Jou, T.S., Ho, Y.L., Lee, W.H., Jeng, Y.T., Hsieh, F.J., Tsai, H.J., 2005. Conditional expression of a myocardium-specific transgene in zebrafish transgenic lines. Dev Dyn 233, 1294-1303.

Kleaveland, B., Zheng, X., Liu, J.J., Blum, Y., Tung, J.J., Zou, Z., Sweeney, S.M., Chen, M., Guo, L., Lu, M.M., Zhou, D., Kitajewski, J., Affolter, M., Ginsberg, M.H., Kahn, M.L., 2009. Regulation of cardiovascular development and integrity by the heart of glass-cerebral cavernous malformation protein pathway. Nature medicine 15, 169-176.

Mably, J.D., Chuang, L.P., Serluca, F.C., Mohideen, M.A., Chen, J.N., Fishman, M.C., 2006. santa and valentine pattern concentric growth of cardiac myocardium in the zebrafish. Development (Cambridge, England) 133, 3139-3146.

Maher, P., Dargusch, R., Bodai, L., Gerard, P.E., Purcell, J.M., Marsh, J.L., 2011. ERK activation by the polyphenols fisetin and resveratrol provides neuroprotection in multiple models of Huntington's disease. Hum Mol Genet 20, 261-270.

Stockton, R.A., Shenkar, R., Awad, I.A., Ginsberg, M.H., 2010. Cerebral cavernous malformations proteins inhibit Rho kinase to stabilize vascular integrity. J Exp Med 207, 881-896.

Uhlik, M.T., Abell, A.N., Johnson, N.L., Sun, W., Cuevas, B.D., Lobel-Rice, K.E., Horne, E.A., Dell'Acqua, M.L., Johnson, G.L., 2003. Rac-MEKK3-MKK3 scaffolding for p38 MAPK activation during hyperosmotic shock. Nature cell biology 5, 1104-1110.

Whitehead, K.J., Chan, A.C., Navankasattusas, S., Koh, W., London, N.R., Ling, J., Mayo, A.H., Drakos, S.G., Jones, C.A., Zhu, W., Marchuk, D.A., Davis, G.E., Li, D.Y., 2009. The cerebral cavernous malformation signaling pathway promotes vascular integrity via Rho GTPases. Nature medicine 15, 177-184.

Whitehead, K.J., Plummer, N.W., Adams, J.A., Marchuk, D.A., Li, D.Y., 2004. Ccm1 is required for arterial morphogenesis: implications for the etiology of human cavernous malformations. Development (Cambridge, England) 131, 1437-1448.

Wustehube, J., Bartol, A., Liebler, S.S., Brutsch, R., Zhu, Y., Felbor, U., Sure, U., Augustin, H.G., Fischer, A., 2010. Cerebral cavernous malformation protein CCM1 inhibits sprouting angiogenesis by activating DELTA-NOTCH signaling. Proceedings of the National Academy of Sciences of the United States of America 107, 12640-12645.

Zawistowski, J.S., Stalheim, L., Uhlik, M.T., Abell, A.N., Ancrile, B.B., Johnson, G.L., Marchuk, D.A., 2005. CCM1 and CCM2 protein interactions in cell signaling: implications for cerebral cavernous malformations pathogenesis. Hum Mol Genet 14, 2521-2531.

Zheng, X., Xu, C., Smith, A.O., Stratman, A.N., Zou, Z., Kleaveland, B., Yuan, L., Didiku, C., Sen, A., Liu, X., Skuli, N., Zaslavsky, A., Chen, M., Cheng, L., Davis, G.E., Kahn, M.L., 2012. Dynamic regulation of the cerebral cavernous malformation pathway controls vascular stability and growth. Dev Cell 23, 342-355.

Appendix: List of hits from yeast 2-hybrid screen, in order of sequencing plate position.

Sequence ID	Contig #	Danio EntrezGene name	Human EntrezGene name	# reads
plate01A01.b	singlet		MAT2B	1
plate01A02.b	singlet	ENSDARG00000078882	-	1
plate01A03.b	49		RNF2	10
plate01A04.b	singlet		ACACA	1
plate01A05.b	45		COL1A2	6
plate01A06.b	50		TTN	10
plate01A07.b	31		SMARCB1	3
plate01A08.b	50		TTN	10
plate01A09.b	49		RNF2	10
plate01A10.b	singlet		TRIP11	1
plate01A11.b	40		FLNA	4
plate01A12.b	singlet		NCLN	1
plate01B01.b	singlet		KDM6A	1
plate01B02.b	singlet	-	-	1
plate01B03.b	40		FLNA	4
plate01B04.b	51		TTN	11
plate01B05.b	41		PIH1D1	4
plate01B06.b	2		CPT1A	1
plate01B07.b	32		GRB10	3
plate01B08.b	31		SMARCB1	3
plate01B09.b	singlet	LOC567179, LOC557901 (weak)	-	1
plate01B10.b	42		CCDC80	4
plate01B11.b	46		DHRS4	6
plate01B12.b	singlet		ELF2	1
plate01C01.b	13		SMOX	2
plate01C02.b	singlet		RPS27A	1
plate01C03.b	50		TTN	10
plate01C04.b	singlet		FBP2	1
plate01C05.b	14		SART3	2
plate01C06.b	15		HMCN1	2
plate01C07.b	43		COL1A2	4
plate01C08.b	singlet		GCAT	1

plate01C09.b	46		DHRS4	6
plate01C10.b	16		C5orf44	2
plate01C11.b	17		RNF2	2
plate01C12.b	17		RNF2	2
plate01D01.b	51		TTN	11
plate01D02.b	singlet		MDH1	1
plate01D03.b	43		COL1A2	4
plate01D04.b	33		CCDC80	3
plate01D05.b	47		KRIT1	6
plate01D06.b	47		KRIT1	6
plate01D07.b	singlet		CDK1	1
plate01D08.b	singlet		GFM2	1
plate01D09.b	40		FLNA	4
plate01D10.b	singlet		-	1
plate01D11.b	18	hbs1l (with intron?)	HBS1L	2
plate01D12.b	31		SMARCB1	3
plate01E01.b	19		TTN	2
plate01E02.b	singlet		PLOD1	1
plate01E03.b	38		LOX	3
plate01E04.b	singlet	-	-	1
plate01E05.b	singlet		TUBGCP4	1
plate01E06.b	14		SART3	2
plate01E07.b	singlet		HSPB1	1
plate01E08.b	51		TTN	11
plate01E09.b	20		MYBPC3	2
plate01E10.b	45		COL1A2	6
plate01E11.b	50		TTN	10
plate01E12.b	21		FLNC	2
plate01F01.b	singlet		ABI3BP	1
plate01F02.b	3		KRIT1	1
plate01F03.b	1		CILP	1
plate01F04.b	singlet		ARCN1	1
plate01F05.b	singlet		PCBP2	1
plate01F06.b	singlet		SHMT1	1
plate01F07.b	singlet		ANXA1	1
plate01F08.b	20		MYBPC3	2
plate01F09.b	32		GRB10	3
plate01F10.b	singlet		TRIM50	1
plate01F11.b	46		DHRS4	6
plate01F12.b	singlet		MANEA	1
plate01G01.b	singlet		DNAJA2	1
plate01G02.b	51		TTN	11
plate01G03.b	singlet		AUH	1

plate01G04.b	singlet		ID2	1
plate01G05.b	47		KRIT1	6
plate01G06.b	43		COL1A2	4
plate01G07.b	singlet		GNB5	1
plate01G08.b	4		SMARCB1	1
plate01G09.b	singlet		SDHA	1
plate01G10.b	singlet		SND1	1
plate01G11.b	singlet	myst3 (in intron?)	-	1
plate01G12.b	singlet		APBA1	1
plate01H01.b	singlet		PKM2	1
plate01H02.b	44		GSR	4
plate01H03.b	43		COL1A2	4
plate01H04.b	33		CCDC80	3
plate01H05.b	41		PIH1D1	4
plate01H06.b	49		RNF2	10
plate01H07.b	singlet		CARKD	1
plate01H08.b	34		FLNA	3
plate01H09.b	48		CILP	6
plate01H10.b	singlet	net1 (5' end?)	-	1
plate01H11.b	singlet		TACO1	1
plate01H12.b	33		CCDC80	3
plate02A01.b	singlet		PPIF	1
plate02A02.b	35		NDUFS2	3
plate02A03.b	34		FLNA	3
plate02A04.b	singlet		NUDT21	1
plate02A05.b	45		COL1A2	6
plate02A06.b	51		TTN	11
plate02A07.b	51		TTN	11
plate02A08.b	22		TBXA2R	2
plate02A09.b	23		HTRA2	2
plate02A10.b	45		COL1A2	6
plate02A11.b	singlet		KIAA0564	1
plate02A12.b	singlet		SRPX	1
plate02B01.b	48		CILP	6
plate02B02.b	44		GSR	4
plate02B03.b	45		COL1A2	6
plate02B04.b	singlet		GPS2	1
plate02B05.b	36		AIP	3
plate02B06.b	singlet		MYLK	1
plate02B07.b	24		FBLN2	2
plate02B08.b	singlet		LAMA4	1
plate02B09.b	41		PIH1D1	4
plate02B10.b	25		SMARCB1	2

plate02B11.b	26		FLNB	2
plate02B12.b	singlet		GIN1	1
plate02C01.b	16		C5orf44	2
plate02C02.b	singlet		KHDRBS1	1
plate02C03.b	singlet		AUP1	1
plate02C04.b	singlet		SH2D4B	1
plate02C05.b	singlet		AKR7A2	1
plate02C06.b	27		POSTN	2
plate02C07.b	singlet		CCNB1	1
plate02C08.b	48		CILP	6
plate02C09.b	singlet	zgc:153607 (3' exon?	-	1
plate02C10.b	singlet	creb3l3l	-	1
plate02C11.b	singlet		L2HGDH	1
plate02C12.b	18	hbs1l (with intron?)	HBS1L	2
plate02D01.b	singlet	alternate exon of si:dkey-21k10.1 (PTPRF)?	-	1
plate02D02.b	35		NDUFS2	3
plate02D03.b	singlet		ttn	1
plate02D04.b	5		GRB10	1
plate02D05.b	singlet		PAPSS2	1
plate02D06.b	37		SMAD6	3
plate02D07.b	singlet		TUBGCP6	1
plate02D08.b	39		CPT1A	3
plate02D09.b	singlet		BAIAP2	1
plate02D10.b	singlet		ABCA5	1
plate02D11.b	singlet		ADCY2	1
plate02D12.b	51		TTN	11
plate02E01.b	singlet		GPS1	1
plate02E02.b	38		LOX	3
plate02E03.b	49		RNF2	10
plate02E04.b	singlet	bnip2	-	1
plate02E05.b	41		PIH1D1	4
plate02E06.b	singlet		SKP2	1
plate02E07.b	48		CILP	6
plate02E08.b	22		TBXA2R	2
plate02E09.b	45		COL1A2	6
plate02E10.b	51		TTN	11
plate02E11.b	47		KRIT1	6
plate02E12.b	singlet		RYBP	1
plate02F01.b	49		RNF2	10
plate02F02.b	singlet	LOC570228 (ARHGEF3)	-	1
plate02F03.b	24		FBLN2	2
plate02F04.b	34		FLNA	3

plate02F05.b	49		RNF2	10
plate02F06.b	6		MYBPC3	1
plate02F07.b	singlet		LGALS3	1
plate02F08.b	39		CPT1A	3
plate02F09.b	38		LOX	3
plate02F10.b	28		CDC20	2
plate02F11.b	singlet	fb06f03 (hmg-like)	-	1
plate02F12.b	39		CPT1A	3
plate02G01.b	51		TTN	11
plate02G02.b	32		GRB10	3
plate02G03.b	50		TTN	10
plate02G04.b	48		CILP	6
plate02G05.b	49		RNF2	10
plate02G06.b	27		POSTN	2
plate02G07.b	46		DHRS4	6
plate02G08.b	singlet		PPT1	1
plate02G09.b	singlet	im:7136729 (MS4A4A)	-	1
plate02G10.b	singlet		CACNA1C	1
plate02G11.b	29		NID2	2
plate02G12.b	singlet		POLDIP2	1
plate02H01.b	7	rfx4 (intron?)	-	1
plate02H02.b	singlet		ADSSL1	1
plate02H03.b	50		TTN	10
plate02H04.b	44		GSR	4
plate02H05.b	30		KRIT1	2
plate02H06.b	15		HMCN1	2
plate02H07.b	51		TTN	11
plate02H08.b	singlet		CTSK	1
plate02H09.b	51		TTN	11
plate02H10.b	8		DHRS4L2	1
plate02H11.b	30		KRIT1	2
plate02H12.b	singlet		SMG5	1
plate03A01.b	47		KRIT1	6
plate03A02.b	9	ADAM12 (5' UTR?)	-	1
plate03A03.b	37		SMAD6	3
plate03A04.b	44		GSR	4
plate03A05.b	23		HTRA2	2
plate03A06.b	singlet		GMPS	1
plate03A07.b	singlet		C16orf13	1
plate03A08.b	48		CILP	6
plate03A09.b	singlet		ABCD3	1
plate03A10.b	singlet		LRRC8A	1
plate03A11.b	49		RNF2	10

plate03A12.b	singlet	-	-	1
plate03B01.b	21		FLNC	2
plate03B02.b	28		CDC20	2
plate03B03.b	19		TTN	2
plate03B04.b	35		NDUFS2	3
plate03B05.b	singlet		ACAA2	1
plate03B06.b	25		SMARCB1	2
plate03B07.b	singlet	repeat?	-	1
plate03B08.b	singlet	LOC566883 (similar to KCNB2)		1
plate03B09.b	36		AIP	3
plate03B10.b	singlet		WDR37	1
plate03B11.b	10		GSR	1
plate03B12.b	47		KRIT1	6
plate03C01.b	50		TTN	10
plate03C02.b	singlet		BAT5	1
plate03C03.b	26		FLNB	2
plate03C04.b	42		CCDC80	4
plate03C05.b	singlet	repeat?	-	1
plate03C06.b	11		KRIT1	1
plate03C07.b	12		CILP	1
plate03C08.b	50		TTN	10
plate03C09.b	49		RNF2	10
plate03C10.b	13		SMOX	2
plate03C11.b	50		TTN	10
plate04A01.b	singlet	-	-	1
plate04A02.b	40		FLNA	4
plate04A03.b	singlet		MAPRE3	1
plate04A04.b	singlet		CCBL2	1
plate04A05.b	singlet		ALDOC	1
plate04A06.b	singlet		PTP4A3	1
plate04A07.b	singlet	-	-	1
plate04A08.b	singlet		PARK2	1
plate04A09.b	37		SMAD6	3
plate04A10.b	49		RNF2	10
plate04A11.b	singlet	-	-	1
plate04A12.b	singlet		CDC23	1
plate04B01.b	singlet	-	-	1
plate04B02.b	36		AIP	3
plate04B03.b	singlet	-	-	1
plate04B04.b	42		CCDC80	4
plate04B05.b	50		TTN	10
plate04B06.b	singlet		CSTF1	1
plate04B07.b	singlet	-	-	1

plate04B08.b	singlet	-	-	1
plate04B09.b	singlet	3' of atp2b4 , 5' of mdm4	-	1
plate04B10.b	42		CCDC80	4
plate04B11.b	29		NID2	2
plate04B12.b	singlet	-	-	1
plate04C01.b	singlet		TBXA2R	1
tube001.b	46		DHRS4	6
tube002.b	46		DHRS4	6